A Systematic Investigation into Bisphosphine Ligands for Nickel-Catalyzed C(sp^2)–N Cross-Coupling

by

Nicole Martinek

Submitted in partial fulfillment of the requirements

For the degree of Master of Science

Dalhousie University

Halifax, Nova Scotia

February 2023

Table of Contents

List of Figures

Abstract

Research into transition metal-catalyzed C–N cross-coupling reactions has been driven by a need for robust and facile synthetic routes towards bioactive molecules which are rich in C–N linkages. The use of Pd-based catalysts in Buchwald-Hartwig Amination (BHA) protocols are the most well studied and utilized within industry. The choice of Pd source, ancillary ligand, base, solvent, and the use of additives have been thoroughly investigated aiding in the selection and optimization of reaction conditions. However, research has refocused towards finding more Earth-abundant and cost-effective transition metals capable of comparable reactivity. Ni has proven to be a competitor with the development of new ancillary ligands after efforts to repurpose well-known ligands in Pd-catalysis had limited success. In particular, bisphosphines within the DalPhos ligand family have enabled the Ni-catalyzed *N*-arylation of challenging substrates including ammonia, alkylamines, heteroarylamines, indole, and amides with (hetero)aryl electrophiles prompting the commercialization of several ligand variants. The effects of varying experimental parameters within these ligand/Ni systems are less established and prompt further investigation in order to determine trends in reactivity and limitations. A systematic evaluation of selected bases and solvents on the effectiveness of leading DalPhos ligand variants in the C–N cross-coupling of structurally varied (hetero)aryl electrophiles with primary and secondary amines is reported herein.

List of Abbreviations Used

API active pharmaceutical ingredient

Ar aryl

BHA Buchwald-Hartwig amination

BINAP 2,2′-bis(diphenylphosphino)-1,1′-binaphthalene

CgP 1,3,5,7-tetramethyl-2,4,8-trioxa-6-phosphaadamantane

COD cycloocta-1,5-diene

Cy cyclohexyl

CyDMEDA *trans*-*N*,*N*'-dimethylcyclohexane-1,2-diamine

CyPF-*t*Bu (R)-(-)-1-[(S)-2-(dicyclohexylphosphino)ferrocenyl]ethyldi-*tert*-butylphosphine

dba dibenzylideneacetone

DiMelHelpt^{Cl} 1,3-bis[2,6-bis[3-methyl-1-(2-methylpropyl)butyl]phenyl]-4,5-dichloro-1,3-dihydro-2*H*-imidazol-2-ylidene

DBU 1,8-diazabicyclo(5.4.0)undec-7-ene

DPPF 1,1′-ferrocenediyl-bis(diphenylphosphine)

DQ duroquinone

GC gas chromatography

h hour

HRMS high-resolution mass spectrometry

HTE high-throughput experimentation

JackiePhos 2-{bis[3,5-bis(trifluoromethyl)phenyl]phosphino}-3,6-dimethoxy -2′,4′,6′-triisopropyl-1,1′-biphenyl

JohnPhos (2-biphenyl)di-*tert*-butylphosphine

LC liquid chromatography

M mol / L

NHC N-heterocyclic carbene

Nf nonaflate

MS mass spectrometry

Ms mesylate

***o*-tol/*o*-tolyl** *ortho*-tolyl

Ph phenyl

PTFE poly(tetrafluoroethylene)

***rac*-BINAP** (±)-2,2′-bis(diphenylphosphino)-1,1′-binaphthalene

rt room-temperature

RuPhos 2-dicyclohexylphosphino-2′,6′-diisopropoxybiphenyl

SET single electron transfer

S_NAr nucleophilic aromatic substitution

***t*BuXPhos** 2-di-*tert*-butylphosphino-2′,4′,6′-triisopropylbiphenyl

TFA trifluoroacetate

THF tetrahydrofuran

OTf triflate

OTs tosylate

X halide substituent or anionic ligand

XantPhos 4,5-bis(diphenylphosphino)-9,9-dimethylxanthene

XPhos 2-dicyclohexylphosphino-2′,4′,6′-triisopropylbiphenyl

Acknowledgments

I would like to extend sincere gratitude to my supervisor, Dr. Mark Stradiotto – Mark, I am beyond grateful your support and generosity. I could not have hoped for a more positive, interesting, or memorable experience right from day one. It has been a blessing to work with you.

Many thanks to past (Connor Simon, Ryan McGuire, Travis Lundrigan, Karlee Bamford and Justin Field, to name a few) and present (Kathleen Morrison, Nicholas Bode, Josh MacMillan, Tim Anderson, Peter Fox, Mike Cotnam, Sam Fisher, Sam Knight, and Jonathan Choi) members of the Stradiotto group. You have each been so helpful over the last two years. Kathleen, you will always have my utmost gratitude and respect for being an extraordinary mentor and one of the kindest people I have ever met.

I would also like to acknowledge and thank Dr. Mike Lumsden, for his technical assistance in running NMR experiments, and Mr. Xiao Feng, for collecting mass-spectrometry data. My committee member, Dr. Alex Speed, and Dr. Carlie Charron are thanked for their time and commitment in supervising my thesis.

Lastly, to my friends and family for supporting me even though I moved across the country – thank you. Dominique, I am most grateful for your continued friendship and unwavering support. Cassidy, Loreal, and Julie – your friendship has made Halifax feel like home.

1 Introduction

1.1 Thesis Overview

Homogeneous transition metal catalysis is used extensively in synthetic organic chemistry. Well-designed catalysts provide improved synthetic protocols, enabling challenging and low yielding reactions to proceed efficiently and can afford more direct access to products that may otherwise require multiple synthetic steps. Cross-coupling reactions are a reliable method for forming C–X bonds (X = C, N, O, S, etc.) and have become essential to the production and modification of organic building blocks and highly functionalized molecules. The production of (hetero)anilines is highly desirable due to their prevalence in pharmaceuticals and natural products. While traditional synthetic methods include S_NAr[1] and sequential nitration/reduction,[2, 3] the metal-catalyzed cross-coupling of (hetero)aryl (pseudo)halides with NH nucleophiles to generate C(sp^2)–N bonds has become a preferred synthetic protocol.[4] The application of such cross-coupling reactions in the pursuit of structurally complex products entails rigorous exploration and optimization of reaction conditions to ensure selection of a robust and cost-effective system.

The success of metal-catalyzed cross-coupling protocols can be largely attributed to the design of ancillary ligands responsible for modulating reactivity at the metal-center through steric and electronic effects.[5, 6] Well-designed ancillary ligands have enabled broad reaction scopes including challenging and deactivated substrates, the use of functional-group tolerant bases, low catalyst loadings, and low temperatures. They can also lend specificity to these systems by enabling chemoselectivity, stereoselectivity, and enantioselectivity that is generally not obtained with more structurally simple ligands (e.g., **PPh_3**).[7] Base and solvent selection must also be considered when constructing a catalytic system, adding to their complexity. The Pd-catalyzed C–

N cross-coupling reaction (i.e., Buchwald-Hartwig Amination, BHA)[8, 9] has been thoroughly studied with a well-accepted Pd(0)/Pd(II) catalytic cycle involving oxidative addition, net transmetalation, and reductive elimination, enabled by a diversity of ancillary ligands. However, there are some disadvantages to using Pd that has spurred research into alternatives. Primarily driven by the scarcity and ensuing cost of Pd, considerable research has focused on the use of highly abundant first row transition metals, such as Ni; while Cu is also useful for such transformations, limited reaction scope in the electrophile reactant renders such protocols as generally unsuitable substitutes for Pd, as discussed below. While preliminary studies employing Ni repurposed ancillary ligands common to Pd chemistry proved to be generally unsuccessful, the design of new ligands has allowed for comparable and in some cases superior reactivity. However, in terms of the mechanism and other reactivity aspects (e.g., redox behavior), these Ni systems are more complex than their Pd counterparts and more research is needed to establish informative trends in reactivity and allow for broader applicability. Such research is aided by advancements in reactor technology and the development of new screening methodology.

1.2 Buchwald-Hartwig Amination

Twenty-eight years ago, Stephen L. Buchwald at the Massachusetts Institute of Technology and John F. Hartwig at Yale University, independently reported the first Pd-catalyzed cross-coupling of aryl bromides with amines (i.e., BHA) presented in **Figure 1.1**.[8, 9] This prompted decades of chemistry centered on understanding and optimizing the metal-catalyzed cross-coupling of (hetero)aryl (pseudo)halides with NH substrates in the formation of C–N bonds. This reaction has become fundamental for the synthesis of aryl amines, which are prominent moieties in many pharmaceuticals,[10, 11, 12] agrochemicals,[11] and functional materials.[13]

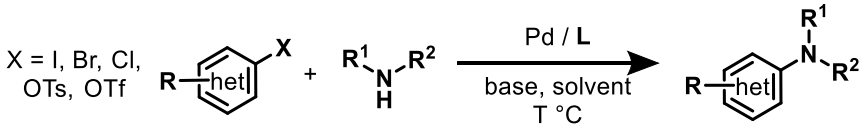

Figure 1.1 General Reaction Scheme for Buchwald-Hartwig Amination.

The drug discovery and late-stage modification of active pharmaceutical ingredients (APIs) often involves highly functionalized and complex substrates, which can pose a significant challenge for most BHA catalyst systems that were developed using more structure simple test substrates.[14] Nonetheless, within the last few years alone Pd-catalyzed BHA has been successfully used in the preparation of several pharmaceutical compounds on kilogram scales including **GDC-0022·pTsOH**[15] and a precursor to **BIIB068**,[16] which are both candidates for treating immune-related diseases, and **T790 M**[17] which is used for the treatment of non-small cell lung cancer (Figure 1.2).[18]

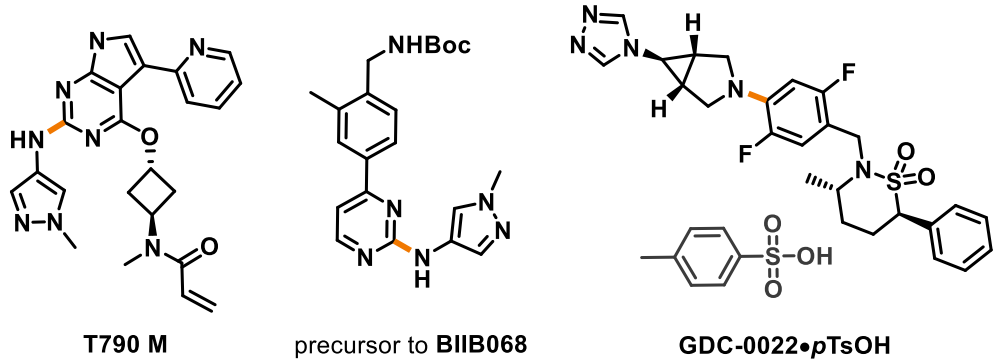

Figure 1.2 Selected examples of drug candidates synthesized on kg scale using Pd-catalyzed BHA to form the bolded C–N bond.

1.2.1 Transition Towards Ni-Catalyzed C–N Cross-Coupling

Although early reports of C–N cross-coupling demonstrated the potential for Ni-based catalysts, the field has recently been dominated by Pd and only in the last decade has research

refocused to include more Earth-abundant metals, such as revisiting Cu (in Ullmann-type coupling) and developing Ni as more economical alternatives to Pd. The first Cu-mediated cross-coupling of an aryl chloride with an aryl amine was reported in 1903 and required stoichiometric quantities of Cu and elevated temperatures (>200 °C),[19] which are common drawbacks to Ullmann-type coupling. While significant advancements have established systems only requiring catalytic quantities of Cu and even mild reaction conditions, they are largely limited to aryl bromide and iodide coupling partners with only select examples using (hetero)aryl chlorides.[20] With aryl chlorides being both cheaper and more widely available than bromo or iodo electrophiles, it is desirable to find a catalytic system capable of accessing these substrates.[21] This has led several research groups to focus on developing Ni-based systems to circumvent the costliness of Pd while overcoming substrate limitations.

1.3 Effect of Ancillary Ligand Design on Transition Metal Reactivity

The putative Pd(0)/Pd(II) cycle of BHA first established by Hartwig[8] is aided by sterically hindering and electronically rich ancillary ligands. Such ligands enable formation of the catalytically active Pd(0) species while preventing inhibitory bis-chelation (i.e., $(L)_2M$) or dimerization and promoting what is commonly rate-limiting oxidative addition of the C(sp^2) –X (X = Br, Cl, etc.) bond by donating electron density to the Pd-center.[5, 22] Phosphines are a common class of ligands employed in BHA and vary from structurally simple bulky monophosphines such as **P(*o*-tol)$_3$** and **P*t*Bu$_3$**, to more complex biaryl monophosphines (e.g., **XPhos** variants) and bisphosphines (P_2, e.g., **XantPhos**, ***rac*-BINAP**) (Figure 1.3). Many of these are regularly used on large scales for the synthesis of pharmaceuticals.[18] Phosphines are advantageous because their sterics and electronics can be easily modified at the phosphorus center with various aryl or alkyl

groups, or by addition of heteroatom linkages and other coordinating functional groups to afford multidentate ligands further tuning reactivity at the metal center.[4, 5]

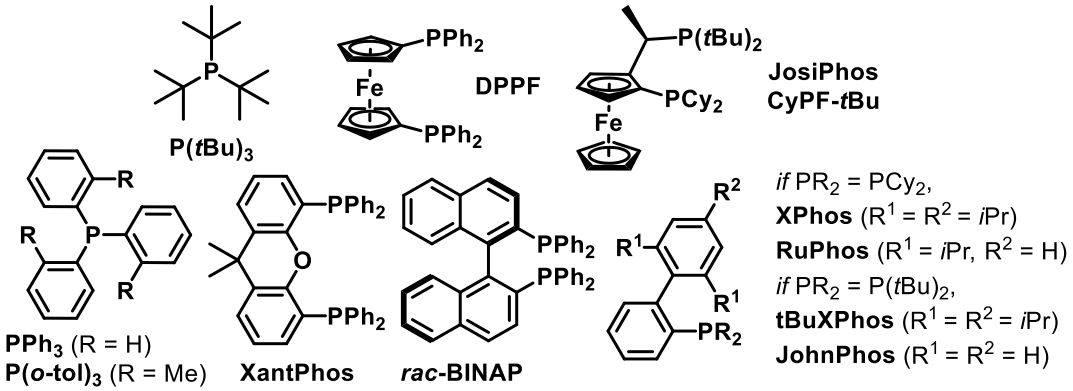

Figure 1.3 Selected examples of mono- and bis-phosphine ancillary ligands commonly employed in BHA.

While these ligands are applicable to Pd-catalysis, the lower electronegativity of Ni benefits from bulky ancillary ligands that are less electron-rich to combat the more challenging reductive elimination step. The sterically encumbering design of these ligands further discourages comproportionation leading to the formation of Ni(I) species enabled by nickel's readily accessible 0, +1, +2, and +3 oxidation states.[23-26] Nickel's ability to engage in single-electron transfer (SET) processes is exploited in redox-enabled cross-coupling approaches which depend upon reductants[27] or photochemical[28]/electrochemical[29] stimuli to drive catalysis. However, these systems are often limited to aryl bromide and/or iodide coupling partners while ligand-enabled Ni catalysts[26] are able to access more challenging substrates. Even early experiments reacting organic halides with Grignard reagents using Pd and Ni catalysts (i.e., Kumada-Corriu cross-coupling) demonstrated nickel's propensity towards oxidative addition of difficult coupling partners such as aryl chlorides, which are more challenging for Pd and still largely inaccessible to Cu catalysts.[30] The poor reactivity of the aryl chloride C(sp^2)–Cl bond can also be advantageous as they can be

introduced early on in synthetic routes for late-stage modification. In addition to these, phenol-derived (pseudo)halides (i.e., tosylates, triflates, mesylates, etc.) are also accessible substrates for ligand-enabled Ni catalysts permitting a broad selection of electrophilic coupling partners.[26, 31-34]

1.3.1 DPPF as an Ancillary Ligand for Ni-Catalyzed C–N Cross-Coupling

The bis(phosphino)ferrocene ligand **DPPF** (Figure 1.3) is a well-known ancillary ligand that was investigated in early C–N cross-couplings catalyzed by both Pd[35] and Ni.[36] In 2014, Buchwald reported the synthesis of an air-stable Ni pre-catalyst, (**DPPF**)Ni(*o*-tol)Cl, with a propensity for cross-coupling aryl chlorides with secondary alkylamines and included several examples using (hetero)aryl (pseudo)halides (i.e., mesylates, triflates, sulfamates, etc.) with (hetero)aryl amines.[31] A subsequent report in 2017 by the Stradiotto group,[37] aimed to elucidate structure-reactivity trends among 1,1′-bis(phosphino)ferrocenes variants as ancillary ligands for Ni-catalysis. This study demonstrated the utility of **DPPF** in the C–N cross-couplings of (hetero)aryl chlorides with furfurylamine, morpholine, and indole as representative primary, secondary, and *N*-heteroaryl amines, respectively. Although a number of other variants were competent in these transformations, they were difficult to obtain as analogous (**L**)Ni(*o*-tol)Cl pre-catalysts and only successfully used in combination with $Ni(COD)_2$, which is both expensive and air/temperature sensitive.

1.3.2 The DalPhos Ligand Series

The so-called DalPhos ligand series began in 2010 with the synthesis of several P,N-type ligands that were first utilized for Pd-catalysis and afforded excellent reactivity. Notably, the combination of $[Pd(cinnamyl)Cl]_2$ with **Mor-DalPhos** (Figure 1.4) enabled room temperature monoarylation of ammonia with a broad scope of aryl chlorides and tosylates.[38] A subsequent

study examining the efficacy of **Mor-DalPhos** and several other ligands common in Pd chemistry (e.g., JosiPhos variants, **DPPF**, and ***rac*-BINAP** shown in Figure 1.3) afforded the first report of Ni-catalyzed ammonia arylation (10 mol%, 110 °C) demonstrating the potential of this first-row transition metal to replace Pd.[39] However, only select JosiPhos variants provided yields greater than 80%[39] and it was not until the development of new P,P-type DalPhos ligands[33] that Ni displayed reactivity competitive to Pd for this cross-coupling (≤5 mol%, 25 °C). These DalPhos bisphosphines contain a bulky 1,3,5,7-tetramethyl-2,4,8-trioxa-6-phosphaadamantane (CgP) unit and a secondary phosphine (i.e., PR_2) group enabling additional ligand modification, which has proven to be integral to the success of Ni-catalyzed cross-couplings (Figure 1.4B).[26, 33]

The effect of minute changes to the sterics and electronics of ancillary ligands (illustrated in Figure 1.4) is evident in the substitution of the *o*-tolyl groups in **PAd-DalPhos** to simple phenyl rings giving **PhPAd-DalPhos**. The absence of two methyl groups in the pre-catalyst provided access to the challenging arylation of bulky α,α,α-branched primary alkylamines at moderate temperatures (≤ 80 °C).[40] The first Ni-catalyzed cross-coupling of cyclopropylamine with several (hetero)aryl (pseudo)halides (chloride, bromide, mesylate, tosylate, triflate, sulfamate, and carbamate) at room temperature was also reported with the synthesis of a cyclohexyl variant, **CyPAd-DalPhos**.[41] Heteroaryl analogues based on pyridine, quinoxaline, and thiophene have also been examined with substitution of the rigid phenylene backbone. Although the majority of these variants proved to be inferior to their parent ligand **PAd-DalPhos**, the 3,4-disubstituted thiophene variant **ThioPAd-DalPhos**[42] displayed improved performance in the coupling of (hetero)aryl (pseudo)halides with primary alkylamines at room temperature with markedly low catalyst loadings (0.125–2.25 mol%). The addition of a second phosphaadamantane cage or phosphonite unit to the original *o*-phenylene backbone afforded access to fluoroalkylamine coupling partners

(**PAd2-DalPhos**)[43] and the chemoselective coupling of (hetero)anilines (**Phen-DalPhos**) over the *N*-arylation of indole (**PAd2-DalPhos**) illustrating the value of these bisphosphines in Ni-catalysis.[44]

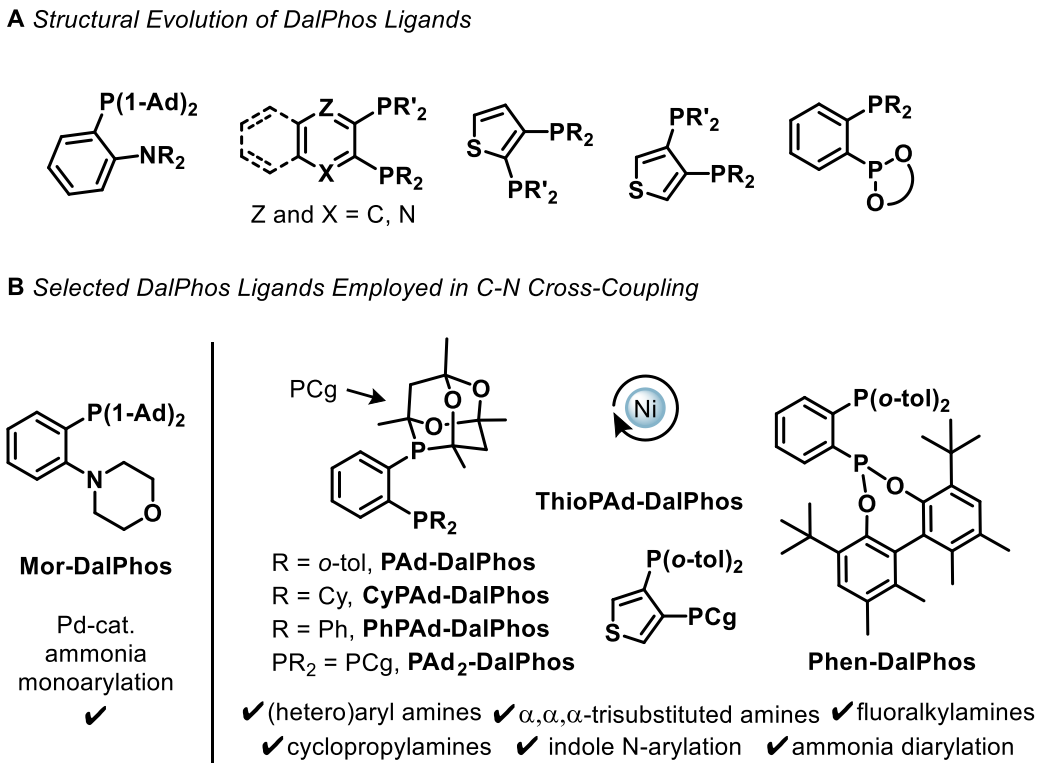

Figure 1.4 A. Structural moieties investigated throughout the development of DalPhos ligand variants. **B.** Selected DalPhos Ligands including the P,N-type ligand **Mor-DalPhos** (left) suited towards BHA and several P,P-type DalPhos ligands (right) used in Ni-catalyzed C–N cross-coupling.

The advancement of Ni-catalyzed C–N cross-couplings is driven by ancillary ligand design and the comparative screening of ligands to establish structure-reactivity relationship. While structural variants within the DalPhos series often display comparable reactivity, there are instances where one variant displays superior reactivity and enables access to challenging substrate classes.[26] Although preliminary ligand screening is often done using $Ni(COD)_2$/**L** mixtures, these ligands can be easily synthesized as air-stable (**L**)Ni(*o*-tol)Cl pre-catalysts analogous to the **DPPF**-

ligated Ni pre-catalyst reported by Buchwald,[31] circumventing the need for $Ni(COD)_2$. The success of these ligands encourages further exploration into their utility.

1.4 High-Throughput Experimentation

High-throughput experimentation (HTE) has transformed screening and optimization processes by allowing anywhere from dozens to a thousand automated experiments to be executed simultaneously with minimal manual handling of reaction materials and equipment. Followed by high-throughput analysis techniques such as gas chromatography (GC) or liquid chromatography (LC), and/or mass spectrometry (MS), this approach can significantly reduce the time needed to discover and optimize catalyst systems. Generally, literature reports are biased towards high yielding reactions with unsuccessful or poorly yielding results omitted. HTE data sets report both 'hits' and 'failures' providing a more comprehensive picture that can better inform subsequent experiments. Currently, this approach is inaccessible to most researchers within academia due to the high cost of HTE and high-throughput analytical (HTA) equipment, which has limited its use almost exclusively to R&D laboratories within industry, although some exceptions exist. The advantages of HTE (data-rich, fast, little-to-no handling of chemicals, reduced waste) cannot be denied and through both collaborative work and the development of smaller albeit less advanced but more affordable HTE systems, it is becoming more widely used.

1.4.1 Practical Considerations for HTE

While HTE screening methods enable testing reaction conditions that may have been excluded by typical 'manual' screening to minimize the workload and use of materials, there are still limitations to this methodology that need to be addressed. Liquid reagents can be delivered with high precision and accuracy while automated dispensing of solids, either dry or as a slurry,

remains a technological challenge that can ultimately result in false negatives.[45-48] This is most evident for reactions dependent upon inorganic phosphate or carbonate bases (i.e. K_3PO_4 or Cs_2CO_3), which are insoluble in conventional solvents (THF, toluene, 1,4-dioxane) and problematic even on larger scales with manual base addition. The reproducibility and scalability of these reactions suffer due to reaction inhomogeneity and poor/unequal particle size distribution.[49] While these bases can be milled prior to use or ground *in situ* with magnetic stirrers[50] to combat these effects, even variation in the reaction vessel[51, 52] used or speed of agitation[53] can be detrimental to the reaction rendering their use unreliable. Soluble organic bases are a promising alternative and have been successfully employed in Ni-catalyzed cross-couplings enabled by photochemical[28] or electrochemical[29] methods, or by the addition of reductants.[27] However, these approaches are often limited to activated aryl bromides or aryl iodides, while traditional thermal reaction conditions, which have concentrated largely on inorganic bases, can provide access to broader substrate scopes. In 2019, Wisniewski and co-workers reported the Pd-catalyzed amination of aryl chlorides using a combination of organic base (1,8-diazabicyclo[5.4.0]undec-7-ene, DBU) and a chloride scavenger (e.g. NaX, X = -TFA, trifluoroacetate) establishing the so-called "dual-base" system.[49] The applicability of DBU in HTE was demonstrated in a BHA study by Newman *et al*.,[47] consisting of 480 experiments conducted on a 0.033 mmol scale. A selection of nucleophiles, aryl chlorides, and commercially available ligands were explored and after analysis by GC-MS, 'hits' (defined as reactions that generated product) were followed up with subsequent optimization on a 0.2 mmol scale. The utility of DBU and other organic bases in ligand-enabled Ni-catalyzed cross-coupling reactions is still limited[43, 54-56] but offers a promising alternative to common bases that could expedite future HTE.

1.5 Overview of Thesis Research

The so-called DalPhos family of P,P-type ancillary ligands have demonstrated competence in various Ni-catalyzed cross-couplings of (hetero)aryl (pseudo)halides with NH substrates. Seemingly minor perturbations to the electronic and steric nature of the ligand, such as the use of phenyl groups in place of *o*-tolyl or cyclohexyl, have proven to have a profound effect on the reactivity emphasizing the need for thorough ligand screening. This inspired the comparative study presented herein, involving DalPhos ligand variants in C–N cross-coupling reactions along with the ancillary ligand **DPPF** as a supplementary bisphosphine that could also be employed as an air-stable (**L**)Ni(*o*-tol)Cl pre-catalyst. The effect of ligand, base, and solvent were systematically probed in the cross-coupling of (hetero)aryl chlorides with primary alkylamines (linear and branched), a primary heteroarylamine, and a secondary alkylamine. In addition to two commonly employed inorganic bases (NaO*t*Bu and K_2CO_3), the 'dual base' DBU/NaTFA system was chosen as a soluble organic base with promising use in HTE. The aim of this head-to-head evaluation was to establish trends in reactivity and limitations to these systems. Ligands displaying superior performance were employed in additional competition experiments and a catalytic system based on **PAd2-DalPhos**/DBU/NaTFA was identified. These results are disclosed in Chapter 2.

Concluding remarks and a proposal for future projects related to this work can be found in Chapter 3. Supplementary figures and experimental data are provided in the Appendix.

2 Comparative Screening of DalPhos/Ni Catalysts in C–N Cross-Couplings of (Hetero)aryl Chlorides Enables Development of Aminopyrazole Cross-Couplings with Amine Base

2.1 Contribution Statement

In this chapter the comparative screening of DalPhos/Ni Catalysts in C–N cross-couplings of (hetero)aryl chlorides is described. Preliminary screening was conducted by N. Martinek aided in part by J. M. Field, an undergraduate student. S. A. Fisher, a fellow graduate student, contributed to the synthesis of several pre-catalysts. The scope of aminopyrazole cross-couplings using an amine base was developed by N. Martinek. K. M. Morrison, a fellow graduate student, acted as a mentor throughout the course of this project, which was proposed by herself and Dr. M. Stradiotto, the graduate supervisor and manuscript author. This work has been published: N. Martinek, K. M. Morrison, J. M. Field, S. A. Fisher, M. Stradiotto, *Chem. Eur. J.* **2022**, e202203394.

2.2 Overview

While variants within the DalPhos ligand family have been able to address outstanding substrate challenges within transition metal-catalyzed C–N cross-coupling, the systematic head-to-head evaluation of **L1**–**L6** (Figure 2.1A) in diverse Ni-catalyzed *N*-arylation chemistry remains unexplored. Such studies are needed to identify optimal ligands for end-user applications, to highlight important limitations of such catalyst systems, and to enable the identification of new and useful Ni-catalyzed C–N cross-couplings.

Herein the results of such a study are reported, involving air-stable DalPhos pre-catalysts **C1**–**C6** (derived from **L1**–**L6**), as well as the commercial pre-catalyst **C7** featuring **DPPF** (**L7**), which has proven useful in Ni-catalyzed C–N cross-couplings.[31, 36, 37] Our catalytic survey probes

the impact of varying important experimental parameters, spanning (Figure 2.1B): sterically and electronically varied (hetero)aryl chloride electrophiles with a focus on heteroatom-dense substrates (**1**–**4**); structurally diverse primary and secondary amines (**a**–**c**) and the aminopyrazole (**d**), as representative nucleophile motifs found in pharmaceuticals and agrochemicals (examples in Figure 2.1C); commonly employed strong and weak inorganic bases (i.e., NaO*t*Bu and K_2CO_3) as well as organic amine bases (DBU) paired with a chloride scavenger (NaTFA); and solvents (toluene and 1,4-dioxane). Key outcomes of this comparative catalyst screening campaign include identification of useful ligands for the targeted Ni-catalyzed C–N cross-couplings, recognition of the ligand-dependent competitive role of C–O coupling when using MO*t*Bu base, and development of the first efficient catalyst system for the *N*-arylation of aminopyrazoles and related nucleophiles with (hetero)aryl chlorides employing an organic amine dual-base system.

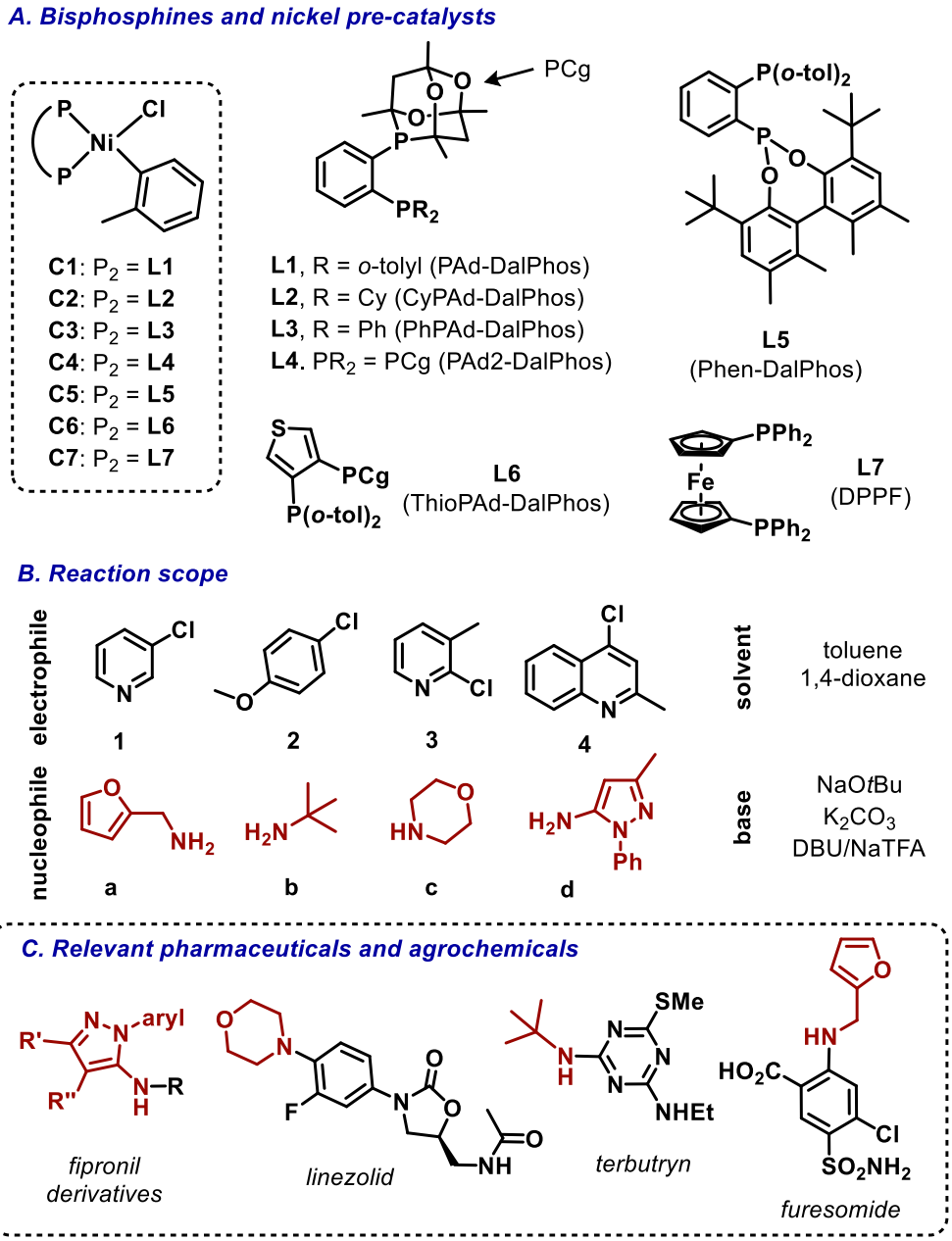

Figure 2.1 **A.** Catalyst survey. **B.** Reaction scope of the Ni-catalyzed C–N cross-coupling reactivity survey featured in this comparative screening campaign. **C.** Chemical structures of pharmaceuticals and agrochemicals with relevant moieties.

2.3 Results and Discussion

Our main catalytic survey involved carrying out 672 individual experiments, as represented in Figure 2.2. Notwithstanding the tremendous utility of high-throughput experimentation[57, 58, 59]

or 'pool-and-split/deconvolution'[60, 61] approaches in terms of identifying promising 'leads' for reaction development at very low scales, we opted to carry out our experiments manually at scales where issues with set-up and reaction progress could be observed and corrected, thereby reducing the potential for false negative results, and enabling fair ligand comparisons across the conditions employed. To intentionally apply somewhat mild and therefore challenging reaction conditions, and to discourage background reactivity, 3 mol% pre-catalyst was used in reactions conducted at 60 °C over the course of 18 h (unoptimized). Only when employing NaO*t*Bu under these conditions did we detect variable amounts of target product formation in the case of **3d** (5–15%) and **4d** (5–20%) in the absence of catalyst (92 additional control experiments). With the exception of selected entries where competing C–O cross-coupling was identified (see below), clean conversion of starting material to product was observed on the basis of GC data, with negligible (<5%) competing side-products detected. Given that the choice of base in such cross-couplings has a profound impact on the reaction outcome, in part because it is employed in greater than stoichiometric quantities relative to the cross-coupling reactants, we partition our analysis of the catalytic survey results in Figure 2.2 by consideration of the base employed.

			NaO*t*Bu				K_2CO_3				DBU/NaTFA			
			a	**b**	**c**	**d**	**a**	**b**	**c**	**d**	**a**	**b**	**c**	**d**
C1	toluene	**1**	78	<5	<5	59	<5	<5	<5	14	19	<5	<5	31
		2	64	11	6	83	<5	<5	<5	<5	<5	<5	<5	16
		3	>95	<5, †	<5, †	21	9	<5	<5	36	>95	<5	11	65
		4	88	5	12	6	6	<5	<5	26	>95	<5	<5	69
	1,4-dioxane	**1**	35	<5	7	29	<5	<5	<5	22	5	<5	<5	15
		2	53	<5	<5	62	<5	<5	<5	<5	<5	<5	<5	<5
		3	81	<5, †	10, †	55	6	<5	<5	17	61	<5	12	39
		4	>95	<5	9	48	75	<5	<5	<5	>95	<5	<5	60
C2	toluene	**1**	>95	13	11	>95	<5	<5	<5	<5	<5	<5	<5	5
		2	83	<5	13	8	<5	<5	<5	<5	<5	<5	<5	<5
		3	>95	<5, †	<5, †	>95	12	<5	<5	90	21	<5	7	86
		4	>95	12	10	25	<5	<5	<5	62	8	<5	<5	44
	1,4-dioxane	**1**	>95	<5	<5	>95	<5	<5	<5	<5	<5	<5	<5	<5
		2	88	<5	<5	8	<5	<5	<5	<5	<5	<5	<5	<5
		3	>95	<5, †	<5, †	>95	<5	<5	<5	76	12	<5	<5	50
		4	>95	<5	7	37	8	<5	<5	43	7	<5	<5	39
C3	toluene	**1**	>95	<5	15	69	<5	<5	<5	<5	<5	<5	<5	<5
		2	65	<5	18	16	<5	<5	<5	<5	<5	<5	<5	<5
		3	>95	<5, †	24, †	47	<5	<5	<5	51	38	<5	<5	>95
		4	>95	20	25	93	>95	<5	<5	5	38	<5	<5	>95
	1,4-dioxane	**1**	>95	33	11	>95	<5	<5	<5	5	<5	<5	<5	<5
		2	81	9	54	12	<5	<5	<5	<5	<5	<5	<5	<5
		3	>95	<5, †	26	88	19	<5	<5	35	29	<5	<5	48
		4	>95	<5	13	>95	82	<5	<5	61	59	<5	<5	>95
C4	toluene	**1**	76	8	<5	70	10	<5	<5	45	21	<5	<5	60
		2	75	17	18	>95	<5	<5	<5	<5	<5	<5	<5	28
		3	>95	<5, †	<5, †	>95	15	<5	<5	46	>95	<5	<5	88
		4	>95	5	11	59	63	<5	<5	61	>95	<5	<5	>95
	1,4-dioxane	**1**	57	<5	7	>95	11	<5	<5	31	5	<5	<5	37
		2	85	<5	<5	>95	<5	<5	<5	<5	<5	<5	<5	<5
		3	>95	<5, †	<5, †	>95	13	<5	<5	8	92	<5	<5	55
		4	>95	<5	<5	41	70	<5	<5	49	>95	<5	<5	>95
C5	toluene	**1**	77	<5	13	43	<5	<5	<5	<5	<5	<5	<5	<5
		2	20	9	13	24	<5	<5	<5	7	<5	<5	<5	20
		3	>95	<5	26	42	<5	<5	<5	6	>95	<5	<5	>95
		4	>95	7	42	26	16	<5	<5	11	37	<5	<5	72
	1,4-dioxane	**1**	26	<5	<5	>95	<5	<5	<5	<5	<5	<5	<5	<5
		2	29	<5	<5	58	<5	<5	<5	<5	<5	<5	<5	<5
		3	>95	<5, †	<5, †	85	<5	<5	<5	<5	5	<5	<5	65
		4	>95	<5	8	90	26	<5	<5	28	13	<5	<5	15
C6	toluene	**1**	>95	<5	8	72	<5	<5	<5	15	<5	<5	<5	<5
		2	75	11	10	>95	<5	<5	<5	19	<5	<5	<5	<5
		3	>95	<5, †	<5, †	6	<5	<5	<5	<5	52	<5	<5	23
		4	>95	9	17	40	17	<5	<5	>95	57	<5	<5	17
	1,4-dioxane	**1**	58	<5	<5	94	<5	<5	<5	30	<5	<5	<5	<5
		2	75	<5	<5	>95	<5	<5	<5	15	<5	<5	<5	<5
		3	>95	<5, †	<5, †	33	<5	<5	<5	14	35	<5	<5	24
		4	>95	<5	7	73	86	<5	<5	>95	82	<5	<5	22
C7	toluene	**1**	18	<5	22	<5	<5	<5	<5	<5	<5	<5	<5	<5
		2	<5	<5	9	<5	<5	<5	<5	<5	<5	<5	<5	<5
		3	18	<5	14	<5	<5	<5	<5	<5	<5	<5	<5	<5
		4	>95	13	91	>95	<5	<5	<5	<5	<5	<5	<5	<5
	1,4-dioxane	**1**	15	<5	27	<5	<5	<5	<5	<5	<5	<5	<5	<5
		2	<5	<5	15	<5	<5	<5	<5	<5	<5	<5	<5	<5
		3	18	<5	5	9	<5	<5	<5	<5	<5	<5	<5	<5
		4	>95	12	>95	>95	<5	<5	<5	<5	<5	<5	<5	<5

Figure 2.2 (caption on following page)

Figure 2.2 Comparative catalytic screening of the Ni-catalyzed C–N cross-coupling of (hetero)aryl chlorides with NH substrates. Unless otherwise indicated, reactions were conducted on 0.12 mmol scale in (hetero)aryl chloride ([0.12] M; 1.1 equiv. amine; 2.0 equiv. base), using 3 mol% pre-catalyst (**C1**–**C7**) at 60 °C over 18 h. The reported yields were determined on the basis of response-factor calibrated GC data using authentic material. Only in the case of **3d** and **4d** when using NaO*t*Bu did we observe variable amounts (5–20%) of product formed in the absence of catalyst; otherwise negligible conversion (<5%) to product observed in the absence of catalyst. The symbol † denotes the presence of products arising from competing C–O cross-coupling involving the *tert*-butoxide base. See Figures S1 and S2 in Appendix A for addition details.

In commencing our studies focusing on the use of NaO*t*Bu as a base, the Ni-catalyzed C–N cross-coupling of furfurylamine (**a**) with 3-chloropyridine (**1**), 4-chloroanisole (**2**), 2-chloro-3-methylpyridine (**3**), or 4-chloroquinaldine (**4**) leading to **1a**, **2a**, **3a**, or **4a**, respectively, was selected as a means of pairing structurally varied (hetero)aryl electrophiles featuring ortho-, meta-, and/or para-substitution with a sterically unhindered heteroaryl-containing primary alkylamine nucleophile for which such cross-couplings are well-established when using NaO*t*Bu.[33,42,62,63,43,37] Under these conditions, several of the DalPhos-derived pre-catalysts **C1**–**C6** provided high levels of conversion to one or more of the target products **1a**–**4a** independent of solvent choice; by comparison, the **DPPF**-containing pre-catalyst **C7** proved inferior. Encouraged by these results, the ability of **C2** or **C4** to promote such reactions at 25 °C was subsequently examined (Appendix A Table S1). In the case of **C2**, >95% conversion to **1a**, **3a**, and **4a** was achieved in each case, even when using only 1 mol% **C2**. Furthermore, in monitoring the formation of **3a** under these conditions (1 mol% **C2**, 25 °C), >95% conversion was noted after 0.5 h (TOF >200 h^{-1}), thus underscoring the high activity of this catalyst system. Related cross-couplings employing the electron-rich (electronically deactivated) 4-chloroanisole proved more challenging, with conversions to **2a** of 51% (toluene) and 66% (1,4-dioxane) being achieved (3 mol% **C2**, 25 °C). While in the case of **C4**, reactions conducted at 25 °C (3 mol% **C4**) resulted in a drop in conversion (typically ~15–20%) for the formation of **1a** and **2a** versus the 60 °C experiments, >95% conversion was still achieved in the case of **3a** and **4a** (Appendix A Table S1).

We subsequently turned our attention to analogous cross-couplings of the hindered primary alkylamine, *tert*-butylamine (**b**), targeting the formation of **1b**–**4b** using NaO*t*Bu (Figure 2.2). While such transformations of α,α,α-trisubstituted primary alkylamine nucleophiles have attracted interest as a means of introducing aliphatic groups that enhance the lipophilicity and other physical properties of aniline derivatives,[64, 65] they remain a persistent challenge in metal-catalyzed C–N cross-coupling. Previous work from our group established **C3** (5 mol% Ni, 25 °C, 18 h, toluene) as being effective in C–N cross-couplings of *t*BuNH$_2$ when using NaO*t*Bu in combination with activated (hetero)aryl chlorides.[40] Our current reactivity survey (3 mol% Ni, 60 °C; Figure 2.2) confirmed the difficulty of such reactions: only in selected cases employing **C3** did we observe even modest (33% maximum) conversion to the target C–N cross-coupling product. Furthermore, scrutiny of the product mixtures in the attempted formation of **3b** (and **3c**, see below) revealed an unusual and distinct selectivity for otherwise challenging C–O cross-coupling[66] arising from NaO*t*Bu (affording **3b'**, Figure 2.3) in the case of **C1**–**C5**. Particularly striking is the >95% conversion to **3b'** that is achieved with **C4** in toluene, when considered alongside the observation that no conversion of **3** is observed nor any detectable **3b'** in analogous reactions where **b** is omitted. While we are uncertain as to the precise origins of these reactivity trends, it is plausible that in this reaction involving **C4** leading to **3b'** nucleophile **b** may serve as a co-base. Consistent with the absence of **3b'** formed when using **C7**, even at higher loadings and temperatures (10 mol% Ni, 120 °C, Figure 2.3), control experiments confirmed that **3b'** is not formed under such conditions in the absence of nickel pre-catalyst.

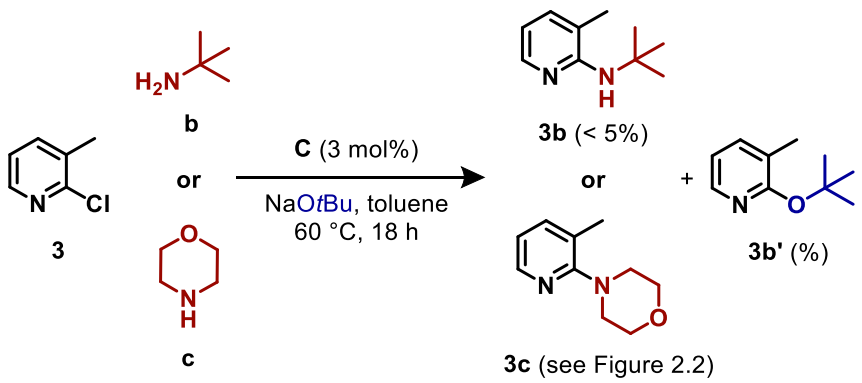

	3b' (%) from reactions of **b**	*3b'* (%) from reactions of **c**
C1	63, 53[a]	38, 56[a]
C2	14, 35[a]	18, 46[a]
C3	13, 79[a]	21, 37[a]
C4	> 95, > 95[a]	> 95, 94[a]
C5	< 5	< 5
C6	19	11
C7	< 5, < 5[b]	< 5, < 5[b,c]

Figure 2.3 Competitive C–N and C–O cross-coupling of **3** with *tert*-butylamine (**b**) or morpholine (**c**). Unless stated, reactions were conducted as in Figure 2.2, with yields of **3b'** reported in toluene (yields in 1,4-dioxane were significantly reduced, see Table S5); in all cases <5% **3b** formed and yields of **3c** are given in Figure 2.2. [a]Reaction conducted using 5 mol% Ni at 110 °C. [b]Reaction conducted using 10 mol% of **C7** at 120 °C (with 5.0 equiv. *tert*-butylamine in reactions of **b**). [c]66% conversion to **3c**.

In exploring more forcing conditions to promote the formation of **1b**, each of **C3** and **C7** provided >95% conversion to product using 5 mol% Ni at 110 °C in toluene (Appendix A Table S2); **C3** also afforded useful levels of conversion to **1b** in toluene (85%) or 1,4-dioxane (68%) when using 10 mol% Ni at 60 °C (Appendix A Table S3). For the formation of **2b** arising from cross-coupling of the deactivated electrophile **2**, pre-catalyst **C3** proved to be uniquely capable amongst the catalyst systems featured in our survey (90%, 10 mol% Ni, 120 °C; Appendix A Table S2).

Under the challenging conditions of our comparative catalytic screening leading to **4b** (Figure 2.2), we were somewhat encouraged that each of **C1**–**C7** displayed some conversion to

product (20% maximum, with **C3**), in the absence of detectable C–O coupling leading to **4b'**. On this basis, we explored further the combined influence of increased loading (10 mol% Ni), temperature, and equivalents of *tert*-butylamine (**b**) and NaO*t*Bu relative to the electrophile (**4**, 1.0 equiv.), in enabling the formation of **4b** when using **C3** (Appendix A Table S4). In using a larger proportion of **b** (**b**: NaO*t*Bu of 3.0 : 1.5, versus 1.1 : 2.0 as in Figure 2.3), 65% conversion to **4b** was achieved at 25 °C in the absence of **4b'**. However, at elevated temperature, competitive formation of the NaO*t*Bu-derived C–O cross-coupling product **4b'** emerged (e. g., 80 °C: 39% **4b**, 32% **4b'**; Appendix A Table S4). With **C3**, efforts to drive the formation of **4b** by using **b**: NaO*t*Bu of 5.0 : 2.0 at 120 °C were selective but with modest conversion (28% **4b**, <5% **4b'**). Although we were unable to achieve complete selectivity for the C–O product, **4b'** could be isolated from **4b** using column chromatography. However, the negligible formation of **3b'** that was noted when using **C7** even under forcing conditions (Figure 2.3) prompted us to try this pre-catalyst under analogous conditions, leading to the selective formation of **4b** in 85% yield (Appendix A Table S4). These results (Figures 2.2 and 2.3, Appendix A Tables S2–S4) reaffirm the general superiority of **C3** amongst the pre-catalysts examined herein for Ni-catalyzed C–N cross-couplings of *tert*-butylamine using NaO*t*Bu. However, the interplay of each of the key experimental parameters (e. g., ligand and electrophile structure, temperature, reagent stoichiometry, other) contributes to the outcome of the reaction, including C–N versus C–O selectivity, with **C7** showing promise for C–N selectivity. As described later herein, our efforts to circumvent the use of NaO*t*Bu as a means of avoiding competitive C–O coupling with **b** have thus far not been successful, with other bases proving ineffective (see below).

Inspired by the ubiquitous nature of the *N*-aryl morpholine motif in biologically active compounds (e. g., linezolid; Figure 2.1C), morpholine (**c**) was chosen as a secondary dialkylamine

test substrate in cross-couplings with **1**–**4** using NaO*t*Bu to give **1c**–**4c** (Figure 2.2). Under the rather challenging screening conditions (3 mol% Ni, 60 °C), **C3** and **C7** emerged as promising candidates for such transformations; notably, >90% conversion to **4c** was achieved by use of **C7**. In the case of reactions leading to **1c**, more forcing conditions (5 mol% Ni, 110 °C, toluene) provided significantly higher conversion to product for **C3** (83%), but not for **C2** (7%), **C4** (6%), or **C7** (25%). In keeping with reactions of *tert*-butylamine (**b**) with 2-chloro-3-methylpyridine (**3**) using NaO*t*Bu in which the C–O coupling product **3b'** was generated, in most reactions targeting **3c** competing and in some cases exclusive C–O cross-coupling leading to **3b'** was found for **C1**–**C6**, but not **C7** (Figures 2.2 and 2.3, Appendix A Table S5). In fact, the general reactivity trends regarding the formation of **3b'** in these reactions of **3** with **b** or **c** appear to be independent of the nucleophile employed, with some noteworthy observations including: i) toluene is typically beneficial for overall conversion of **3** versus 1,4-dioxane; ii) **C4** offers high and selective conversion to the C–O cross-coupling product **3b'**; and iii) under the conditions surveyed, **C7** exhibits negligible propensity for C–O cross-coupling of NaO*t*Bu, while offering useful conversion to C–N cross-couplings products in the case of morpholine (**c**).

To complete our comparative catalytic examination involving the use of NaO*t*Bu as a base, we turned our attention to cross-couplings of the aminopyrazole (**d**) as a representative primary five-membered heteroarylamine (Figures 2.1 and 2.2). While *N*-arylated variants of **d** and related aminopyrazoles are of interest in terms of their biological[67-70] and photophysical[71, 72] properties, such primary five-membered heteroarylamines have proven to be challenging reaction partners in comparison to alkylamines or anilines in metal-catalyzed C–N cross-coupling chemistry. Our 2019 report on Ni-catalyzed C–N cross-couplings of heteroarylamines included the first base-metal transformations involving an aminopyrazole with (hetero)aryl chlorides (three entries involving 5-

amino-1,3-dimethylpyrazole), enabled by use of **C4** (5 mol% Ni, 80 °C, 16 h, 2-MeTHF) in combination with NaOPh.[62] While this 2-MeTHF/ NaOPh combination (inspired by a report from Buchwald and co-workers[73] regarding Pd-catalyzed C–N cross-couplings of aminooxazole/thiazoles) proved effective in our study,[62] we did with some electrophiles note the formation of base-derived C–O products in the absence of nickel catalyst, thus prompting us to explore herein alternative bases for such transformations. Under the conditions outlined in Figure 2.2 using NaO*t*Bu, we did not observe the formation of unwanted C–O cross-coupling products in the presence or absence of nickel catalyst. However, in the absence of nickel catalyst we did confirm that NaO*t*Bu enables the formation of **3d** (12%, toluene; <5%, 1,4-dioxane) and **4d** (21%, toluene; 6%, 1,4-dioxane) under these conditions.

The data collected in Figure 2.2 for Ni-catalyzed C–N cross-couplings of **d** with **1**–**4** employing NaO*t*Bu reveal that each of **C1**–**C7** demonstrate competence for one or more of the targeted transformations under the conditions employed. While some exceptions exist (e. g., the formation of **1d** or **2d** by use of **C5** in 1,4-dioxane, Figure 2.2), >50% conversion to **1a**–**4a** proved to be a necessary but not sufficient predictor for success with the electrophile in question leading to **1d**–**4d**, with 1,4-dioxane generally leading to superior performance over toluene. Beyond this, some notable trends in electrophile compatibility were observed: i) **C4** and **C5** were the only pre-catalysts that displayed >50% conversion of all four electrophiles (**C3** hit for **3** of **4**); ii) **C2** afforded >95% to the pyridine derivatives **1d** and **3d**, yet performed poorly in the formation of **2d** and **4d**; iii) **C6** generally out-performed the phenylene analogue **C1**, and emerged as being particularly well-suited for the formation of **2d** arising from the electron-rich 4-chloroanisole **2** (>95%); and iv) **C7** offered negligible conversion to **1d**–**3d**, yet enabled >95% conversion to the 4-chloroquinaldine-derived **4d**.

Encouraged by our successful cross-coupling of the aminopyrazole (**d**) with NaO*t*Bu when using several pre-catalysts under investigation herein (Figure 2.2), we carried out selected competition experiments under conditions in Figure 2.2 to learn more about the selectivity preferences, and possible substrate inhibition phenomena, exhibited in these reactions (Appendix A Tables S6–S8). The poor performance of **C2** in the cross-coupling of **2** leading to **2d** (8%) does not appear to arise from inhibition by **2**, given that high conversion to **1d** was retained in cross-couplings involving mixtures of **1** and **2** (1.0 equiv. each, Appendix A Table S6). Analogous competitions employing **1** and **3** (1.0 equiv. each, Appendix A Table S7) established that while **C2** is capable of individually catalyzing the formation of **1d** and **3d** in high yield (>95%, Figure 2.2), in competition 3-chloropyridine (**1**) was the preferred electrophile (**1d**:**3d** = 3.3:1). A nucleophile competition employing 4-chloroquinaldine (**4**, 1.0 equiv.) with morpholine (**c**, 1.1 equiv.) and the aminopyrazole (**d**, 1.1 equiv.), for which **C7** enables high conversion to both of the target products **4c** and **4d** (Figure 2.2), revealed the aminopyrazole to be the preferred NH coupling partner in this system (**4c**:**4d** = 1:12.5; Appendix A Table S8). Strong preference for the formation of the aminopyrazole-derived **2d** over the furfurylamine-derived **2a** (**2a**:**2d** = 1:>25; Appendix A Table S9) was also noted in analogous nucleophile competitions involving the generally challenging electrophile 4-chloroanisole (**2**, 1.0 equiv.) with either **C3** or **C4**. These nucleophile competitions highlight the suitability of the aminopyrazole motif in Ni-catalyzed C–N cross-couplings under the conditions outlined in Figure 2.2 involving NaO*t*Bu.

Overall, our comparative catalytic examination of **C1**–**C7** in Ni-catalyzed C–N cross-couplings using NaO*t*Bu as a base enabled the identification of catalysts that are competent for 15 of the 16 targeted transformations (**3b** was unsuccessful), in some cases operating under more mild conditions (e.g., reactions of **a**) and in other cases requiring more forcing conditions (e.g., reactions

of **b**) than those employed in the broad screen presented in Figure 2.2. However, considering the complications associated with using NaO*t*Bu as a base, including competitive C–O cross-coupling, we turned our attention to the use of a weaker inorganic base that might circumvent such reactivity issues and ultimately provide broader reaction scope, especially with base-sensitive and/or heteroatom-dense substrates. Efforts to use K_2CO_3 in place of NaO*t*Bu were largely unsuccessful (Figure 2.2); only in the formation of **3d** (**C2**), **4a** (**C1**, **C3**, **C4**, and **C6**), and **4d** (**C6**) was ≥70% conversion to the target product observed. Given that such bases can suffer from poor solubility and inconsistent reactivity profiles arising from particle size variation,[74] we did not pursue further optimization. Rather, we opted to conduct an alternative screening campaign using the inexpensive and soluble organic amine base DBU, paired with the presumptive chloride scavenger NaTFA (so-called 'dual-base' system[49]). While we have successfully applied this approach in Ni-catalyzed C–N cross-couplings of fluoroalkylamines and amides,[54, 55, 63] as well as in challenging α-arylation chemistry,[56] the application of dual-base systems remains unexplored in the context of Ni-catalyzed C–N cross-couplings involving nucleophiles **a**–**d** with (hetero)aryl chlorides. As with K_2CO_3, the catalytic performance achieved when using DBU/NaTFA was found to be inferior to that observed with NaO*t*Bu (Figure 2.2), with ≥70% conversion to the target complex being limited to following cases: **3a** (**C1**, **C4**, and **C5**), **3d** (**C2**–**C5**), **4a** (**C1**, **C4**, and **C6**), and **4d** (**C3**–**C5**). However, on closer inspection we were encouraged by the fact that under these somewhat challenging screening conditions (3 mol% Ni, 60 °C) **C4** with DBU/NaTFA enabled appreciable conversions of the aminopyrazole (**d**) to each of **1d**–**4d** in a manner that was not demonstrated in our survey by any other pre-catalyst/nucleophile combination using either K_2CO_3 or DBU/NaTFA. Given current interest in the development of metal-catalyzed C–N cross-couplings that make use of soluble organic amine bases such as DBU,[47] especially in the construction of heteroatom-dense

molecules of biological relevance,[14,75] we sought to improve the catalytic performance of the **C4**/DBU/NaTFA system in transformations leading to **1d**–**4d**. By applying only modestly higher loading and temperature (5 mol% Ni, 80 °C), >90% conversion to each of **1d**, **3d**, and **4d** was achieved (Appendix A Table S10); cross-couplings of 4-chloroanisole (**2**) remained difficult under these conditions (<30% **2d**).

In exploring the scope of reactivity under these conditions (Figure 2.4), a range of nucleophiles based on the aminopyrazole motif proved to be suitable cross-coupling substrates, including substituted/isomeric variants of the test nucleophile **d** leading **5a**–**5d**, as well as the nitrogen-rich 1-methyl-1*H*-pyrazolo[3,4-b]pyridin-3-yl product **5e**. Chemoselective *N*-arylation of the amino group in parent 3-aminopyrazole, leading to **5f** and **5g**, was also achieved, despite the presence of a potentially contending pyrazole NH unit. Bridging the amino and pyrazolyl fragments by an *ortho*-phenylene unit, as in 2-(1*H*-pyrazol-1-yl)aniline, was also well-tolerated leading **5h**–**5j**. Throughout the course of these transformations, electrophiles featuring pyridine, quinaldine, and quinoxaline core structures, and/or various ortho-, meta-, and para-substituents proved to be compatible. Finally, the practical, user-friendly nature of the protocol was demonstrated via the successful benchtop preparation of **5b**. In such cases, a vial was loaded with the reaction components in-air, the contents of the reaction vial were then sparged with nitrogen, and the headspace purged with nitrogen for 30 s prior to sealing. Full conversion of the aryl chloride was observed under the conditions outlined in Figure 2.4, with a triplicate average isolated yield of 80% following purification by column chromatography.

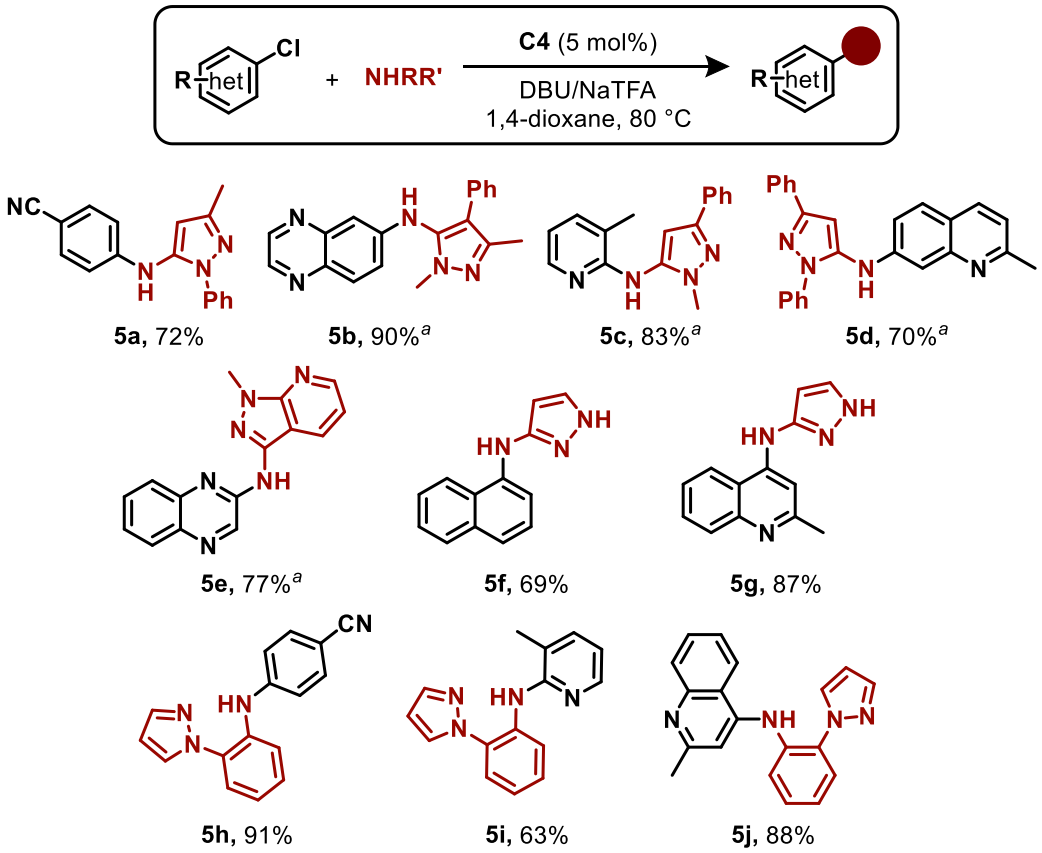

Figure 2.4 Scope of Ni-catalyzed C–N cross-couplings of pyrazole-containing nucleophiles, with isolated yields reported. Unless otherwise indicated, reactions were conducted at 80 °C over 18 h (unoptimized) on 0.48 mmol scale in (hetero)aryl chloride ([0.12] M in 1,4-dioxane), with pyrazole nucleophile (1.1 equiv.), DBU (2.0 equiv.), and NaTFA (2.0 equiv.). [a]Reactions conducted in toluene.

Furthermore, a 'pool-and-split/deconvolution'[60, 61] approach was taken examining the Ni-catalyzed C–N cross-coupling of **4** with furfurylamine (**a**) by combining **C1**–**C3**, and **C7** in a 'pool' under the conditions outlined in Figure 2.2. The pool generated substantial 'hits' (>95%) with NaO*t*Bu and the 'dual-base' system DBU/NaTFA prompting these reactions to be 'split/deconvoluted' for identification of the effective pre-catalyst(s). However, the yield generated using K_2CO_3 was appreciably diminished (27% in toluene and 16% in 1,4-dioxane) relative to the 'split' conditions in which yields greater than 75% were obtained using **C1** and **C3** (Appendix A Table S11), potentially due to inhibitory interactions between pre-catalysts.

2.4 Summary

Our systematic catalytic survey of pre-catalysts featuring the DalPhos ligands **L1**–**L6**, along with **DPPF** (**L7**), in the context of the Ni-catalyzed C–N cross-coupling of some representative nucleophilic NH substrates with (hetero)aryl chlorides revealed that a complex interplay of experimental parameters influences the outcome of such reactions. Nonetheless, some important reactivity trends emerged from our investigation:

1. The overall trend in catalytic performance as a function of base was found to be NaO*t*Bu ⋙DBU/NaTFA>K_2CO_3, with the last of these being generally ineffective under the conditions examined. The influence of solvent was more nuanced, with 1,4-dioxane being comparable to toluene, and in some case preferred. While electrophile compatibility varied with pre-catalyst and nucleophile, 4-chloroanisole (**2**) in general proved to be the most challenging. The somewhat differing catalytic performance of **C1** and **C6** underscores the potential influence of ancillary backbone modification.
2. Cross-couplings of furfurylamine (**a**) using NaO*t*Bu proved to be straightforward, with each of pre-catalysts **C2**, **C3**, **C4**, and **C6** displaying particularly useful catalytic performance. Subsequent testing showed **C2** to function well in such reactions conducted using only 1 mol% Ni at 25 °C.
3. Attempted cross-couplings of *tert*-butylamine (**b**) using NaO*t*Bu under the conditions in Figure 2.2 afforded generally poor results, including previously unobserved competitive C–O cross-coupling involving the base that was found to be the dominant reaction in some cases involving **C4** (Figure 2.3); the generality of this latter observation warrants further investigation. Although **C3** showed promise for C–N bond formation involving this bulky amine, the lack of competitive C–O bond formation observed using **C7** at higher

temperature and loading suggests its use may be advantageous when C–N selectivity is required. Similar reactivity trends were noted in reactions of morpholine (**c**), with **C3** and **C7** proving particularly effective.

4. Each of **C1**–**C7** demonstrated competence in cross-couplings of aminopyrazole (**d**) using NaO*t*Bu under the conditions in Figure 2.2, with **C3**–**C5** proving to be the most useful in general. Competitions involving furfurylamine (a) versus d (with **C3** or **C4**), as well as morpholine (**c**) versus **d** (with **C2** or **C7**), established a marked preference for **d**, despite the competence of the competing nucleophiles **a** and **c** in each case.
5. The DBU/NaTFA dual-base system proved effective with several pre-catalysts in C–N cross-couplings of furfurylamine (**a**) or aminopyrazole (**d**). Encouraged by these observations, the first efficient catalyst system for C–N cross-couplings of aminopyrazoles and related nucleophiles with (hetero)aryl chlorides using a dual-base system was developed (5 mol% **C4**, 80 °C), enabling a range of substrate pairings leading to nitrogen-dense products (Figure 2.4), including examples conducted on the benchtop without the use of an inert atmosphere glovebox. The broader application of this catalyst system in cross-couplings of primary five-membered heteroarylamine nucleophiles is under investigation currently in our laboratory.

Collectively, the results presented herein underscore the complementary nature of ligands **L1**–**L7** (Figure 2.1) in otherwise challenging Ni-catalyzed C–N cross-couplings of (hetero)aryl chlorides, with **L2** (**CyPAd-DalPhos**), **L3** (**PhPAd-DalPhos**), and **L4** (**PAd2-DalPhos**), along with **L7** (**DPPF**), comprising a core 'go-to' set of commercial ligands for such transformations. Herein we have shown these to enable such C–N cross-couplings in some cases under mild conditions and/or employing soluble organic amine base, in transformations leading to sought-

after heteroatom-dense products. We will report in due course on our efforts to gain a mechanistic understanding of the divergent ligand-enabled reactivity exhibited by the catalysts under investigation herein, to support the further development of high-performing catalysts for these and other transformations.

2.5 Experimental

2.5.1 General Considerations

Unless otherwise indicated, all experimental procedures were conducted in a nitrogen-filled, inert-atmosphere glovebox using oven-dried glassware and purified solvents, with workup procedures carried out on the benchtop in air using unpurified solvents. Toluene and 1,4-dioxane when used in the glovebox were deoxygenated by purging with nitrogen followed by storage over activated 4 Å molecular sieves for 24 h. K_2CO_3 was dried under vacuum at 180 °C for 24 h and stored under nitrogen in the glovebox prior to use. (**PAd-DalPhos**)Ni(*o*-tol)Cl, (**CyPAd-DalPhos**)Ni(*o*-tol)Cl, (**PhPAd-DalPhos**)Ni(*o*-tol)Cl, (**PAd2-DalPhos**)Ni(*o*-tol)Cl, (**Phen-DalPhos**)Ni(*o*-tol)Cl, (**ThioPAd-DalPhos**)Ni(*o*-tol)Cl, and (**DPPF**)Ni(*o*-tol)Cl were prepared according to literature procedures (**C1**–**C7**),[31, 33, 40, 41, 44, 62, 63] as were **2a**,[63] **2c**,[31] **4a**,[31] and **4c**.[31] All other commercial solvents, reagents, and materials were used as received. GC data were obtained on an instrument equipped with an SGE BP-5 column (30 m, 0.25 mm i.d.). Automated flash chromatography was carried out on a Biotage Isolera One automated flash purification system using 10 g Biotage SNAP KP-SIL (particle size 30−90 μm) or 12 g Silicycle SiliaSep (particle size 40−63 μm, 230−400 mesh) silica flash cartridges with a typical gradient of 6−12−6 column volumes and a flow rate of 10 mL/min, unless otherwise indicated. Manual flash chromatography was carried out on silica gel using Silicycle SiliaFlash 60 silica (particle size 40−63 μm, 230−400

mesh), or alumina (activated, neutral Brockmann I) where indicated. All ^{1}H NMR (500.1 MHz) and ^{13}C{^{1}H} NMR (125.8 MHz) spectra were recorded on a Bruker AV 500 MHz spectrometer at 300 K and were referenced to residual protio solvent peaks (^{1}H) or deuterated solvent peaks (^{13}C{^{1}H}). Splitting patterns are indicated as follows: br, broad; s, singlet; d, doublet; t, triplet; q, quartet; m, multiplet. All coupling constants (*J*) are reported in Hertz (Hz). Mass spectra were obtained using ion trap electrospray ionization (ESI) instruments operating in positive or negative mode, as indicated.

2.5.2 General Procedures

Screening Procedure for the Cross-Coupling of (Hetero)aryl Chlorides and Amines (GSP). In a nitrogen-filled glovebox, a glass screw-capped 1-dram vial was charged with base (0.24 mmol, 2.0 equiv.), (hetero)aryl chloride (0.12 mmol, 1.0 equiv.), amine (0.13 mmol, 1.1 equiv.), pre-catalyst (3.6 μmol, 3 mol%, delivered from a stock solution in toluene or 1,4-dioxane, 0.12 M (hetero)aryl chloride), and a magnetic stir bar. The vial was sealed with a cap containing a PTFE septum, removed from the glovebox, the joint was taped, and the vial placed in a temperature-controlled aluminum heating block set to the indicated temperature (60 °C unless otherwise stated). Magnetic stirring was initiated. The mixture was allowed to stir at this temperature for 18 h (unless otherwise stated), after which time the vial was removed from the heat source and cooled to room temperature. In air the reaction mixture in the vial was diluted with methanol (MeOH, ~0.5 mL) and phenyldodecane or hexadecane (0.12 mmol, 1.0 equiv.) was added as an internal standard. An aliquot of the reaction mixture was filtered through a short celite/silica plug eluting with ethyl acetate (EtOAc, ~1.0 mL) and subjected to GC analysis. The reported yields were determined on the basis of response-factor calibrated GC data using authentic material.

General Competition Procedure (**GCP**). In a nitrogen-filled glovebox, a glass screw-capped 4-dram vial was charged with pre-catalyst (3.6 μmol, 3 mol%), NaO*t*Bu (0.24 mmol, 2.0 equiv.), (hetero)aryl halide(s) (0.12 mmol, 1.0 equiv.), nucleophilic NH coupling partner(s) (0.13 mmol, 1.1 equiv.) and toluene (0.12 M) followed by a magnetic stir bar. The vial was then sealed with a cap containing a PTFE septum, removed from the glovebox, the joint was taped, and the vial placed in a temperature-controlled aluminum heating block set to 60 °C. The mixture was stirred at this temperature for 18 h, after which time the vial was removed from the heat source and cooled to room temperature. In air the reaction mixture was diluted with MeOH (~0.5 mL) and phenyldodecane (0.12 mmol, 1.0 equiv.) was added as an internal standard. An aliquot of the reaction mixture was filtered through a short celite/silica plug eluting with EtOAc (~1.0 mL) and subjected to GC analysis. The reported yields were determined on the basis of response-factor calibrated GC data using authentic material.

General Procedure for the Cross-Coupling of (Hetero)aryl Chlorides and Amines (**GP1**). In a nitrogen-filled glovebox, a glass screw-capped 4-dram vial was charged with base (0.96 mmol, 2.0 equiv.), (hetero)aryl chloride (0.48 mmol, 1.0 equiv.), amine (0.53 mmol, 1.1 equiv.), pre-catalyst (0.014 mmol/3 mol% unless specified and delivered from a stock solution in toluene or 1,4-dioxane, 0.12 M (hetero)aryl chloride), and a magnetic stir bar. The vial was sealed with a cap containing a PTFE septum, the joint was taped, and the vial placed in a temperature-controlled aluminum heating block set to 60 °C, unless otherwise indicated. Magnetic stirring was initiated. The mixture was allowed to stir at this temperature for 18 h. Unless otherwise stated, **GWP** described below was then followed.

General Workup Procedure (**GWP**). Following GP1, the reaction mixture was cooled to room temperature and then diluted with EtOAc (~15 mL). The mixture was washed with brine (3 x 30

mL) and dried over Na_2SO_4 then dried *in vacuo* and subjected to column chromatography as indicated.

2.6 Synthesis and Characterization of Cross-Coupled Products

N-(furan-2-ylmethyl)pyridin-3-amine (1a)

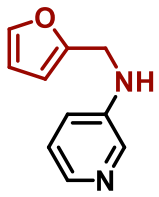

GP1 was followed using NaO*t*Bu (92.3 mg, 0.96 mmol), 3-chloropyridine (45.6 µL, 0.48 mmol), furfurylamine (46.7 µL, 0.53 mmol), **C5** (12.4 mg, 0.0144 mmol), and toluene (2 mL). After automated flash chromatography (90% EtOAc in hexanes), the title compound was obtained (63 mg, 75%) as a brown oil. ^{1}H NMR (500.1 MHz, $CDCl_3$): δ 8.07 (d, J = 2.7 Hz, 1H), 7.96 (dd, J = 4.6, 1.1 Hz, 1H), 7.34 (m, 1H), 7.06 (dd, J = 8.3, 4.7 Hz, 1H), 6.92 (ddd, J = 8.3, 2.8, 1.3 Hz, 1H), 6.30 (dd, J = 3.2, 1.9 Hz, 1H), 6.22 (d, J = 3.0 Hz, 1H), 4.30 (s, 3H). ^{13}C{^{1}H} UDEFT (125.8 MHz, $CDCl_3$): δ 151.97, 143.75, 142.19, 139.13, 136.21, 123.75, 119.04, 110.44, 107.40, 40.94. Spectroscopic data are in agreement with those previously reported.[76] HRMS-ESI Calc'd for $C_{10}H_{11}N_2O$ $[M+H]^+$: 175.0866. Found: 175.0867.

N-(*tert*-butyl)pyridin-3-amine (1b)

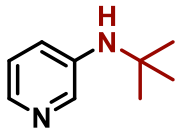

GP1 was followed using NaO*t*Bu (92.3 mg, 0.96 mmol), 3-chloropyridine (45.6 µL, 0.48 mmol), *tert*-butylamine (151 µL, 1.44 mmol), **C3** (32 mg, 0.048 mmol), and toluene (4 mL) at 110 °C. After 18 h the reaction mixture was diluted with EtOAc (20 mL) and filtered over celite, then dried *in vacuo* and subjected to flash chromatography (60% acetone in hexanes) to give the title compound (19 mg, 26%) as a colourless oil. ^{1}H NMR (500.1 MHz, $CDCl_3$): δ 8.10 (s, 1H), 7.98 (s, 1H), 7.06 (d, J = 2.5 Hz, 2H), 3.32 (br s, 1H), 1.35 (s, 9H). ^{13}C{^{1}H} UDEFT (125.8 MHz, $CDCl_3$): δ 143.19, 139.44, 139.18, 123.56, 123.00, 51.75, 29.98. Spectroscopic data are in agreement with those previously reported.[77] HRMS-ESI Calc'd for $C_9H_{15}N_2$ $[M+H]^+$: 151.1230. Found: 151.1230.

4-(pyridin-3-yl)morpholine (1c)

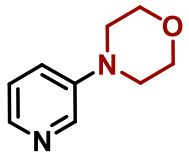

GP1 was followed using NaO*t*Bu (92.3 mg, 0.96 mmol), 3-chloropyridine (45.6 µL, 0.48 mmol), morpholine (46.7 µL, 0.53 mmol), **C3** (16 mg, 0.024 mmol), and toluene (4 mL) at 110 °C. After automated flash chromatography (70–100% EtOAc in hexanes), the title compound was obtained (28.3 mg, 36%) as a yellow oil. ^{1}H NMR (500.1 MHz, $CDCl_3$): δ 8.31 (s, 1H), 8.13 (s, 1H), 7.17 (s, 2H), 3.87 (m, 4H), 3.18 (m, 4H). ^{13}C{^{1}H} UDEFT (125.8 MHz, $CDCl_3$): δ 147.08, 141.20, 138.42, 123.66, 122.24, 66.81, 48.77. Spectroscopic data are in agreement with those previously reported.[78] HRMS-ESI Calc'd for $C_9H_{13}N_2O$ $[M+H]^+$: 165.1022. Found: 165.1022.

***N*-(3-methyl-1-phenyl-1*H*-pyrazol-5-yl)pyridin-3-amine (1d)**

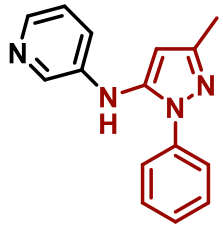

GP1 was followed using NaO*t*Bu (92.3 mg, 0.96 mmol), 3-chloropyridine (45.6 µL, 0.48 mmol), 5-amino-3-methyl-1-phenylpyrazole (92 mg, 0.53 mmol), **C4** (10 mg, 0.0144 mmol), and toluene (4 mL) at 60 °C. After automated flash chromatography (0–80% EtOAc in hexanes), the title compound was obtained (69 mg, 57%) as a pale brown solid. ^{1}H NMR (500.1 MHz, $CDCl_3$): δ 8.19 (d, *J* = 2.7 Hz, 1H), 8.10 (d, *J* = 4.5 Hz, 1H), 7.49 (m, 2H), 7.41 (dd, *J* = 10.7, 4.8 Hz, 2H), 7.31 (dd, *J* = 10.8, 4.0 Hz, 1H), 7.25 (m, 1H), 7.14 (dd, *J* = 8.3, 4.7 Hz, 1H), 5.99 (s, 1H), 5.86 (br, s, 1H), 2.31 (s, 3H). ^{13}C{^{1}H} UDEFT (125.8 MHz, $CDCl_3$): δ 149.55, 141.80, 140.30, 140.01, 138.45, 138.19, 129.51, 127.68, 124.32, 123.97, 121.91, 97.21, 14.24. HRMS-ESI Calc'd for $C_{15}H_{15}N_4$ $[M+H]^+$: 251.1291. Found: 251.1290.

***N*-(*tert*-butyl)-4-methoxyaniline (2b)**

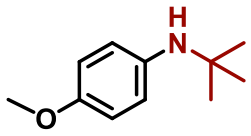

GP1 was followed using NaO*t*Bu (92.3 mg, 0.96 mmol), 4-chloroanisole (58.8 µL, 0.48 mmol), *tert*-butylamine (55.5 µL, 0.53 mmol), **C3** (32 mg, 0.048 mmol), and toluene (4 mL) at 120 °C. After 18 h the reaction mixture was diluted with EtOAc (20 mL) and filtered over celite then dried *in vacuo* and subjected to flash chromatography (40% EtOAc in hexanes). The title compound was obtained (53 mg, 62%) as a pale-yellow oil. ^{1}H NMR (500.1 MHz, $CDCl_3$): δ 6.85 – 6.71 (m, 4H), 3.76 (s, 3H), 2.82 (br s, 1H), 1.23 (s, 9H). ^{13}C{^{1}H} UDEFT (125.8 MHz, $CDCl_3$): δ 154.54, 139.81, 122.98, 114.24, 55.67, 52.46, 30.25. Spectroscopic data are in agreement with those previously reported.[79] HRMS-ESI Calc'd for $C_{11}H_{18}NO$ $[M+H]^+$: 180.1383. Found: 180.1381.

***N*-(4-methoxyphenyl)-3-methyl-1-phenyl-1*H*-pyrazol-5-amine (2d)**

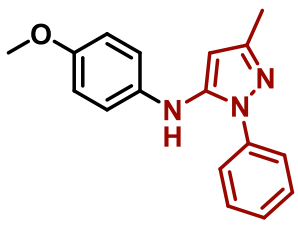

GP1 was followed using NaO*t*Bu (92.3 mg, 0.96 mmol), 4-chloroanisole (58.8 µL, 0.48 mmol), 5-amino-3-methyl-1-phenylpyrazole (92 mg, 0.53 mmol), **C4** (10 mg, 0.0144 mmol), and 1,4-dioxane (4 mL) at 60 °C. After automated flash chromatography (0–50% EtOAc in hexanes), the title compound was obtained (76 mg, 57%) as a pale-yellow solid.^{1}H NMR (500.1 MHz, $CDCl_3$): δ 7.55 (dd, *J* = 8.5, 1.1 Hz, 2H), 7.43 (t, *J* = 7.6, 2H), 7.32 (t, *J* = 7.4 Hz, 1H), 6.93 (m, 2H), 6.83 (m, 2H), 5.81 (s, 1H), 5.44 (s, 1H), 3.77 (s, 3H), 2.28 (s, 3H). ^{13}C{^{1}H} UDEFT (125.8 MHz, $CDCl_3$): δ 154.82, 149.42, 143.51, 138.70, 136.28, 129.49, 127.33, 124.31, 118.86, 114.87, 93.89, 55.71, 14.20. Spectroscopic data are in agreement with those previously reported.[72] HRMS-ESI Calc'd for $C_{17}H_{18}N_3O$ $[M+H]^+$: 280.1444. Found: 280.1441.

***N*-(furan-2-ylmethyl)-3-methylpyridin-2-amine (3a)**

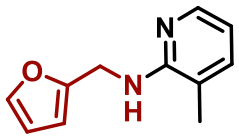

GP1 was followed using NaO*t*Bu (92.3 mg, 0.96 mmol), 2-chloro-3-methylpyridine (52.3 µL, 0.48 mmol), furfurylamine (46.7 µL, 0.53 mmol), **C4** (10 mg, 0.0144 mmol), and toluene (4 mL) at 60 °C. After automated flash chromatography (30% EtOAc in hexanes), the title compound was obtained (49 mg, 54%) as a yellow oil. ^{1}H NMR (500.1 MHz, $CDCl_3$): δ 8.09 – 8.01 (m, 1H), 7.38 (dd, *J* = 1.7, 0.8 Hz, 1H), 7.23 (ddd, *J* = 7.1, 1.7, 0.8 Hz, 1H), 6.56 (dd, *J* = 7.1, 5.1 Hz, 1H), 6.33 (dd, *J* = 3.1, 1.9 Hz, 1H), 6.26 (dd, *J* = 3.1, 0.7 Hz, 1H), 4.69 (d, *J* = 5.2 Hz, 2H), 4.40 (br s, 1H), 2.09 (s, 3H). ^{13}C{^{1}H} UDEFT (125.8 MHz, $CDCl_3$): δ 156.40, 153.36, 145.51, 142.01, 137.06, 116.92, 113.34, 110.49, 107.03, 38.97, 17.05. Spectroscopic data are in agreement with those previously reported.[80] HRMS-ESI Calc'd for $C_{11}H_{13}N_2O$ $[M+H]^+$: 189.1022. Found: 189.1024.

2-(*tert*-butoxy)-3-methylpyridine (3b')

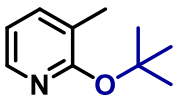

GP1 was followed using NaO*t*Bu (92.3 mg, 0.96 mmol), 2-chloro-3-methylpyridine (52.3 µL, 0.48 mmol), *tert*-butylamine (55.5 µL, 0.53 mmol), **C4** (10 mg, 0.0144 mmol), and toluene (4 mL) at 60 °C. The crude reaction mixture was filtered over celite/silica (1:1) using EtOAc (~20 mL) then dried *in vacuo*. The title compound was obtained (27 mg, 34%) as a pale-yellow oil. ^{1}H NMR (500.1 MHz, $CDCl_3$): δ 7.94 (dd, *J* = 4.9, 1.4 Hz, 1H), 7.33 (dd, *J* = 7.1, 1.9 Hz, 1H), 6.70 (dd, *J* = 7.1, 5.0 Hz, 1H), 2.13 (s, 3H), 1.59 (s, 9H). ^{13}C{^{1}H} UDEFT (125.8 MHz, $CDCl_3$): δ 143.78, 138.21, 116.16, (quaternary carbons could not be identified unequivocally due to low solubility, despite long acquisitions), 28.95, 16.67. HRMS-ESI Calc'd for $C_{10}H_{16}NO$ $[M+H]^+$: 166.1226. Found: 166.1226.

4-(3-methylpyridin-2-yl)morpholine (3c)

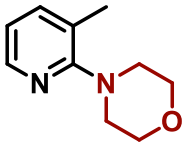

GP1 was followed using NaO*t*Bu (92.3 mg, 0.96 mmol), 2-chloro-3-methylpyridine (52.3 µL, 0.48 mmol), **C7** (36 mg, 0.048 mmol), and toluene (4 mL) at 120 °C. After automated flash chromatography (50–70% EtOAc in hexanes), the title compound was obtained (20 mg, 23%) as an orange oil. ^{1}H NMR (500.1 MHz, $CDCl_3$): δ 8.17 (dd, *J* = 4.7, 1.5 Hz, 1H), 7.41 (dd, *J* = 7.3, 0.9 Hz, 1H), 6.87 (dd, *J* = 7.3, 4.9 Hz, 1H), 3.86 (t, *J* = 5 Hz, 4H), 3.16 (t, *J* = 5 Hz, 4H), 2.29 (s, 3H). ^{13}C{^{1}H} UDEFT (125.8 MHz, $CDCl_3$): δ 161.51, 145.48, 139.59, 124.99, 118.26, 67.35, 50.25, 18.47. Spectroscopic data are in agreement with those previously reported.[81] HRMS-ESI Calc'd for $C_{10}H_{15}N_2O$ $[M+H]^+$: 179.1179. Found: 179.1180.

3-methyl-*N*-(3-methyl-1-phenyl-1*H*-pyrazol-5-yl)pyridin-2-amine (3d)

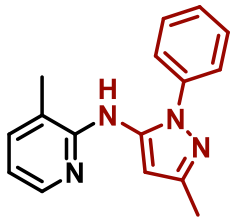

GP1 was followed using NaO*t*Bu (92.3 mg, 0.96 mmol), 2-chloro-3-methylpyridine (52.3 µL, 0.48 mmol), 5-amino-3-methyl-1-phenylpyrazole (92 mg, 0.53 mmol), **C4** (10 mg, 0.0144 mmol), and 1,4-dioxane (4 mL) at 60 °C. After automated flash chromatography (70% EtOAc in hexanes), the title compound was obtained (110.5 mg, 87%) as a pink oil. ^{1}H NMR (500.1 MHz, $CDCl_3$): δ 8.15 (m, 1H), 7.55 (dd, *J* = 8.4, 1.1 Hz, 2H), 7.47 (t, *J* = 7.9 Hz, 2H), 7.34 (m, 2H), 6.74 (dd, *J* = 7.2, 5.0 Hz, 1H), 6.59 (s, 1H), 6.30 (br s, 1H), 2.34 (s, 3H), 2.06 (s, 3H).^{13}C{^{1}H} UDEFT (125.8 MHz, $CDCl_3$): δ 152.28, 149.72, 145.93, 139.23, 138.68, 138.15, 129.69, 127.77, 127.15, 124.69, 123.96, 117.74, 116.06, 96.95, 90.89, 16.94, 14.31. HRMS-ESI Calc'd for $C_{16}H_{16}N_4Na$ $[M+Na]^+$: 287.1267. Found: 287.1268.

***N*-(*tert*-butyl)-2-methylquinolin-4-amine (4b)**

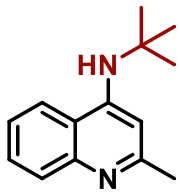

GP1 was followed using NaO*t*Bu (92.3 mg, 0.96 mmol), 4-chloroquinaldine (96.8 µL, 0.48 mmol), tert-butylamine (151 µL, 1.44 mmol), **C7** (35.5 mg, 0.048 mmol), and toluene (4 mL) at 120 °C. After flash chromatography (10% MeOH in DCM), the title compound was obtained (88 mg, 86%) as an off-white solid. ^{1}H NMR (500.1 MHz, $CDCl_3$): 7.95 (d, *J* = 8.4 Hz, 1H), 7.65 (dd, *J* = 8.4, 0.7 Hz, 1H), 7.57 (ddd, *J* = 8.3, 6.9, 1.2 Hz, 1H), 7.35 (ddd, *J* = 8.2, 6.9, 1.2 Hz, 1H), 6.55 (s, 1H), 5.06 (br s, 1H), 2.63 (s, 3H), 1.54 (s, 9H). ^{13}C{^{1}H} UDEFT (125.8 MHz, $CDCl_3$): δ 158.18, 148.88, 146.95, 129.53, 128.17, 124.29, 119.26, 117.88, 101.24, 51.88, 29.37, 25.11. HRMS-ESI Calc'd for $C_{14}H_{19}N_2$ $[M+H]^+$: 215.1543. Found: 215.1546.

4-(*tert*-butoxy)-2-methylquinoline (4b')

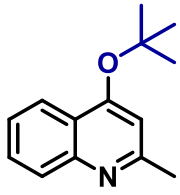

GP1 was followed using NaO*t*Bu (92.3 mg, 0.96 mmol), 4-chloroquinaldine (96.8 µL, 0.48 mmol), *tert*-butylamine (55.5 µL, 0.53 mmol), **C3** (31.8 mg, 0.048 mmol), and toluene (4 mL) at 120 °C. After flash chromatography (100% EtOAc in hexanes), the title compound was obtained (50 mg, 49%) as a yellow oil from a mixture of **4b** and **4b'**. ^{1}H NMR (500.1 MHz, $CDCl_3$): δ 8.12 (dd, *J* = 8.3, 1.1 Hz, 1H), 7.92 (d, *J* = 8.4 Hz, 1H), 7.62 (ddd, *J* = 8.4, 6.9, 1.5 Hz, 1H), 7.40 (ddd, *J* = 8.1, 7.0, 1.0 Hz, 1H), 6.81 (s, 1H), 2.68 (s, 3H), 1.62 (s, 9H). ^{13}C{^{1}H} UDEFT (125.8 MHz, $CDCl_3$): δ 159.66, 159.57, 149.45, 129.60, 128.28, 124.71, 122.68, 122.59, 107.33, 80.55, 28.90, 26.18. HRMS-ESI Calc'd for $C_{14}H_{17}NNaO$ $[M+Na]^+$: 238.1202. Found: 238.1212.

2-methyl-*N*-(3-methyl-1-phenyl-1*H*-pyrazol-5-yl)quinolin-4-amine (4d)

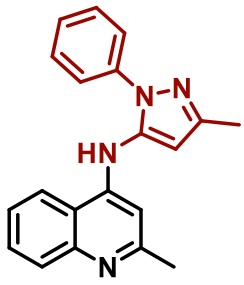

GP1 was followed using DBU (144 µL, 0.96 mmol), NaTFA (131 mg, 0.96 mmol), 4-chloroquinaldine (96.8 µL, 0.48 mmol), 5-amino-3-methyl-1-phenylpyrazole (92 mg, 0.53 mmol), **C3** (9.5 mg, 0.0144 mmol), and toluene (4 mL) at 60 °C. After flash chromatography (50% EtOAc in hexanes), the title compound was obtained (124 mg, 82%) as a pale-yellow solid. ^{1}H NMR (500.1 MHz, $CDCl_3$): δ 7.96 (d, J = 8.4 Hz, 1H), 7.65 (m, 2H), 7.49 (m, 2H), 7.39 – 7.42 (m, 3H), 7.30 (m, 1H), 6.76 (s, 1H), 6.49 (br s, 1H), 6.21 (s, 1H), 2.60 (s, 3H), 2.40 (s, 3H). ^{13}C{^{1}H} UDEFT (125.8 MHz, $CDCl_3$): δ 149.74, 138.43, 129.76–129.58 (overlapping signals), 127.77, 125.04, 123.82, 119.11, 117.54, 103.16, 101.02, 25.71, 14.41. HRMS-ESI Calc'd for $C_{20}H_{19}N_4$ $[M+H]^+$: 315.1604. Found: 315.1602.

4-((3-methyl-1-phenyl-1*H*-pyrazol-5-yl)amino)benzonitrile (5a)

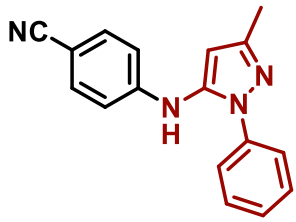

GP1 was followed using DBU (144 µL, 0.96 mmol), NaTFA (131 mg, 0.96 mmol), 4-chlorobenzonitrile (66 mg, 0.48 mmol), 5-amino-3-methyl-1-phenylpyrazole (92 mg, 0.53 mmol), **C4** (16.6 mg, 0.024 mmol), and 1,4-dioxane (4 mL) at 80 °C. After flash chromatography (40% EtOAc in hexanes), the title compound was obtained (94 mg, 72%) as a white powder. ^{1}H NMR (500.1 MHz, $CDCl_3$): δ 7.50 (m, 2H), 7.47 – 7.41 (m, 4H), 7.34 (m, 1H), 6.87 (m, 2H), 6.10 (s, 1H), 5.80 (br s, 1H), 2.35 (s, 3H). ^{13}C{^{1}H} UDEFT (125.8 MHz, $CDCl_3$): 149.65, 147.41, 138.51, 138.23, 134.04, 129.60, 127.95, 124.25, 119.55, 114.78, 102.98, 99.72, 14.28. HRMS-ESI Calc'd for $C_{17}H_{15}N_4$ $[M+H]^+$: 275.1291. Found: 275.1292.

***N*-(1,3-dimethyl-4-phenyl-1*H*-pyrazol-5-yl)quinoxalin-6-amine (5b)**

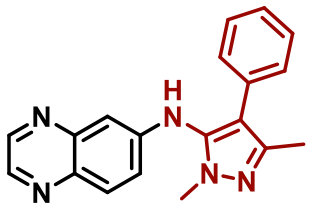

GP1 was followed using DBU (144 µL, 0.96 mmol), NaTFA (131 mg, 0.96 mmol), 2-chloroquinoxaline (79 mg, 0.48 mmol), 2,5-dimethyl-4-phenylpyrazol-3-amine (99 mg, 0.53 mmol), **C4** (16.6 mg, 0.024 mmol), and toluene (4 mL) at 80 °C. The crude mixture was immediately filtered over a pad of silica on celite (1:1) with EtOAc (~50 mL) then dried *in vacuo*. After flash chromatography on alumina (25% EtOAc in hexanes was followed by 50% EtOAc in hexanes then 100% MeOH), the title compound was obtained (137 mg, 90%) as a yellow solid. ^{1}H NMR (500.1 MHz, $CDCl_3$): δ 8.69 (d, J = 1.9 Hz, 1H), 8.62 (d, J = 1.9 Hz, 1H), 7.97 (d, J = 9.0 Hz, 1H), 7.31 – 7.27 (m, 2H), 7.25 – 7.18 (m, 4H), 7.05 (d, J = 2.6 Hz, 1H), 5.77 (s, 1H), 3.73 (s, 3H), 2.37 (s, 3H). ^{13}C{^{1}H} UDEFT (125.8 MHz, $CDCl_3$): δ 147.14, 145.97, 145.52, 144.95, 142.12, 138.96, 135.43, 132.59, 131.22, 128.78, 128.76, 126.80, 120.86, 115.87, 108.19, 35.33, 13.57. HRMS-ESI Calc'd for $C_{19}H_{17}N_5Na$ $[M+Na]^+$: 338.1376. Found: 338.1372.

3-methyl-*N*-(1-methyl-3-phenyl-1*H*-pyrazol-5-yl)pyridin-2-amine (5c)

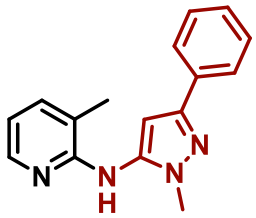

GP1 was followed using DBU (144 µL, 0.96 mmol), NaTFA (131 mg, 0.96 mmol), 2-chloro-3-methylpyridine (52.3 µL, 0.48 mmol), 1-methyl-3-phenyl-1*H*-pyrazol-5-amine (91 mg, 0.53 mmol), **C4** (16.6 mg, 0.024 mmol), and toluene (4 mL) at 80 °C. The crude mixture was immediately filtered over a pad of silica on celite (1:1) with EtOAc (~50 mL) then dried *in vacuo*. After flash chromatography on alumina (0% MeOH in DCM followed by flushing with 100% MeOH), the title compound was obtained (105 mg, 83%) as a pale-pink oil. ^{1}H NMR (500.1 MHz, $CDCl_3$): δ 8.08 (dd, *J* = 5.0, 1.2 Hz, 1H), 7.79 (dd, *J* = 8.3, 1.2 Hz, 2H), 7.41 (ddd, *J* = 7.3, 1.7, 0.8 Hz, 1H), 7.39 – 7.35 (m, 2H), 7.28 (dt, *J* = 3.6, 1.6 Hz, 1H), 6.77 (dd, *J* = 7.3, 5.0 Hz, 1H), 6.49 (s, 1H), 6.04 (br s, 1H), 3.79 (s, 3H), 2.25 (s, 3H). ^{13}C{^{1}H} UDEFT (125.8 MHz, $CDCl_3$): δ 154.12, 150.04, 145.60, 139.71, 138.89, 133.98, 128.61, 127.57, 125.53, 117.89, 116.12, 97.44, 35.83, 17.30. HRMS-ESI Calc'd for $C_{16}H_{16}N_4Na$ $[M+Na]^+$: 287.1267. Found: 287.1270.

***N*-(1,3-diphenyl-1*H*-pyrazol-5-yl)-2-methylquinolin-7-amine (5d)**

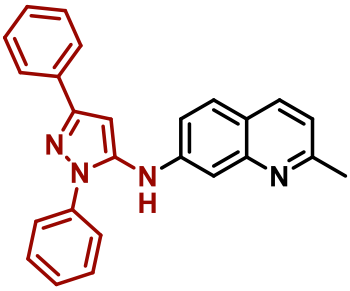

GP1 was followed using DBU (144 µL, 0.96 mmol), NaTFA (131 mg, 0.96 mmol), 7-chloroquinaldine (85 mg, 0.48 mmol), 5-amino-1,3-diphenyl-1*H*-pyrazole (124 mg, 0.53 mmol), **C4** (16.6 mg, 0.024 mmol), and toluene (4 mL) at 80 °C. The crude mixture was immediately filtered over a pad of silica on celite (1:1) with EtOAc (~50 mL) then dried *in vacuo*. After flash chromatography on alumina (0% MeOH in DCM followed by 5% MeOH in DCM) the title compound was obtained (127 mg, 70%) as white solid. ^{1}H NMR (500.1 MHz, $CDCl_3$): δ 7.95 (d, *J* = 8.3 Hz, 1H), 7.90 (d, *J* = 7.3 Hz, 2H), 7.65 (m, 3H), 7.56 (s, 1H), 7.50 – 7.39 (m, 4H), 7.35 (m, 2H), 7.11 (m, 2H), 6.73 (s, 1H), 5.87 (br s, 1H), 2.71 (s, 3H). ^{13}C{^{1}H} UDEFT (125.8 MHz, $CDCl_3$): δ 159.79, 151.86, 144.73, 140.60, 138.57, 136.36, 133.30, 129.62, 129.14, 128.75, 128.23-127.99 (overlapping signals), 125.86, 124.61, 121.82, 119.82, 117.38, 109.80, 96.41, 25.29. HRMS-ESI Calc'd for $C_{25}H_{21}N_4$ $[M+H]^+$: 377.1761. Found: 377.1760.

***N*-(1-methyl-1*H*-pyrazolo[3,4-b]pyridin-3-yl)quinoxalin-2-amine (5e)**

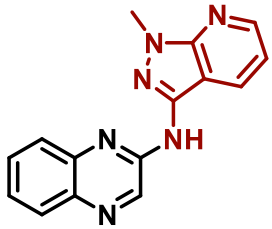

GP1 was followed using DBU (144 µL, 0.96 mmol), NaTFA (131 mg, 0.96 mmol), 2-chloroquinoxaline (79 mg, 0.48 mmol), 1-methyl-1*H*-pyrazolo[3,4-b]pyridin-3-ylamine (78 mg, 0.53 mmol), **C4** (16.6 mg, 0.024 mmol), and toluene (4 mL) at 80 °C. The crude mixture was immediately filtered over a pad of silica on celite (1:1) with EtOAc (~50 mL) then dried *in vacuo* then washed with MeOH (3 x 10 mL). The title compound was obtained (101 mg, 77%) as a bright yellow solid. ^{1}H NMR (500.1 MHz, $(CD_3)_2SO$): δ 9.88 (s, 1H), 8.79 (d, *J* = 1.9 Hz, 1H), 8.67 (d, *J* = 1.9 Hz, 1H), 8.63 (d, *J* = 2.4 Hz, 1H), 8.56 (dd, *J* = 4.5, 1.5

Hz, 1H), 8.47 (dd, J = 8.0, 1.5 Hz, 1H), 7.99 (d, J = 9.1 Hz, 1H), 7.91 (dd, J = 9.1, 2.5 Hz, 1H), 7.19 (dd, J = 8.0, 4.5 Hz, 1H), 4.03 (s, 3H). $^{13}C\{^1H\}$ UDEFT (125.8 MHz, $(CD_3)_2SO$): δ 149.68, 149.66, 145.45, 144.27, 143.08, 141.92, 141.89, 137.91, 129.82, 129.38, 123.05, 115.08, 109.75, 106.93, 33.23. HRMS-ESI Calc'd for $C_{15}H_{11}N_6$ $[M-H]^-$: 275.1051. Found: 275.1049.

***N*-(naphthalen-1-yl)-1*H*-pyrazol-3-amine (5f)**

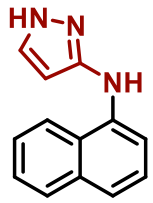

GP1 was followed using DBU (144 µL, 0.96 mmol), NaTFA (131 mg, 0.96 mmol), 1-chloronapthalene (65.4 µL, 0.48 mmol), 3-aminopyrazole (43.9 mg, 0.53 mmol), **C4** (16.6 mg, 0.024 mmol), and 1,4-dioxane (4 mL) at 80 °C. After flash chromatography (50% EtOAc in hexanes), the title compound was obtained (69 mg, 69%) as yellow oil. ^1H NMR (500.1 MHz, $CDCl_3$): δ 8.02 (d, J = 8.2 Hz, 1H), 7.84 (d, J = 7.8 Hz, 1H), 7.57 – 7.31 (m, 7H), 6.12 (d, J = 2.2 Hz, 1H), one NH signal not observed. $^{13}C\{^1H\}$ UDEFT (125.8 MHz, $CDCl_3$): δ 152.21, 139.17, 134.63, 130.29, 128.71, 126.29–126.07 (overlapping signals), 125.50, 121.14, 121.01, 111.45, 95.40. HRMS-ESI Calc'd for $C_{13}H_{10}N_3$ $[M-H]^-$: 208.0880. Found: 208.0882

2-methyl-*N*-(1*H*-pyrazol-3-yl)quinolin-4-amine (5g)

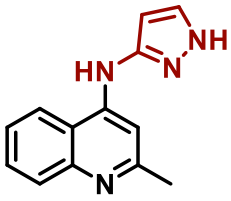

GP1 was followed using DBU (144 µL, 0.96 mmol), NaTFA (131 mg, 0.96 mmol), 4-chloroquinaldine (96.8 µL, 0.48 mmol), 3-aminopyrazole (43.9 mg, 0.53 mmol), **C4** (16.6 mg, 0.024 mmol), and 1,4-dioxane (4 mL) at 80 °C. After flash chromatography (20% MeOH in DCM), the title compound was obtained (94 mg, 87%) as a white solid. ^1H NMR (500.1 MHz, $(CD_3)_2SO$): δ 12.42 (br s, 1H), 9.13 (br s, 1H), 8.42 (d, J = 8.3 Hz, 1H), 7.77 (dd, J = 8.4, 0.9 Hz, 1H), 7.72 (s, 1H), 7.67 – 7.59 (m, 2H), 7.45 (ddd, J = 8.2, 6.9, 1.2 Hz, 1H), 6.20 (d, J = 2.1 Hz, 1H), 2.49 (s, 3H; overlaps with DMSO). $^{13}C\{^1H\}$ UDEFT (125.8 MHz, $(CD_3)_2SO$): δ 158.56, 149.40, 147.72, 146.58, 129.09, 128.96, 128.04, 123.74, 121.60, 117.46, 102.52, 96.60, 25.06. HRMS-ESI Calc'd for $C_{13}H_{13}N_4$ $[M+H]^+$: 225.1135. Found: 225.1142.

4-((2-(1*H*-pyrazol-1-yl)phenyl)amino)benzonitrile (5h)

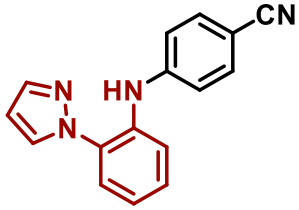

GP1 was followed using DBU (144 µL, 0.96 mmol), NaTFA (131 mg, 0.96 mmol), 4-chlorobenzonitrile (66 mg, 0.48 mmol), 1-(2-aminophenyl)-1*H*-pyrazole (84.1 mg, 0.53 mmol), **C4** (16.6 mg, 0.024 mmol), and 1,4-dioxane (4 mL) at 80 °C. After flash chromatography (30% EtOAc in hexanes), the title compound was obtained (114 mg, 91%) as pale-yellow powder. ^1H NMR (500.1 MHz, $CDCl_3$) δ 8.82 (s, 1H), 7.79 (d, J = 2.2 Hz, 2H), 7.57 (dd, J = 8.2, 1.0 Hz, 1H), 7.48 (dd, J = 9.0, 2.1 Hz, 2H), 7.36 (dd, J = 7.9, 1.3 Hz, 1H), 7.32 (m, 1H), 7.10 (m, 3H), 6.48 (t, J = 2.2 Hz, 1H). $^{13}C\{^1H\}$ UDEFT (125.8 MHz, $CDCl_3$) δ 146.94, 141.11, 134.73, 133.79, 130.50, 130.04, 128.16, 124.28, 122.79,

120.40, 119.84, 116.50, 107.14, 102.49. HRMS-ESI Calc'd for $C_{16}H_{12}N_4Na$ $[M+Na]^+$: 283.0954. Found: 283.0951.

***N*-(2-(1*H*-pyrazol-1-yl)phenyl)-3-methylpyridin-2-amine (5i)**

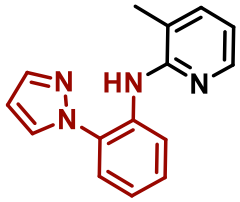

GP1 was followed using DBU (144 µL, 0.96 mmol), NaTFA (131 mg, 0.96 mmol), 2-chloro-3-methylpyridine (52.3 µL, 0.48 mmol), 1-(2-aminophenyl)-1*H*-pyrazole (84.1 mg, 0.53 mmol), **C4** (16.6 mg, 0.024 mmol), and 1,4-dioxane (4 mL) at 80 °C. After flash chromatography (30% EtOAc in hexanes), the title compound was obtained (76 mg, 63%) as a yellow oil. ^{1}H NMR (500.1 MHz, $CDCl_3$): δ 9.17 (s, 1H), 8.59 (dd, *J* = 8.4, 1.2 Hz, 1H), 8.08 (dd, *J* = 4.9, 1.5 Hz, 1H), 7.81 (d, *J* = 1.8 Hz, 1H), 7.77 (dd, *J* = 2.4, 0.4 Hz, 1H), 7.40 – 7.35 (m, 1H), 7.33 (ddd, *J* = 7.2, 1.7, 0.8 Hz, 1H), 7.30 (dd, *J* = 7.9, 1.5 Hz, 1H), 7.02 (td, *J* = 7.8, 1.4 Hz, 1H), 6.69 (dd, *J* = 7.2, 5.0 Hz, 1H), 6.52 – 6.43 (m, 1H), 2.23 (s, 3H). ^{13}C{^{1}H} UDEFT (125.8 MHz, $CDCl_3$): δ 153.89, 144.94, 140.74, 137.93, 135.10, 130.51, 128.97, 128.25, 123.46, 121.45, 121.18, 119.62, 115.41, 106.90, 17.55. HRMS-ESI Calc'd for $C_{15}H_{14}N_4Na$ $[M+Na]^+$: 273.1111. Found: 273.1113.

***N*-(2-(1*H*-pyrazol-1-yl)phenyl)-2-methylquinolin-4-amine (5j)**

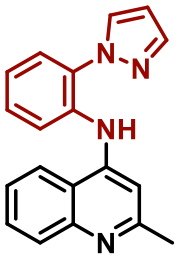

GP1 was followed using DBU (144 µL, 0.96 mmol), NaTFA (131 mg, 0.96 mmol), 4-chloroquinaldine (96.8 µL, 0.48 mmol), 1-(2-aminophenyl)-1*H*-pyrazole (84.1 mg, 0.53 mmol), **C4** (16.6 mg, 0.024 mmol), and 1,4-dioxane (4 mL) at 80 °C. After flash chromatography on alumina (95% EtOAc in hexanes), the title compound was obtained (126 mg, 88%) as yellow oil. ^{1}H NMR (500.1 MHz, $CDCl_3$): δ 8.94 (br s, 1H), 8.68 (d, *J* = 1.4 Hz, 1H), 8.60 (s, 1H), 7.94 (d, *J* = 9.1 Hz, 1H), 7.82 (t, *J* = 2.3 Hz, 2H), 7.78 (dd, *J* = 8.2, 1.1 Hz, 1H), 7.71 (d, *J* = 2.4 Hz, 1H), 7.49 (dd, *J* = 9.1, 2.5 Hz, 1H), 7.40 – 7.32 (m, 2H), 7.11 (td, *J* = 7.9, 1.3 Hz, 1H), 6.49 (t, *J* = 2.2 Hz, 1H), 3.49 (s, 3H). ^{13}C{^{1}H} UDEFT (125.8 MHz, $CDCl_3$): δ 145.11, 144.77, 144.59, 141.92, 141.10, 139.39, 135.46, 130.53, 130.24–130.14 (overlapping signals), 128.34, 124.50, 124.24, 122.43, 120.12, 110.04, 107.08, 51.00. HRMS-ESI Calc'd for $C_{19}H_{17}N_4$ $[M+H]^+$: 301.1448. Found: 301.1446.

3 Conclusions and Future Work

3.1 Concluding Remarks

In summary, this work encompasses an extensive evaluation of leading DalPhos ligand variants in the Ni-catalyzed C–N cross-coupling of (hetero)aryl chlorides with NH substrates. This comparative study, utilizing a comprehensive screening strategy similar to that used in high-throughput studies, enabled reactivity trends to be established related to the choice of ligand, base, and solvent that can be used to inform subsequent experimentation. In particular, while the strong inorganic base NaO*t*Bu proved to be a superior choice for these reactions, competitive C–O cross-coupling was observed, which prompts further exploration into this limitation and the propensity for these ligands for C–O cross-coupling reactions. The potential for employing organic bases in future screening studies was also illustrated by the success of **PAd2-DalPhos** and the 'dual base' system DBU/NaTFA. Most importantly, limitations discovered throughout this study provide motivation to improve this methodology and further develop ligand-enabled Ni catalysts in order to tackle these challenges and related cross-coupling reactions. The following section describes related NH substrates of importance that have proven to be challenging in metal-catalyzed C–N cross-coupling reactions and a proposal for improving this methodology based on literature precedence.

3.2 Future Work

3.2.1 Introduction to Amides and Sulfonamides

Amide bond forming reactions are predominant throughout literature[12] due to the prevalence of the amide functional group in biologically active molecules and functional materials.[82] They are most commonly synthesized from carboxylic acids and amines with the use

of coupling reagent(s) responsible for activation or conversion of the carboxylic acid into a more reactive derivative.[82, 83]The transition metal catalyzed *N*-arylation of amides is a promising route for their direct functionalization with many Cu[20] and Pd[84] catalysts having been reported. There are selected examples employing bisphosphine ligated Ni catalysts demonstrating exemplary reactivity overcoming the limitations often associated with Cu and Pd (discussed in Chapter 1). Sulfur containing functional groups are also common in medicinal chemistry with sulfonamides being the most prominent.[85-87] They are also prevalent in agrochemicals[88] and can function as carboxylic isosteres[99] and organocatalysts.[90] Analogous to amides, sulfonamide groups can also be functionalized through transition metal catalyzed *N*-arylation.

3.2.2 Transition Metal Catalyzed N-Arylation of Primary and Secondary Sulfonamides

The transition metal catalyzed *N*-arylation of sulfonamides has generally employed Cu and Pd based catalysts with fewer reports using Ni catalysts. The utility of Cu catalysts in this chemistry has been illustrated by the large scale (>50 kg) sulfamidation of a (hetero)aryl bromide using CuI/cyDMEDA in the synthesis of AZD5069, a drug candidate for treating asthma.[91] Until recently, the Cu-catalyzed synthesis of *N*-arylsulfonamides has been limited to (hetero)aryl bromide and/or iodide coupling partners.[92-96] A publication from the Ma group[97] in 2022 demonstrated an impressive scope of (hetero)aryl chlorides but required elevated catalyst loadings and temperatures (10–20 mol% at ≥ 120 °C) and was limited to primary sulfonamides. Conversely, Pd catalysts have afforded access to modest scopes coupling primary sulfonamides with (hetero)aryl chlorides,[98-100] but examples coupling (hetero)aryl (pseudo)halides (ArBr, ArCl, ArOTf, and/or ArONfl)[46, 93, 99, 101] with secondary sulfonamides are limited.

Most Ni-catalyzed *N*-arylations of sulfonamides have relied heavily on photochemistry[102-104] with limited examples employing electrolytic[105] or ligand-enabled approaches.[106, 107] More

recently, T. You and J. Li[107] reported the use of the air-stable pre-catalyst Ni(COD)(DQ) without the need for additional ligands, which afforded a broad scope in both (hetero)aryl bromides and secondary *N*-arylsulfonamides but employed high loading (20 mol%) and temperature (150 °C). An earlier report using the air-stable pre-catalyst (**PhPAd-DalPhos**)Ni(*o*-tol)Cl included a broad scope of (hetero)aryl chlorides coupled to primary sulfonamides (aryl and alkyl) at modest loading and temperature (5 mol%, 80 °C). Selected examples with *N*-methyl substituted secondary sulfonamides were also reported but required elevated temperatures (110 °C) and electron-rich (hetero)aryl chlorides were challenging coupling partners.[106] In contrast to the Ni-catalyzed *N*-arylation of primary and secondary sulfonamides, the analogous functionalization of amides employing DalPhos ligands has been more extensively investigated.

3.2.3 Efficacy of DalPhos Ligands in the N-Arylation of Primary and Secondary Amides

The first Ni-catalyzed amide *N*-arylation was reported in 2016.[108] Enabled by the air-stable pre-catalyst (**PAd-DalPhos**)Ni(*o*-tol)Cl, primary amides were coupled to a variety of electrophilic coupling partners including (hetero)aryl bromides, chlorides, triflates, tosylates, mesylates, and sulfamates. Several base/solvent combinations were found to be useful (NaO*t*Bu/toluene, Cs_2CO_3/1,4-dioxane, and K_3PO_4/*t*BuOH) for this transformation. Five years later, a catalytic system employing the 'dual base' DBU/NaTFA system was developed, however slightly elevated temperatures (100 °C vs 90 °C) were needed in addition to the use of $Ni(COD)_2$ rather than an air-stable pre-catalyst. The cyclohexyl DalPhos variant, **CyPAd-DalPhos**, displayed superior performance at modest loading (5 mol%) with a comparable scope of (hetero)aryl (pseudo)halides and primary amides reported in addition to several examples coupling (hetero)aryl chlorides to more challenging secondary amides.[54] Shortly after this another DalPhos/DBU/NaTFA system was published reporting the cross-coupling of primary and secondary amides with 2'-

(pseudo)halide-substituted acetophenones. The double cage ligand **PAd2-DalPhos** was successfully employed as an air-stable (**L**)Ni(4-CN-Ph)Cl pre-catalyst, analogous to the JosiPhos bearing pre-catalyst developed by the Hartmann group,[109] and displayed superior performance to the previously reported **CyPAd-DalPhos**/Ni(COD)$_2$ system and (**L**)Ni(*o*-tol)Cl derivatives, with several transformations conducted at room temperature.[55]

3.2.4 The Effect of Various Additives in Pd-catalyzed Amidations

The use of Lewis acids in catalytic or stoichiometric quantities to facilitate catalytic turnover is well-known[110] and a variety of Lewis acids have proven to be effective additives in Pd-catalyzed amidations. In 2017, J. Becica and G. E. Dobereiner investigated metal triflates (i.e., M(OTf)$_3$, M = Al, In, Sc, Yb, Zn) as co-catalysts in the Pd-catalyzed *N*-arylation of primary and secondary amides with (hetero)aryl bromides. Although each of these metal triflates proved to be beneficial, Pd(dba)$_2$/XantPhos (2 mol%) and Al(OTf)$_3$ (5 mol%), the most cost-effective additive, were employed in a modest scope with up to a 45% increase in the product yield. It was also observed that the use of M(OTf)$_3$:Pd ratios greater than 1:1 reduced the rate of catalysis resulting in depreciated yields.[111] In 2007, Hartwig reported the amidation of (hetero)aryl bromides catalyzed by Pd(dba)$_2$/XantPhos in which the addition of 20 mol% BEt$_3$ was found to accelerate reductive elimination.[112] This inspired a subsequent study coupling (hetero)aryl chlorides with primary amides in the presence of borane additives in 2017.[113] Although the use of pyrophoric reagents is not ideal, by employing a bulky N-heterocyclic carbene (NHC) ligated Pd catalyst ((DiMelHelpt^{Cl})Pd(cinnamyl)Cl) and 20 mol% of either BEt$_3$, B(*sec*Bu)$_3$, or B(C$_6$F$_5$)$_3$ full conversion was observed compared to negligible or modest conversion (0–20%) in the absence of these boranes. Other additives that were tested but proved to be inferior included B(OMe)$_3$, ZnCl$_2$, and Et$_2$AlCl. A 2008 study from the Buchwald group[101] using [(allyl)PdCl]$_2$ with the

biarylmonophosphine ligand JackiePhos, also demonstrated the benefit of adding 3 Å powdered molecular sieves in their optimization for the coupling of 4-*tert*-butylphenyl nonaflate with *N*-butyl acetamide in which a modest increase in yield from 69 to 87% was observed without the formation of side products. These conditions were subsequently employed in the cross-coupling of both secondary amides and secondary sulfonamides with aryl nonaflates, triflates, and chlorides.

3.2.5 Proposed Investigation

The use of DalPhos ancillary ligands in Ni-catalyzed cross-coupling has afforded promising results in the *N*-arylation of amides and sulfonamides with (hetero)aryl (pseudo)halides.[54, 55, 106, 108] However, electron-rich electrophiles and secondary substrates remain a challenge and have typically required elevated temperatures or loading. Given the prevalence of these functional groups in medicinal chemistry[12, 82, 85-90] and the potential for additional modification by *N*-arylation of secondary motifs, it is desirable to develop a robust catalytic system for this chemistry. An investigation into the effects of molecular sieves and Lewis acids in established Ni/DalPhos systems is motivated by the success of additives in analogous Pd-catalyzed amidations[100, 111-113] and could enable facile *N*-arylation of challenging substrates (Figure 3.1).

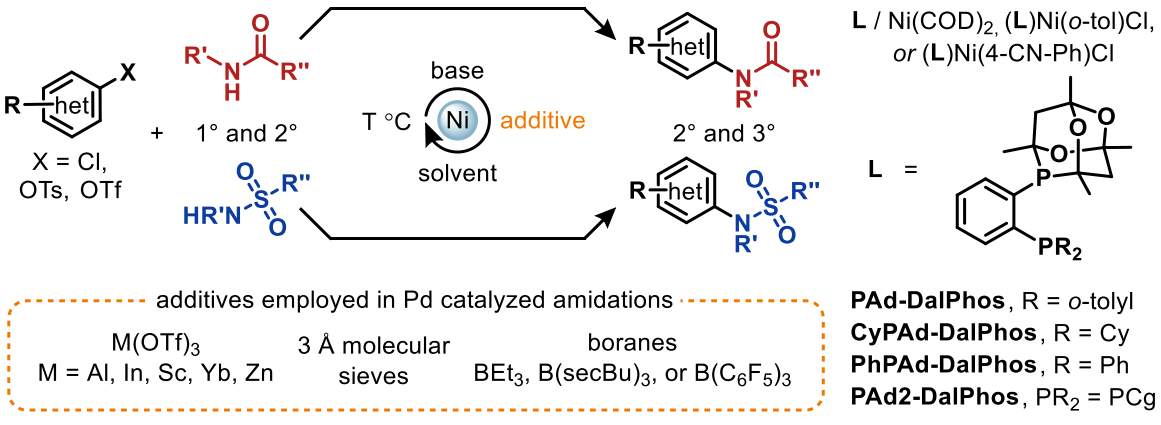

Figure 3.1 Proposed investigation into the effect of $M(OTf)_3$, molecular sieves, and alkyl/aryl borane additives in established Ni/DalPhos catalytic systems.

References

1. In *Modern Nucleophilic Aromatic Substitution*, John Wiley & Sons, Ltd, **2013**, pp. 1–94.

2. M. Orlandi, D. Brenna, R. Harms, S. Jost, M. Benaglia, *Org. Process Res. Dev.* **2018**, *22*, 430–445.

3. Amines by Reduction. In *Kirk-Othmer Encyclopedia of Chemical Technology*, John Wiley & Sons, Ltd, **2021**, pp. 1–34.

4. In *Methodologies in Amine Synthesis: Challenges and Applications*, John Wiley & Sons, Ltd, **2021**, pp. 377–444.

5. In *Ligand Design in Metal Chemistry*, John Wiley & Sons, Ltd, **2016**, pp. 1–14.

6. C. J. Elsevier, J. Reedijk, P. H. Walton, M. D. Ward, *Dalton Trans*. **2003**, 1869–1880.

7. R. J. Lundgren, M. Stradiotto, *Chem. Eur. J.* **2012**, *18*, 9758–9769.

8. J. Louie, J. F. Hartwig, *Tetrahedron Lett.* **1995**, *36*, 3609–3612.

9. A. S. Guram, R. A. Rennels, S. L. Buchwald, *Angew. Chem. Int. Ed. Engl.* **1995**, *34*, 1348–1350.

10. E. Vitaku, D. T. Smith, J. T. Njardarson, *J. Med. Chem*. **2014**, *57*, 10257−10274.

11. N. A. McGrath, M. Brichacek, J. T. Njardarson, *J. Chem. Educ.* **2010**, *87*, 1348–1349.

12. D. G. Brown, J. Bostrom, *J. Med. Chem.* **2016**, *59*, 4443–4458.

13. P. Ruiz-Castillo, S. L. Buchwald, *Chem. Rev.* **2016**, *116*, 12564–12649.

14. A. B. Santanilla, E. L. Regalado, T. Pereira, M. Shevlin, K. Bateman, L. C. Campeau, J. Schneeweis, S. Berritt, Z.-C. Shi, P. Nantermet, Y. Liu, R. Helmy, C. J. Welch, P. Vachal, I. W. Davies, T. Cernak, S. D. Dreher, *Science* **2015**, *347*, 49–53.

15. L. E. Sirois, D. Lao, J. Xu, R. Angelaud, J. Tso, B. Scott, P. Chakravarty, S. Malhotra, F. Gosselin, *Org. Process Res. Dev.* **2020**, *24*, 567–578.

16. C. Li, L. Franklin, R. Chen, T. Mack, M. Humora, B. Ma, B. T. Hopkins, J. Guzowski, F. Zheng, M. MacPhee, Y. Lin, S. Ferguson, D. Patience, G. A. Moniz, W. F. Kiesman, E. M. O'Brien, *Org. Process Res. Dev.* **2020**, *24*, 1199–1206.

17. H. Cheng, S. K. Nair, B. W. Murray, C. Almaden, S. Bailey, S. Baxi, D. Behenna, S. Cho-Schultz, D. Dalvie, D. M. Dinh, M. P. Edwards, J. L. Feng, R. A. Ferre, K. S. Gajiwala, M. D. Hemkens, A. Jackson-Fisher, M. Jalaie, T. O. Johnson, R. S. Kania, S.

Kephart, J. Lafontaine, B. Lunney, K. K.-C. Liu, Z. Liu, J. Matthews, A. Nagata, S. Niessen, M. A. Ornelas, S. T. M. Orr, M. Pairish, S. Planken, S. Ren, D. Richter, K. Ryan, N. Sach, H. Shen, T. Smeal, J. Solowiej, S. Sutton, K. Tran, E. Tseng, W. Vernier, M. Walls, S. Wang, S. L. Weinrich, S. Xin, H. Xu, M.-J. Yin, M. Zientek, R. Zhou, J. C. Kath, *J. Med. Chem*. **2016**, *59*, 2005–2024.

18. Y. Tao, N. F. Keene, K. E. Wiglesworth, B. Sitter, J. C. McWilliams, *Org. Process Res. Dev.* **2019**, *23*, 382–388.

19. F. Ullmann, *Ber. Dtsch. Chem. Ges.* **1903**, *36*, 2382−2384.

20. Q. Yang, Y. Zhao, D. Ma, *Org. Process Res. Dev.* **2022**, *26*, 1690−1750.

21. S. Kim, M. J. Goldfogel, M. M. Gilbert, D. J. Weix, *J. Am. Chem. Soc.* **2020**, *142*, 9902–9907.

22. D. S. Surry, S. L. Buchwald, *Angew. Chem. Int. Ed.* **2008**, *47*, 6338–6361.

23. S. Z. Tasker, E. A. Standley, T. F. Jamison, *Nature* **2014**, *509*, 299−309.

24. S, Bajo, G. Laidlaw, A. R. Kennedy, S. Sproules, D. J. Nelson, *Organometallics* **2017**, *36*, 1662−1672.

25. M. M. Beromi, G. Banerjee, G. W. Brudvig, D. J. Charboneau, N. Hazari, H. M. C Lant, B. Q. Mercado, *Organometallics* **2018**, *37*, 3943−3955.

26. C. M. Lavoie, M. Stradiotto, *ACS Catal.* **2018**, *8*, 7228–7250.

27. R. Sun, Y. Z. Qin, D. G. Nocera, *Angew. Chem. Int. Ed.* **2020**, *59*, 9527–9533.

28. E. B. Corcoran, M. T. Pirnot, S. Lin, S. D. Dreher, D. A. DiRocco, I. W. Davies, S. L. Buchwald and D. W. C. MacMillan, *Science*, 2016, **353**, 279–283.

29. Y. Kawamata, J. C. Vantourout, D. P. Hickey, P. Bai, L. Chen, Q. Hou, W. Qiao, K. Barman, M. A. Edwards, A. F. Garrido-Castro, J. N. deGruyter, H. Nakamura, K. Knouse, C. Qin, K. J. Clay, D. Bao, C. Li, J. T. Starr, C. Garcia-Irizarry, N. Sach, H. S. White, M. Neurock, S. D. Minteer and P. S. Baran, *J. Am. Chem. Soc.*, **2019**, *141*, 6392–6402.

30. V. V. Grushin, H. Alper, *Chem. Rev*. **1994**, *94*, 1047–1062.

31. N. H. Park, G. Teverovskiy, S. L. Buchwald, *Org. Lett.* **2014**, *16*, 220–223.

32. Iranpoor, N.; Panahi, F. *Adv. Synth. Catal.* **2014**, *356*, 3067–3073.

33. C. M. Lavoie, P. M. MacQueen, N. L. Rotta-Loria, R. S. Sawatzky, A. Borzenko, A. J. Chisholm, B. K. V. Hargreaves, R. McDonald, M. J. Ferguson, M. Stradiotto, *Nat. Commun.* **2016**, *7*, 11073.

34. P. M. MacQueen, M. Stradiotto, *Synlett.* **2017**, *28*, 1652–1656.

35. M. S. Driver, J. F. Hartwig, *J. Am. Chem. Soc.* **1996**, *118*, 7217–7218.

36. J. P. Wolfe, S. L. Buchwald, *J. Am. Chem. Soc.* **1997**, *119,* 6054–6058.

37. J. S. K. Clark, C. N. Voth, M. J. Ferguson, M. Stradiotto, *Organometallics* **2017**, *36*, 679−686.

38. R. J. Lundgren, B. D. Peters, P. G. Alsabeh, M. Stradiotto, *Angew. Chem. Int. Ed.* **2010**, *49*, 4071–4074.

39. A. Borzenko, N. L. Rotta-Loria, P. M. MacQueen, C. M. Lavoie, R. McDonald, M. Stradiotto, *Angew. Chem. Int. Ed.* **2015**, *54*, 3773–3777.

40. J. P. Tassone, E. V. England, P. M. MacQueen, M. J. Ferguson, M. Stradiotto, *Angew. Chem. Int. Ed.* **2019**, *58*, 2485–2489.

41. J. P. Tassone, P. M. MacQueen, C. M. Lavoie, M. J. Ferguson, R. McDonald, M. Stradiotto, *ACS Catal.* **2017**, *7*, 6048−6059.

42. J. S. K. Clark, C. M. Lavoie, P. M. MacQueen, M. J. Ferguson, M. Stradiotto, *Organometallics*, **2016**, *35*, 3248–3254.

43. R. T. McGuire, A. A. Yadav, M. Stradiotto, *Angew. Chem. Int. Ed.* **2021**, *60*, 4080–4084.

44. R. T. McGuire, J. F. J. Paffile, Y. Q. Zhou, M. Stradiotto, *ACS Catal.* **2019**, *9*, 9292–9297.

45. M. N. Bahr, D. B. Damon, S. D. Yates, A. S. Chin, J. D. Christopher, S. Cromer, N. Perrotto, J. Quiroz, V. Rosso, *Org. Process Res. Dev.* **2018**, *22*, 1500–1508.

46. J. Becica, D. P. Hruszkewycz, J. E. Steves, J. M. Elward, D. C. Leitch and G. E. Dobereiner, *Org. Lett.*, **2019**, *21*, 8981–8986.

47. S. K. Kashani, J. E. Jessiman and S. G. Newman, *Org. Process Res. Dev.* **2020**, *24*, 1948–1954.

48. M. N. Bahr, M. A. Morris, N. P. Tu, A. Nandkeolyar, *Org. Process Res. Dev.* **2020**, *24*, 2752–2761.

49. G. L. Beutner, J. R. Coombs, R. A. Green, B. Inankur, D. Lin, J. Qiu, F. Roberts, E. M. Simmons and S. R. Wisniewski, *Org. Process Res. Dev.* **2019**, *23*, 1529–1537.

50. S. A. Derhamine, T. Krachko, N. Monteiro, G. Pilet, J. Schranck, A. Tlili, A. Amgoune, *Angew. Chem. Int. Ed.* **2020**, *59*, 18948–18953.

51. D. B. Damon, R. W. Dugger, S. E. Hubbs, J. M. Scott, R. W. Scott, *Org. Process Res. Dev.* **2006**, *10*, 472−480.

52. B. M. Cohen, B. Inankur, K. T. Lauser, J. Lott, W. Chen, *Org. Process Res. Dev*. **2018**, *22*,1481−1488.

53. D. M. Barnes, S, Shekhar, T. B. Dunn, J. H. Barkalow, V. S. Chan, T. S. Franczyk, A. R. Haight, J. E. Hengeveld, L. Kolaczkowski, B. J. Kotecki, G. Liang, J. C. Marek, M. A. McLaughlin, D. K. Montavon, J. J. Napier, *J. Org. Chem.* **2019**, *84*, 4873−4892.

54. T. Lundrigan, J. P. Tassone, M. Stradiotto, *Synlett.* **2021**, *32*, 1665–1669.

55. R. T. McGuire, T. Lundrigan, J. W. M. MacMillan, K. N. Robertson, A. A. Yadav, M. Stradiotto, *Angew. Chem. Int. Ed*. **2022**, *61*, e202200352.

56. J. W. M. MacMillan, R. T. McGuire, M. Stradiotto, *Chem. Eur. J*. **2022**, *28*, e202200764.

57. S. M. Mennen, C. Alhambra, C. L. Allen, M. Barberis, S. Berritt, T. A. Brandt, A. D. Campbell, J. Castañón, A. H. Cherney, M. Christensen, D. B. Damon, J. Eugenio de Diego, S. García-Cerrada, P. García-Losada, R. Haro, J. Janey, D. C. Leitch, L. Li, F. Liu, P. C. Lobben, D. W. C. MacMillan, J. Magano, E. McInturff, S. Monfette, R. J. Post, D. Schultz, B. J. Sitter, J. M. Stevens, I. I. Strambeanu, J. Twilton, K. Wang, M. A. Zajac, *Org. Process Res. Dev.* **2019**, *23*, 1213–1242.

58. D. Schultz, L. C. Campeau, *Nat. Chem.* **2020**, *12*, 661–664.

59. R. Grainger, S. Whibley, *Org. Process Res. Dev.* **2021**, *25*, 354–364.

60. K. Troshin, J. F. Hartwig, *Science* **2017**, *357*, 175–181.

61. J. M. Fordham, P. Kollmus, M. Cavegn, R. Schneider, M. Santagostino, *J. Org. Chem.* **2022**, *87*, 4400–4414.

62. J. S. K. Clark, M. J. Ferguson, R. McDonald, M. Stradiotto, *Angew. Chem. Int. Ed.* **2019**, *58*, 6391–6395.

63. J. S. K. Clark, R. T. McGuire, C. M. Lavoie, M. J. Ferguson, M. Stradiotto, *Organometallics* **2019**, *38*, 167–175.

64. T. W. Johnson, R. A. Gallego, M. P. Edwards, *J. Med. Chem.* **2018**, *61*, 6401–6420.

65. J. P. Tassone, T. Lundrigan, T. D. Ashton, M. Stradiotto, *Org. Chem.* **2022**, *87*, 6492–6498.

66. K. M. Morrison, R. T. McGuire, M. J. Ferguson, M. Stradiotto, *ACS Catal.* **2021**, *11*, 10878–10884.

67. N. Griebenow, L. Bärfacker, H. Meier, D. Schneider, N. Teusch, K. Lustig, R. Kast, P. Kolkhof, *Bioorg. Med. Chem. Lett.* **2010**, *20*, 5891–5894.

68. S. Patel, S. F. Harris, P. Gibbons, G. Deshmukh, A. Gustafson, T. Kellar, H. Lin, X. Liu, Y. Liu, Y. Liu, C. Ma, K. Scearce-Levie, A. S. Ghosh, Y. G. Shin, H. Solanoy, J. Wang, B. Wang, J. Yin, M. Siu, J. W. Lewcock, *J. Med. Chem.* **2015**, *58*, 8182–8199.

69. D. Anand, P. K. Yadav, O. P. S. Patel, N. Parmar, R. K. Maurya, P. Vishwakarma, K. S. R. Raju, I. Taneja, M. Wahajuddin, S. Kar, P. P. Yadav, *J. Med. Chem.* **2017**, *60*, 1041–1059.

70. D. C. Blakemore, L. Castro, I. Churcher, D. C. Rees, A. W. Thomas, D. M. Wilson, A. Wood, *Nat. Chem.* **2018**, *10*, 383–394.

71. K. Wojtasik, A. Danel, M. Wojtasik, M. Lukasiewicz, *ChemistrySelect* **2021**, *6*, 4330–4335.

72. M. Kucharek, A. Danel, *Chem. Heterocycl. Compd.* **2021**, *57*, 633–639.

73. E. P. K. Olsen, P. L. Arrechea, S. L. Buchwald, *Angew. Chem. Int. Ed.* **2017**, *56*, 10569–10572; *Angew. Chem.* **2017**, *129*, 10705–10708.

74. T. R. Puleo, S. J. Sujansky, S. E. Wright, J. S. Bandar, *Chem. Eur. J.* **2021**, *27*, 4216–4229.

75. S. D. Dreher, *React. Chem. Eng.* **2019**, *4*, 1530–1535.

76. J. M. Dennis, N. A White, R. Y. Liu, S. L. Buchwald, *J. Am. Chem. Soc.* **2018**, *140*, 4721–4725.

77. Q. Shen, T. Ogata, J. F. Hartwig, *J. Am. Chem. Soc.* **2008**, *130*, 6586–6596.

78. G. D. Roiban, G. Mehler, M. T. Reetz, *Eur. J. Org. Chem.* **2014**, 2070–2076.

79. T. J. Barker, E. R. Jarvo, *Angew. Chem Int. Ed.* **2011**, *50*, 8325–8328.

80. W. Weickmann, W. Frey, B. Plietker, *Chem. Eur. J.* **2013**, *19*, 2741–2748.

81. F.-D. Huang, C. Xu, D.-D. Lu, D.-S. Shen, T. Li, F.-S. Liu, *J. Org. Chem*. **2018**, *83*, 9144−9155.

82. In *The Amide Linkage: Selected Structural Aspects in Chemistry, Biochemistry, and Materials Science*, Wiley-Interscience, **2000**.

83. E. Valeur, M. Bradley, *Chem. Soc. Rev.* **2009**, *38*, 606–631.

84. R. Dorel, C. P. Grugel, A. M. Haydl, *Angew. Chem. Int. Ed.* **2019**, *58*, 17118–17129.

85. K. A. Scott, J. T. Njardarson, *Top. Curr. Chem.* **2018**, *376*, 1–34.

86. S. Apaydın, M. Török, *Bioorg. Med. Chem. Lett.* **2019**, *29*, 2042–2050.

87. K. A. Scott, M. H. Qureshi, P. B. Cox, C. M. Marshall, B. C. Bellaire, M. Wilcox, B. A. R. Stuart, J. T. Njardarson, *J. Med. Chem.* **2020**, *63*, 15449−1548.

88. P. Devendar, G.-F. Yang, *Top. Curr. Chem.* **2017**, *375*, 82.

89. C. Ballatore, D. M. Huryn, A. B. Smith, *ChemMedChem* **2013**, *8*, 385–395.

90. Y.-R. Zhu, J. Xu, H.-F. Jiang, R.-J. Fang, Y.-J. Zhang, L. Chen, C. Sun, F. Xiong, *Eur. J. Org. Chem.* **2022**, e202201081.

91. N. K. Adlington, P. S. Siedlecki, I. Derrick, S. D. Yates, A. D. Campbell, P. Tomlin, T. Langer, *Org. Process Res. Dev.* **2022**, 26, 2337−2350.

92. W. Deng, L. Liu, C. Zhang, M. Liu, Q. X. Guo, *Tetrahedron Lett.* **2005**, *46*, 7295–7298.

93. D. Steinhuebel, M. Palucki, D. Askin, U. Dolling, T*etrahedron Lett.* **2004**, *45*, 3305–3307.

94. X. J. Han, *Tetrahedron Lett.* **2010**, *51*, 360–362.

95. J. Baffoe, M. Y. Hoe, B. B. Toure, *Org. Lett.* **2010**, *12*, 1532–1535.

96. X. Wang, A. Guram, M. Ronk, J. E. Milne, J. S. Tedrow, M. M. Faul, *Tetrahedron Lett.* **2012**, *53*, 7–10.

97. Q. Li, L. Xu, D. Ma, *Angew. Chem. Int. Ed.* **2022**, *61*, e202210483.

98. S. M. Crawford, C. B. Lavery, M. Stradiotto, *Chem. Eur. J.* **2013**, *19*, 16760–16771.

99. J. D. Laffoon, V. S. Chan, M. G. Fickes, B. Kotecki, A. R. Ickes, J. Henle, J. G. Napolitano, T. S. Franczyk, T. B. Dunn, D. M. Barnes, A. R. Haight, R. F. Henry, S.

Shekhar, *ACS Catal*. **2019**, *9*, 11691−11708.

100. P. Anjanappa, D.Mullick, K. Selvakumar, M. Sivakumar, *Tetrahedron Lett.* **2008**, *49*, 4585–4587.

101. J. D. Hicks, A. M. Hyde, A. M. Cuezva, S. L. Buchwald, *J. Am. Chem. Soc.* **2009**, *131*, 16720–16734.

102. T. Kim, S. J. McCarver, C. Lee, D. W. C. MacMillan, *Angew. Chem. Int. Ed.* **2018**, *57*, 3488–3492.

103. C. Cavedon, S. Gisbertz, S. Reischauer, S. Vogl, E. Sperlich, J. H. Burke, R. F. Wallick, S. Schrottke, W.-H. Hsu, L. Anghileri, Y. Pfeifer, N. Richter, C. Teutloff, H. Müller-Werkmeister, D. Cambié, P. H. Seeberger, J. Vura-Weis, R. M. van der Veen, A. Thomas, B. Pieber, *Angew. Chem. Int. Ed.* **2022**, *61,* e202211433.

104. T.-T. Zhao, H.-N. Qin, P.-F. Xu, *Org. Lett.* **2023**, *25*, 636−641.

105. C. Zhu, A. P. Kale, H. Yue, M. Rueping, *JACS Au* **2021**, *1*, 1057–1065.

106. R. T. McGuire, C. M. Simon, A. A. Yadav, M. J. Ferguson, M. Stradiotto, *Angew. Chem. Int. Ed*. **2020**, *59*, 8952–8956.

107. T. You, J. Li, *Org. Lett.* **2022**, *24*, 6642−6646.

108. C. M. Lavoie, P. M. MacQueen, M. Stradiotto, *Chem. Eur. J.* **2016**, *22*, 18752–18755.

109. J. Schranck, P. Furer, V. Hartmann, A. Tlili, *Eur. J. Org. Chem.* **2017**, 3496–3500.

110. In *Comprehensive Organometallic Chemistry IV,* Elsevier Ltd, **2022**, pp. 555–582.

111. J. Becica, G. E. Dobereiner, *ACS Catal*. **2017**, *7*, 5862−5870.

112. Q. Shen, J. F. Hartwig, *J. Am. Chem. Soc.* **2007**, *129*, 7734−35.

113. S. Sharif, J. Day, H. N. Hunter, Y. Lu, D. Mitchell, M. J. Rodriguez, M. G. Organ, *J. Am. Chem. Soc.* **2017**, *139*, 18436−18439.

Appendices

Appendix A. Supporting Figures and Tables

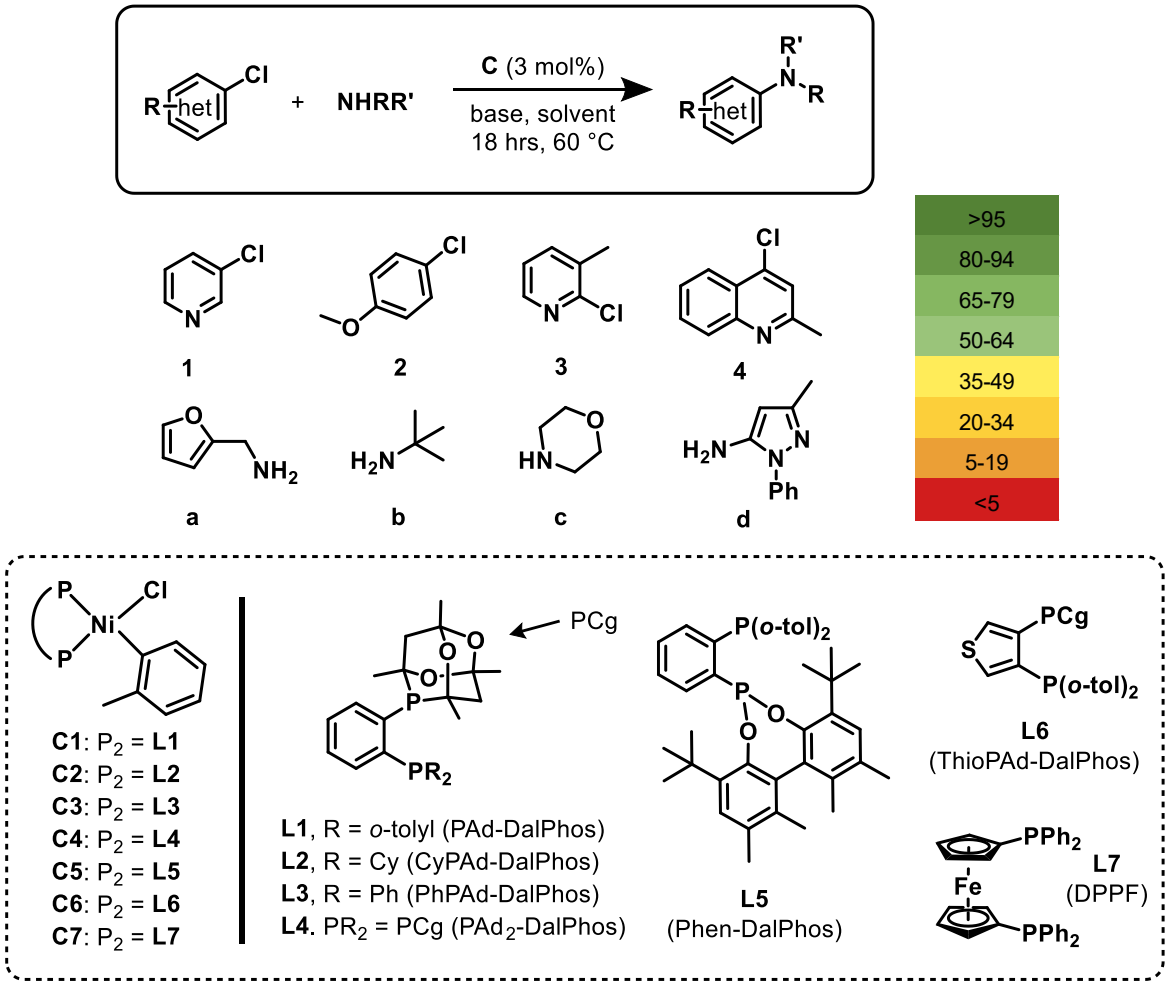

Figure S1. Substrates and ligands/pre-catalysts examined in the comparative catalytic screening of the Ni-catalyzed C–N cross-coupling of (hetero)aryl chlorides with NH substrates, showing the legend for the heat-map featured in the manuscript. The ligands used herein are reported in the references, [31, 33, 40, 41, 44, 62, 63] and compounds **2a**,[63] **2c**,[31] **4a**,[31] and **4c**[31] were prepared according to literature methods.

			NaO*t*Bu				K_2CO_3				DBU/NaTFA			
			a	**b**	**c**	**d**	**a**	**b**	**c**	**d**	**a**	**b**	**c**	**d**
C1	toluene	**1**	78	<5	<5	59	<5	<5	<5	14	19	<5	<5	31
		2	64	11	6	83	<5	<5	<5	<5	<5	<5	<5	16
		3	>95	<5, †	<5, †	21	9	<5	<5	36	>95	<5	11	65
		4	88	5	12	6	6	<5	<5	26	>95	<5	<5	69
	1,4-dioxane	**1**	35	<5	7	29	<5	<5	<5	22	5	<5	<5	15
		2	53	<5	<5	62	<5	<5	<5	<5	<5	<5	<5	<5
		3	81	<5, †	10, †	55	6	<5	<5	17	61	<5	12	39
		4	>95	<5	9	48	75	<5	<5	<5	>95	<5	<5	60
C2	toluene	**1**	>95	13	11	>95	<5	<5	<5	<5	<5	<5	<5	5
		2	83	<5	13	8	<5	<5	<5	<5	<5	<5	<5	<5
		3	>95	<5, †	<5, †	>95	12	<5	<5	90	21	<5	7	86
		4	>95	12	10	25	<5	<5	<5	62	8	<5	<5	44
	1,4-dioxane	**1**	>95	<5	<5	>95	<5	<5	<5	<5	<5	<5	<5	<5
		2	88	<5	<5	8	<5	<5	<5	<5	<5	<5	<5	<5
		3	>95	<5, †	<5, †	>95	<5	<5	<5	76	12	<5	<5	50
		4	>95	<5	7	37	8	<5	<5	43	7	<5	<5	39
C3	toluene	**1**	>95	<5	15	69	<5	<5	<5	<5	<5	<5	<5	<5
		2	65	<5	18	16	<5	<5	<5	<5	<5	<5	<5	<5
		3	>95	<5, †	24, †	47	<5	<5	<5	51	38	<5	<5	>95
		4	>95	20	25	93	>95	<5	<5	5	38	<5	<5	>95
	1,4-dioxane	**1**	>95	33	11	>95	<5	<5	<5	5	<5	<5	<5	<5
		2	81	9	54	12	<5	<5	<5	<5	<5	<5	<5	<5
		3	>95	<5, †	26	88	19	<5	<5	35	29	<5	<5	48
		4	>95	<5	13	>95	82	<5	<5	61	59	<5	<5	>95
C4	toluene	**1**	76	8	<5	70	10	<5	<5	45	21	<5	<5	60
		2	75	17	18	>95	<5	<5	<5	<5	<5	<5	<5	28
		3	>95	<5, †	<5, †	>95	15	<5	<5	46	>95	<5	<5	88
		4	>95	5	11	59	63	<5	<5	61	>95	<5	<5	>95
	1,4-dioxane	**1**	57	<5	7	>95	11	<5	<5	31	5	<5	<5	37
		2	85	<5	<5	>95	<5	<5	<5	<5	<5	<5	<5	<5
		3	>95	<5, †	<5, †	>95	13	<5	<5	8	92	<5	<5	55
		4	>95	<5	<5	41	70	<5	<5	49	>95	<5	<5	>95
C5	toluene	**1**	77	<5	13	43	<5	<5	<5	<5	<5	<5	<5	<5
		2	20	9	13	24	<5	<5	<5	7	<5	<5	<5	20
		3	>95	<5	26	42	<5	<5	<5	6	>95	<5	<5	>95
		4	>95	7	42	26	16	<5	<5	11	37	<5	<5	72
	1,4-dioxane	**1**	26	<5	<5	>95	<5	<5	<5	<5	<5	<5	<5	<5
		2	29	<5	<5	58	<5	<5	<5	<5	<5	<5	<5	<5
		3	>95	<5, †	<5, †	85	<5	<5	<5	<5	5	<5	<5	65
		4	>95	<5	8	90	26	<5	<5	28	13	<5	<5	15
C6	toluene	**1**	>95	<5	8	72	<5	<5	<5	15	<5	<5	<5	<5
		2	75	11	10	>95	<5	<5	<5	19	<5	<5	<5	<5
		3	>95	<5, †	<5, †	6	<5	<5	<5	<5	52	<5	<5	23
		4	>95	9	17	40	17	<5	<5	>95	57	<5	<5	17
	1,4-dioxane	**1**	58	<5	<5	94	<5	<5	<5	30	<5	<5	<5	<5
		2	75	<5	<5	>95	<5	<5	<5	15	<5	<5	<5	<5
		3	>95	<5, †	<5, †	33	<5	<5	<5	14	35	<5	<5	24
		4	>95	<5	7	73	86	<5	<5	>95	82	<5	<5	22
C7	toluene	**1**	18	<5	22	<5	<5	<5	<5	<5	<5	<5	<5	<5
		2	<5	<5	9	<5	<5	<5	<5	<5	<5	<5	<5	<5
		3	18	<5	14	<5	<5	<5	<5	<5	<5	<5	<5	<5
		4	>95	13	91	>95	<5	<5	<5	<5	<5	<5	<5	<5
	1,4-dioxane	**1**	15	<5	27	<5	<5	<5	<5	<5	<5	<5	<5	<5
		2	<5	<5	15	<5	<5	<5	<5	<5	<5	<5	<5	<5
		3	18	<5	5	9	<5	<5	<5	<5	<5	<5	<5	<5
		4	>95	12	>95	>95	<5	<5	<5	<5	<5	<5	<5	<5

Figure S2. Grey-scale version of the conversion heat-map featured in the comparative catalytic screening of the Ni-catalyzed C–N cross-coupling of (hetero)aryl chlorides with NH substrates (Figure 2.2). The symbol † denotes the presence of products arising from competing C–O cross-coupling involving the *tert*-butoxide base.

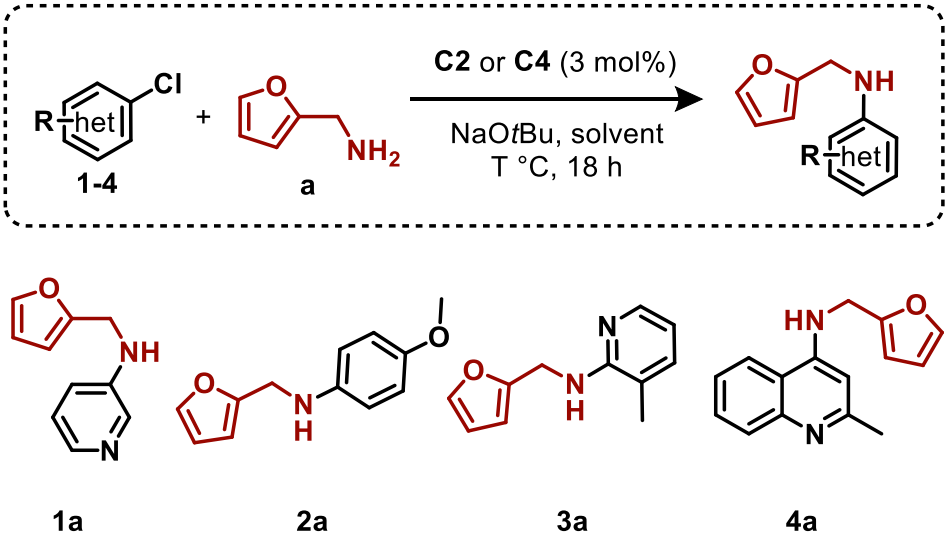

			1a (%)	2a (%)	3a (%)	4a (%)
C2	25 °C	toluene	>95, 94[b]	51, 36[b]	>95[a], >95[b]	>95, >95[b]
		1,4-dioxane	86	66	>95	>95
	60 °C	toluene	>95	83	>95	>95
		1,4-dioxane	>95	88	>95	>95
C4	25 °C	toluene	56	59	>95	>95
		1,4-dioxane	57	66	>95	>95
	60 °C	toluene	76	75	>95	>95
		1,4-dioxane	57	85	>95	>95

Table S1. Reaction optimization for the Ni-catalyzed C–N cross-coupling of **1**–**4** with furfurylamine **a**. Reactions were conducted on a 0.12 mmol scale using **C2** or **C4** following **GSP**. Yields determined on the basis of response-factor-calibrated GC data using authentic material, with remaining mass balance corresponding to unreacted starting material. [a]Reaction reached completion within 30 minutes. [b]Using 1 mol% of **C2** and 1.5 equivalents of NaO*t*Bu.

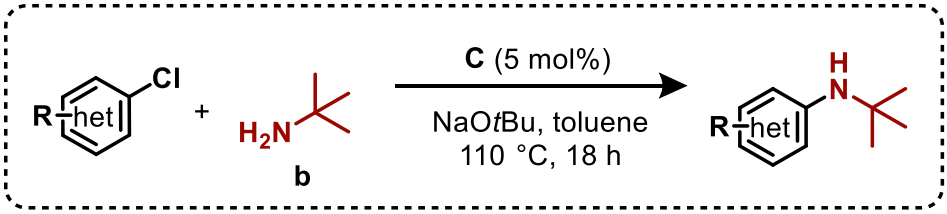

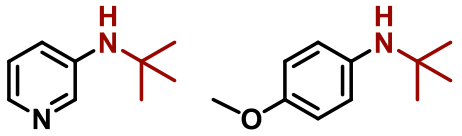

1b **2b**

pre-catalyst	**1b** (%)	**2b** (%)
C1	<5	5
C2	10	5
C3	>95	30, 90[a]
C4	<5	16
C7	>95	NA

Table S2. Temperature and loading screens for the Ni-catalyzed C–N cross-coupling of **1** with *tert*-butylamine **b** (5 mol% Ni, 110 °C, unless stated). Reactions were conducted on a 0.12 mmol scale following **GSP**. Yields determined on the basis of response-factor-calibrated GC data using authentic material, with remaining mass balance corresponding to unreacted starting material. [a]Reactions conducted using 10 mol% of **C3** at 120 °C.

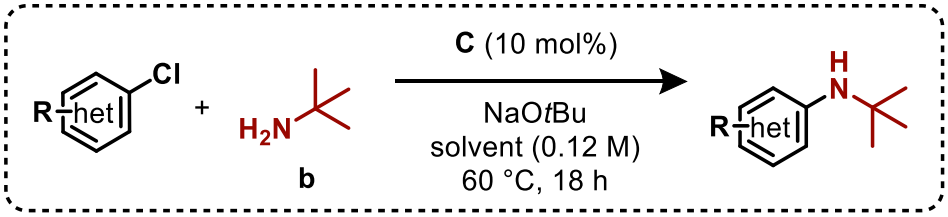

		1b (%)		2b (%)	
		3 mol% **C**	10 mol% **C**	3 mol% **C**	10 mol% **C**
C3	toluene	<5	85	<5	17
	1,4-dioxane	33	68	9	12
C4	toluene	8	<5	17	50
	1,4-dioxane	<5	<5	<5	<5
C5	toluene	<5	9	9	8
	1,4-dioxane	<5	<5	<5	<5
C6	toluene	<5	<5	11	12
	1,4-dioxane	<5	<5	<5	<5

Table S3. Loading screens for the Ni-catalyzed C–N cross-coupling of **1** and **2** with *tert*-butylamine **b** at 60 °C. Reactions were conducted on a 0.12 mmol scale using **C3**, **C4**, **C5**, and **C6** following **GSP**. Yields determined on the basis of response-factor-calibrated GC data using authentic material, with remaining mass balance corresponding to unreacted starting material.

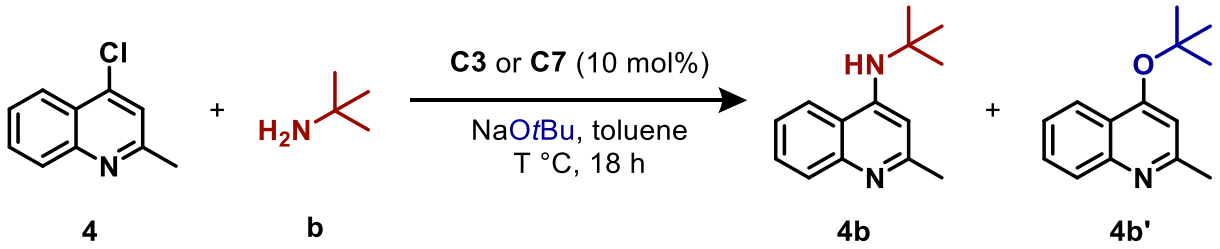

4 **b** **4b** **4b'**

pre-catalyst	equiv *t*BuNH$_2$	equiv NaO*t*Bu	T (°C)	**4b** (%)	**4b'** (%)
C3	3.0	1.1	25	57	<5
C3	3.0	1.5	25	65	<5
C3	3.0	1.1	60	46	11
C3	3.0	1.5	60	58	9
C3	3.0	1.1	80	39	18
C3	3.0	1.5	80	39	32
C3	1.1	2.0	120	16[a]	49[a]
C3	5.0	2.0	120	28	<5
C7	5.0	2.0	120	85	<5

Table S4. Competitive Ni-catalyzed C–N and C–O cross-coupling of **4** with *tert*-butylamine **b** and NaO*t*Bu, exploring stoichiometry and temperature. Reactions were conducted on a 0.12 mmol scale using **C3** or **C7** following **GSP**. Yields determined on the basis of response-factor-calibrated GC data using authentic material, with remaining mass balance corresponding to unreacted starting material. [a]Isolated yields following **GP1**, purified by flash column chromatography (**4b'** obtained with 100% EtOAc, **4b** obtained upon flushing with 100% MeOH).

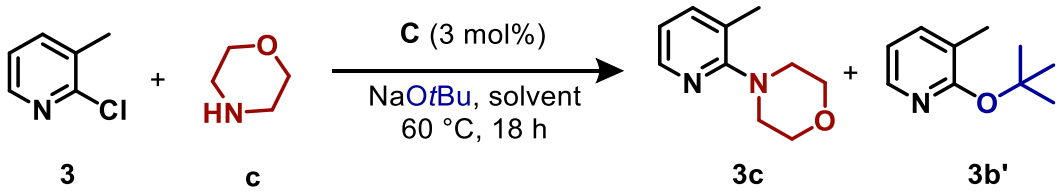

		3c (%)	3b' (%)
C1	toluene	<5, <5[a]	38, 56[a]
	1,4-dioxane	10	18
C2	toluene	<5, 6[a]	18, 46[a]
	1,4-dioxane	<5	8
C3	toluene	24, 41[a]	21, 37[a]
	1,4-dioxane	26	<5
C4	toluene	<5, <5[a]	>95, 94[a]
	1,4-dioxane	<5	13
C5	toluene	26	<5
	1,4-dioxane	<5	9
C6	toluene	<5	11
	1,4-dioxane	<5	17
C7	toluene	14, 27[a], 66[b]	<5, <5[a], <5[b]
	1,4-dioxane	5	<5

Table S5. Competitive Ni-catalyzed C–N and C–O cross-coupling of **3** with morpholine **c**. Reactions were conducted on a 0.12 mmol scale following **GSP**. Yields determined on the basis of response-factor-calibrated GC data using authentic material, with remaining mass balance corresponding to unreacted starting material. [a]Reactions conducted using 5 mol% **C** at 110 °C. [b]Reaction conducted using 10 mol% of **C7** at 120 °C.

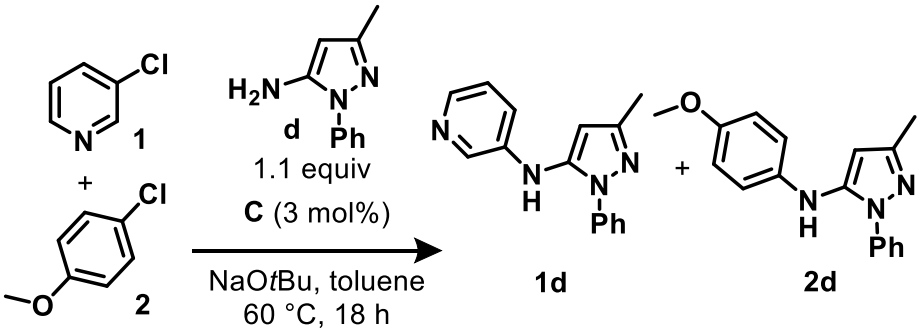

pre-catalyst	**1** (% remaining)	**2** (% remaining)	product ratio **1d:2d**
C2	22	83	>25:1
C4	17	87	16:1

Table S6. Electrophile competition experiments for **1** *vs* **2** with 5-amino-3-methyl-1-phenylpyrazole **d** using **C2** and **C4**. Reactions were conducted following **GCP** and yields were determined on the basis of response-factor-calibrated GC data using authentic material.

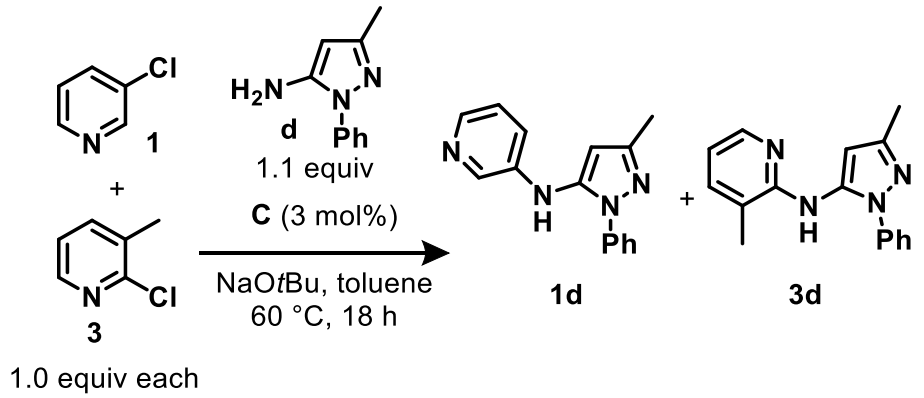

pre-catalyst	**1** (% remaining)	**3** (% remaining)	product ratio **1d:3d**
C2	25	85	3.3:1
C6	>95%	88	1:>25

Table S7. Electrophile competition experiments for the cross-coupling of **1** *vs* **3** with 5-amino-3-methyl-1-phenylpyrazole **d** using **C2** and **C6**. Reactions were conducted following **GCP** and yields were determined on the basis of response-factor-calibrated GC data using authentic material.

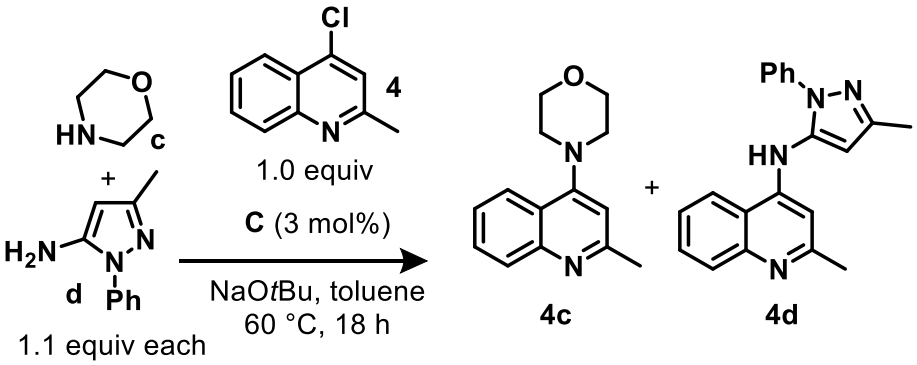

pre-catalyst	**4** (% remaining)	ratio **4c:4d**
C2	84	1:11.5
C7	14	1:12.5

Table S8. Nucleophile competition experiments for the cross-coupling of **4** with morpholine **c** *vs* 5-amino-3-methyl-1-phenylpyrazole **d** using **C2** and **C7**. Reactions were conducted following **GCP** and yields were determined on the basis of response-factor-calibrated GC data using authentic material.

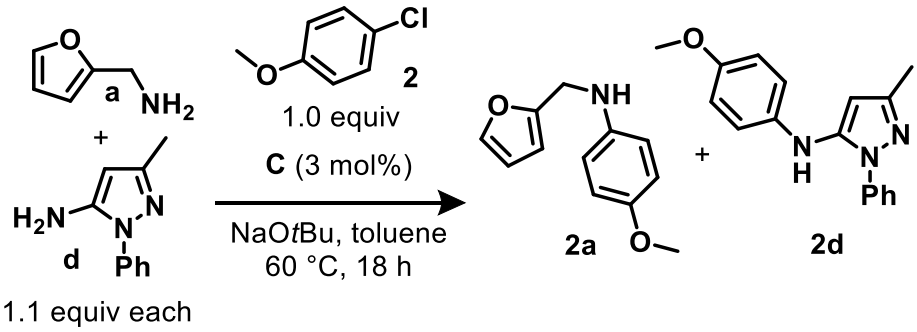

pre-catalyst	**2** (% remaining)	ratio **2a:2d**
C3	23	1:>25
C4	<5	1:>25

Table S9. Nucleophile competition experiments for the cross-coupling of **2** with furfurylamine **a** *vs* 5-amino-3-methyl-1-phenylpyrazole **d** using **C3** and **C4**. Reactions were conducted following **GCP** and yields were determined on the basis of response-factor-calibrated GC data using authentic material.

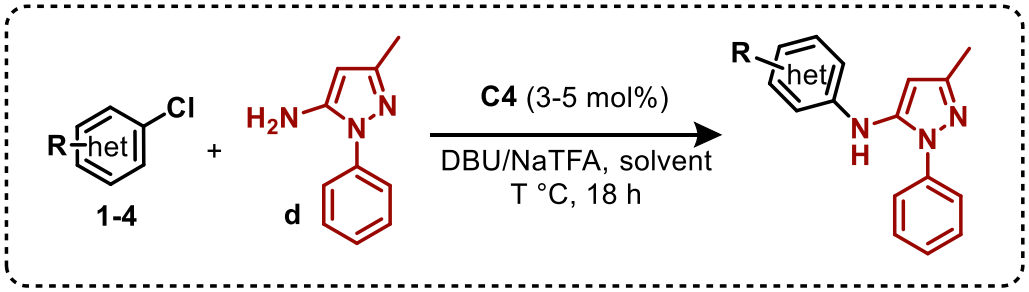

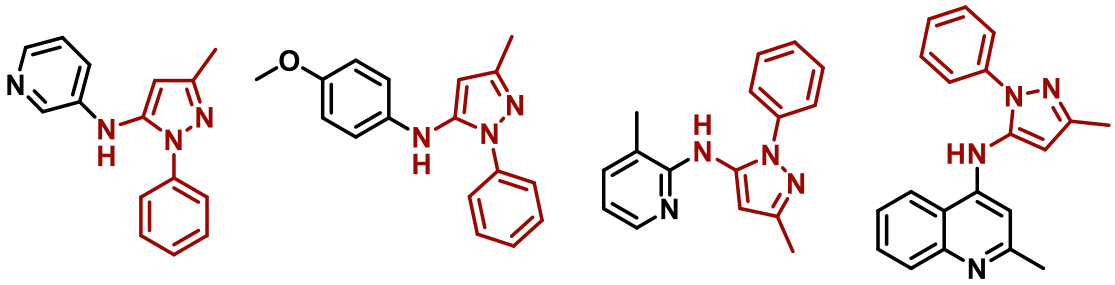

1d **2d** **3d** **4d**

		1d (%)	**2d** (%)	**3d** (%)	**4d** (%)
60 °C 3 mol% **C4**	toluene	60%	28%	88%	>95%
	1,4-dioxane	37%	<5%	55%	>95%
80 °C 5 mol% **C4**	toluene	90%	27%	74%	>95%
	1,4-dioxane	92%	20%	>95%	>95%

Table S10. Reaction optimization for the Ni-catalyzed C–N cross-coupling of electrophiles **1** through **4** with 5-amino-3-methyl-1-phenylpyrazole **d**. Reactions were conducted on a 0.12 mmol scale using **C4** following **GSP**. Yields determined on the basis of response-factor-calibrated GC data using authentic material, with remaining mass balance corresponding to unreacted starting material.

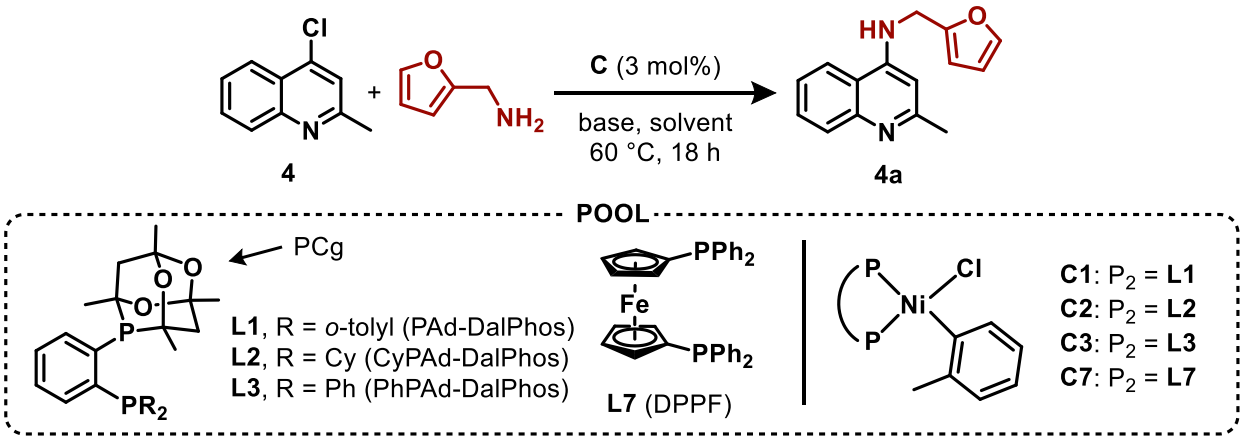

		NaO*t*Bu	K_2CO_3	DBU/NaTFA
C1+C2+C3+C7	toluene	>95	27	>95
	1,4-dioxane	>95	16	>95
C1	toluene	88	6	>95
	1,4-dioxane	>95	75	>95
C2	toluene	>95	0	8
	1,4-dioxane	>95	8	7
C3	toluene	>95	>95	38
	1,4-dioxane	>95	82	59
C7	toluene	>95	0	0
	1,4-dioxane	>95	0	0

Table S11. Attempted 'pool-and-split/deconvolution' for the nickel-catalyzed cross-coupling of **4** with furfurylamine **a** using **C1**–**C3** and **C7**. Reactions were conducted on a 0.12 mmol scale and yields were determined on the basis of response-factor-calibrated GC data using authentic material, with remaining mass balance corresponding to unreacted starting material.

Appendix B. NMR Spectra

Figure A1. ^{1}H NMR spectrum of *N*-(furan-2-ylmethyl)pyridin-3-amine, **1a** (500.1 MHz, CDCl3).

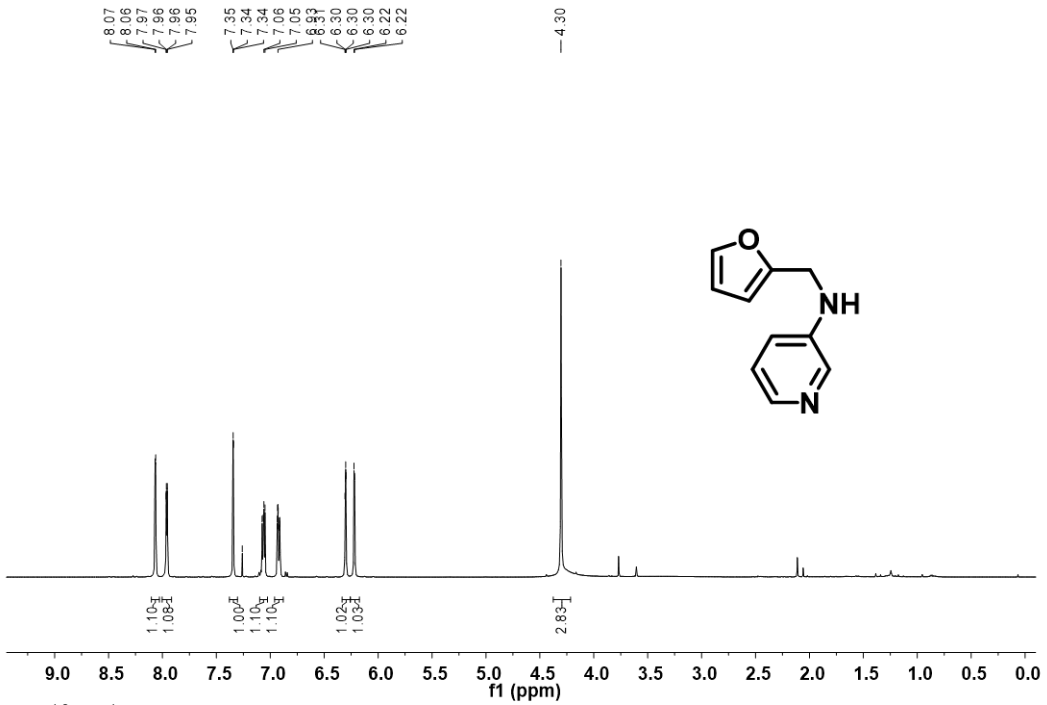

Figure A2. ^{13}C{^{1}H} UDEFT NMR spectrum of *N*-(furan-2-ylmethyl)pyridin-3-amine, **1a** (125.8 MHz, $CDCl_3$).

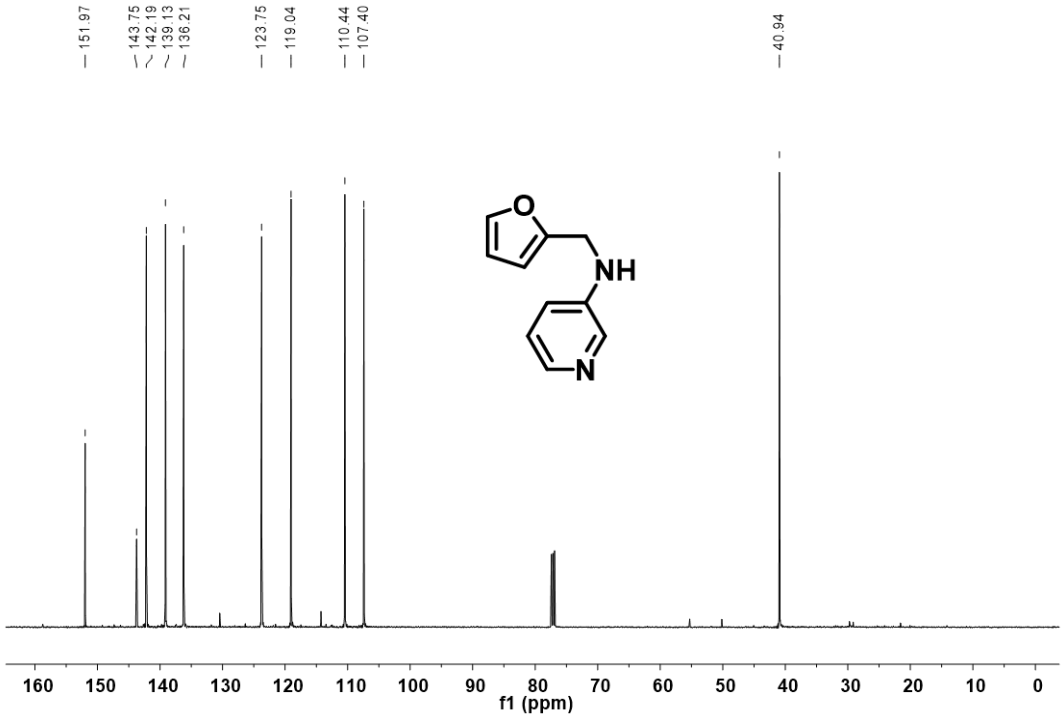

Figure A3. ^{1}H NMR spectrum of *N*-(*tert*-butyl)pyridin-3-amine, **1b** (500.1 MHz, $CDCl_3$).

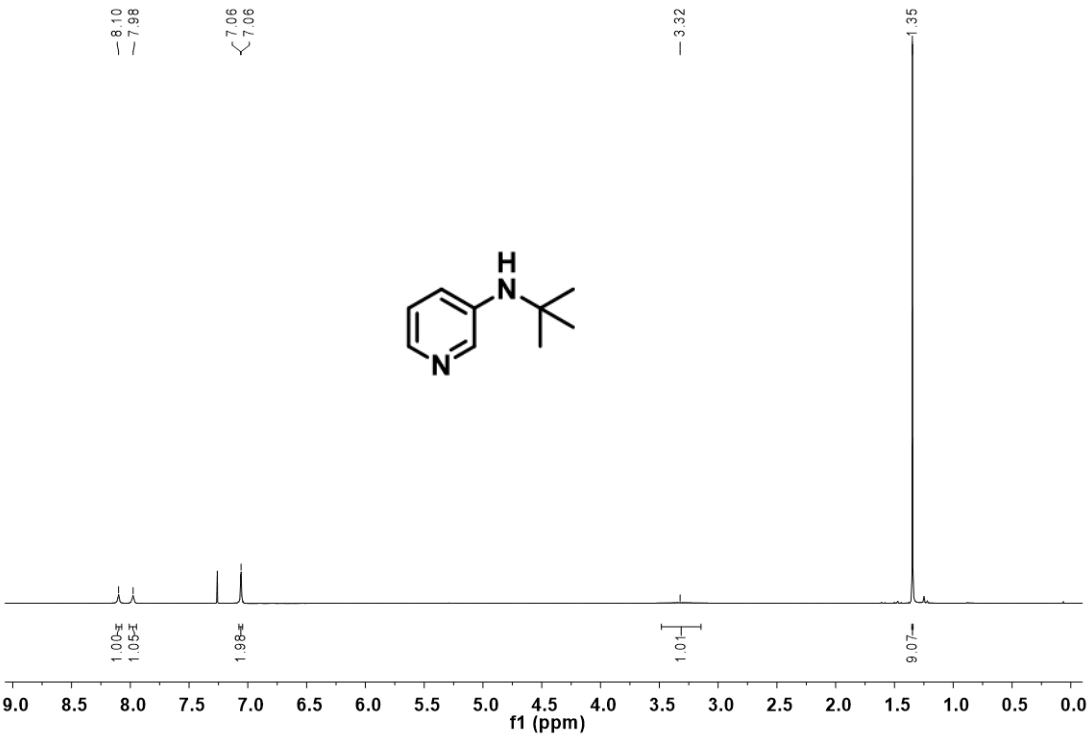

Figure A4. $^{13}C\{^{1}H\}$ UDEFT NMR spectrum of *N*-(*tert*-butyl)pyridin-3-amine, **1b** (125.8 MHz, $CDCl_3$).

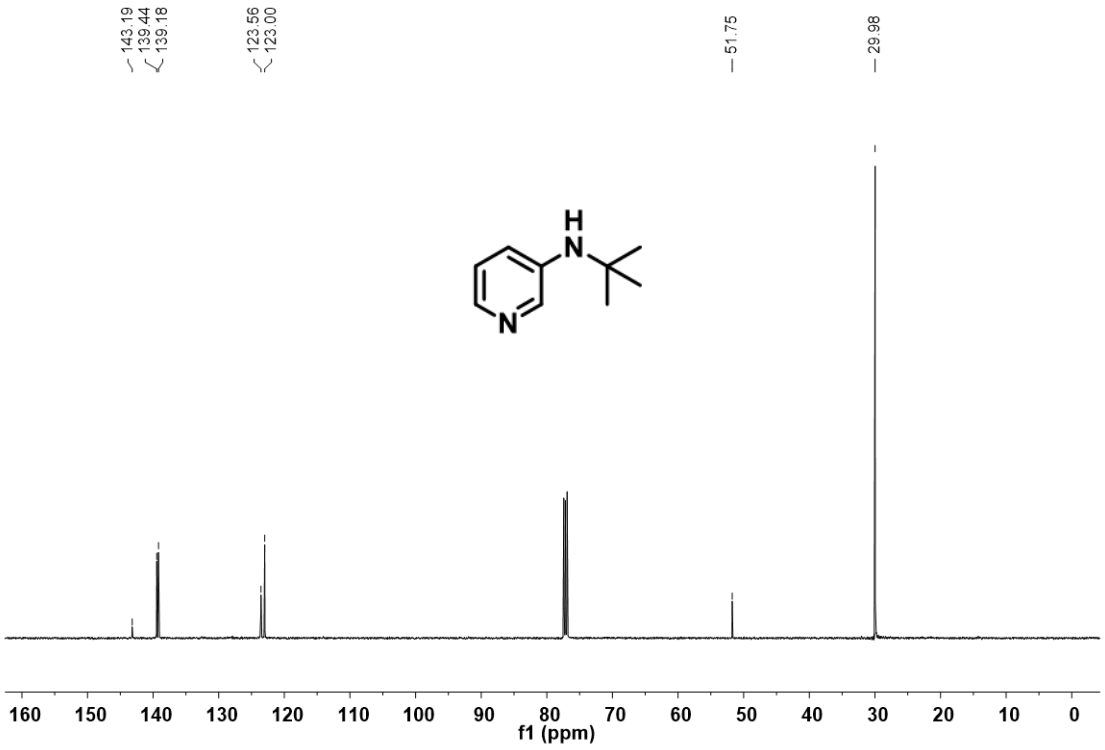

Figure A5. ^{1}H NMR spectrum of 4-(pyridin-3-yl)morpholine, **1c** (500.1 MHz, $CDCl_3$).

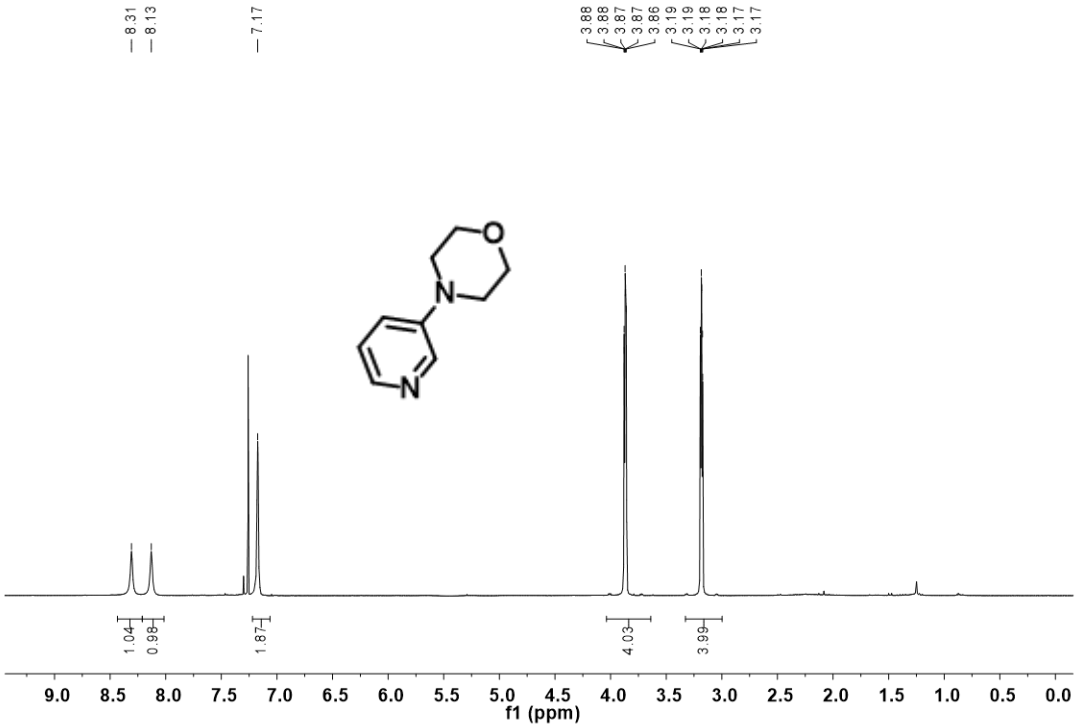

Figure A6. $^{13}C\{^{1}H\}$ UDEFT NMR spectrum of 4-(pyridin-3-yl)morpholine, **1c** (125.8 MHz, $CDCl_3$).

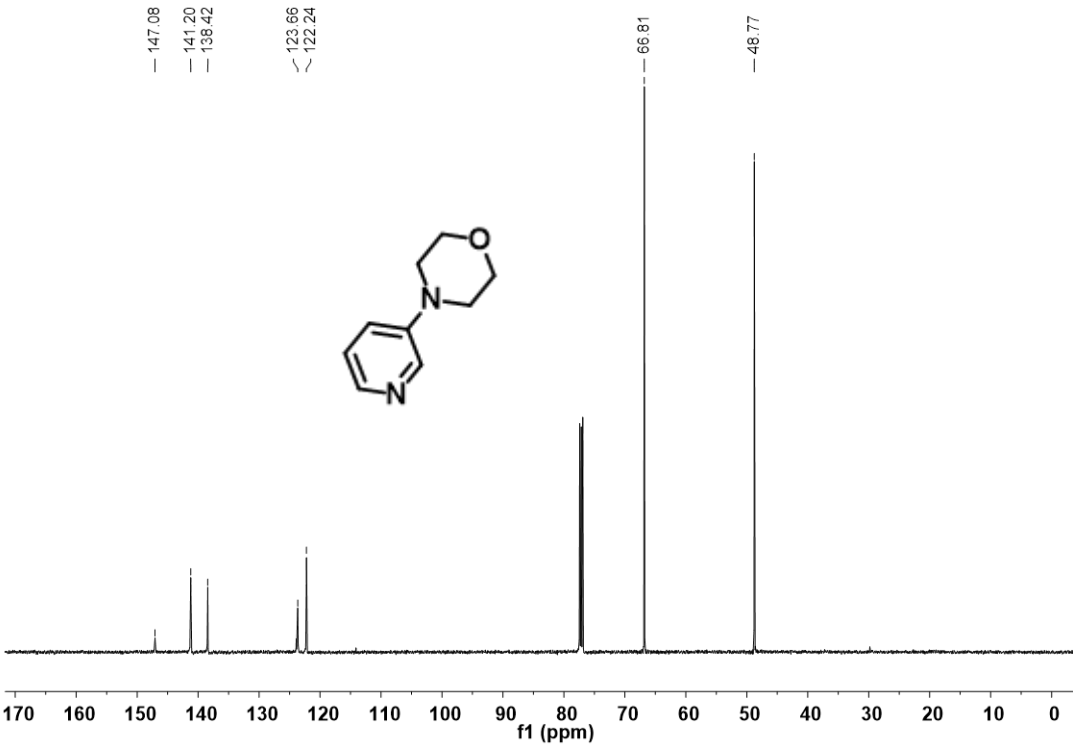

Figure A7. ^{1}H NMR spectrum of *N*-(3-methyl-1-phenyl-1*H*-pyrazol-5-yl)pyridin-3-amine, **1d** (500.1 MHz, $CDCl_3$).

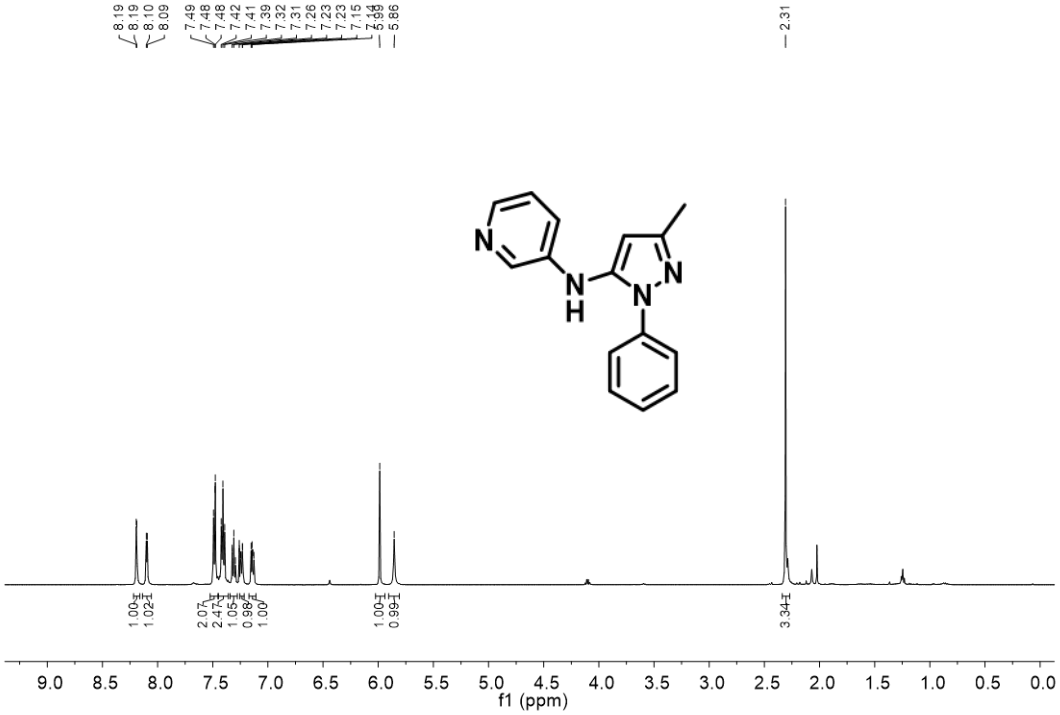

Figure A8. ^{13}C{^{1}H} UDEFT NMR spectrum of *N*-(3-methyl-1-phenyl-1*H*-pyrazol-5-yl)pyridine-3-amine, **1d** (125.8 MHz, $CDCl_3$).

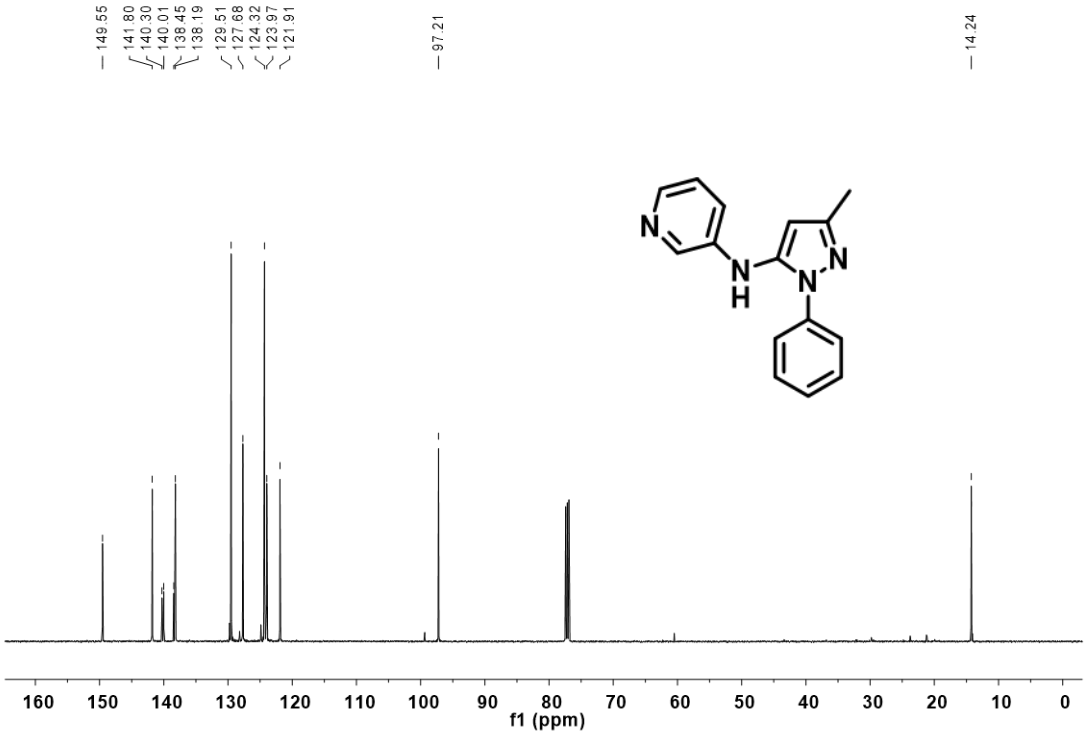

Figure A9. ^{1}H NMR spectrum of *N*-(*tert*-butyl)-4-methoxyaniline, **2b** (500.1 MHz, $CDCl_3$).

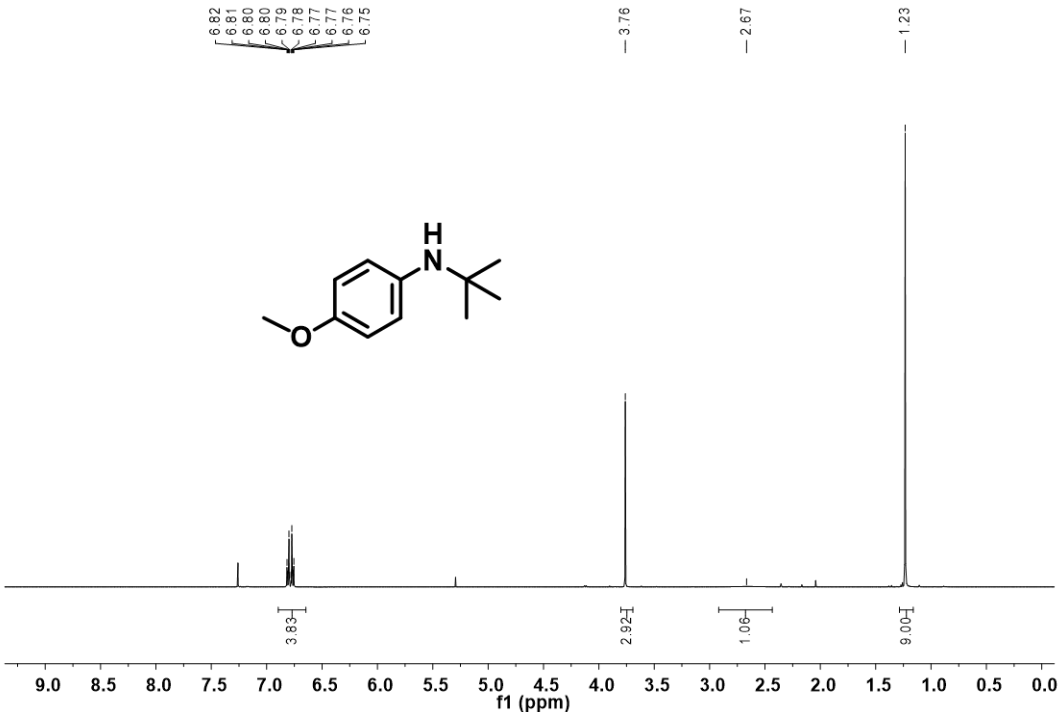

Figure A10. $^{13}C\{^{1}H\}$ UDEFT NMR spectrum of *N*-(*tert*-butyl)-4-methoxyaniline, **2b** (125.8 MHz, $CDCl_3$).

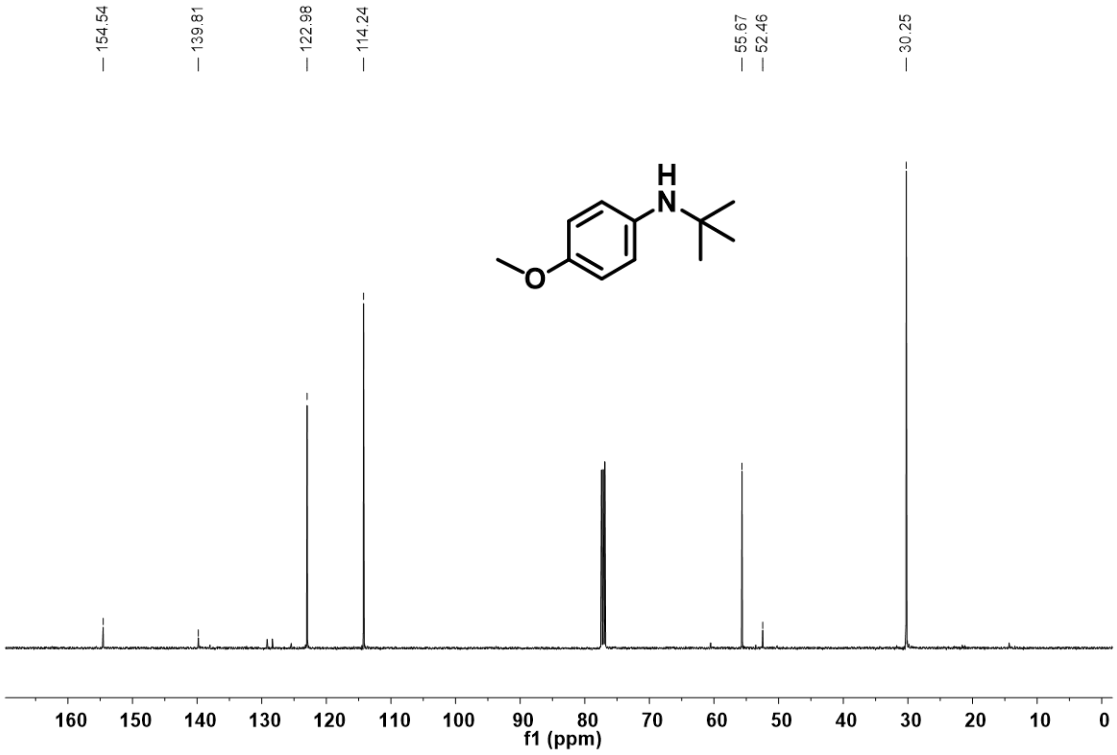

Figure A11. ^{1}H NMR spectrum of *N*-(4-methoxyphenyl)-3-methyl-1-phenyl-1*H*-pyrazol-5-amine, **2d** (500.1 MHz, $CDCl_3$).

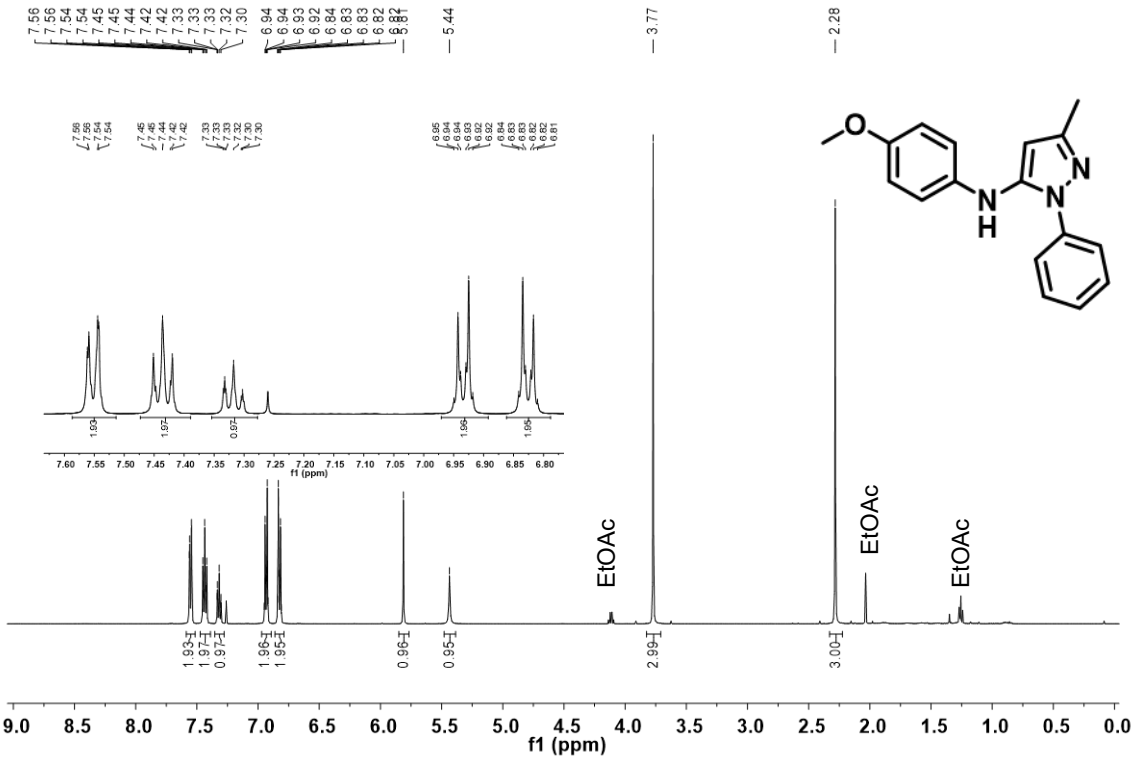

Figure A12. ^{13}C{^{1}H} UDEFT NMR spectrum of *N*-(4-methoxyphenyl)-3-methyl-1-phenyl-1*H*-pyrazol-5-amine, **2d** (125.8 MHz, $CDCl_3$).

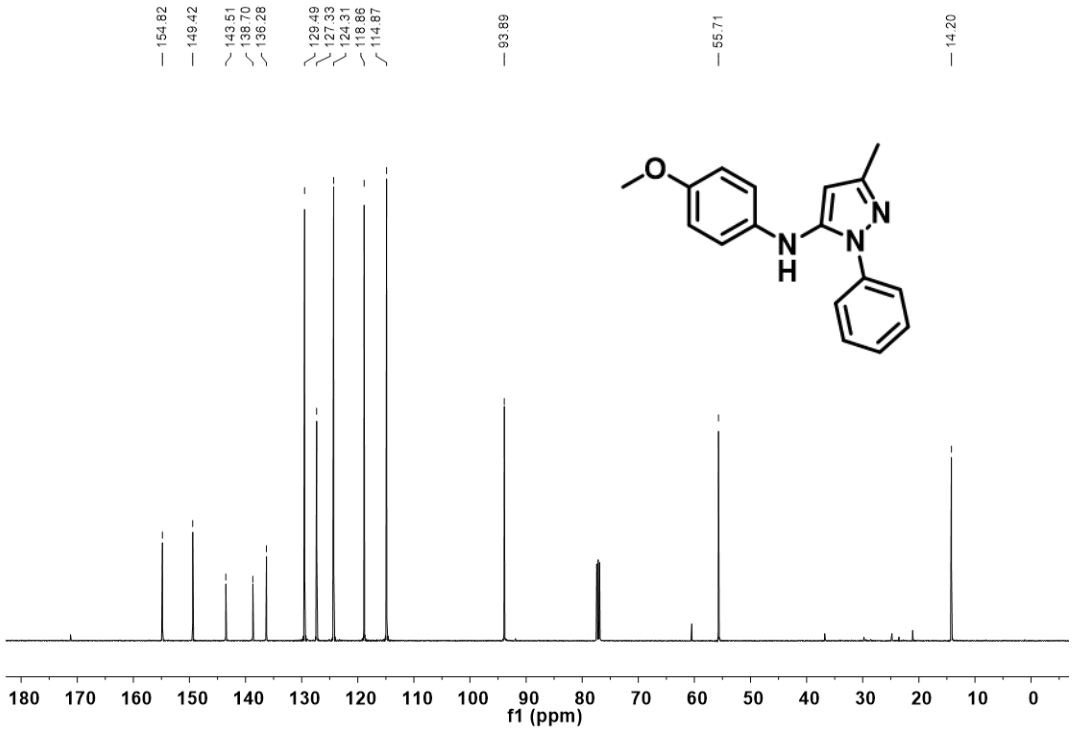

Figure A13. ^{1}H NMR spectrum of *N*-(furan-2-ylmethyl)-3-methylpyridin-2-amine, **3a** (500.1 MHz, $CDCl_3$).

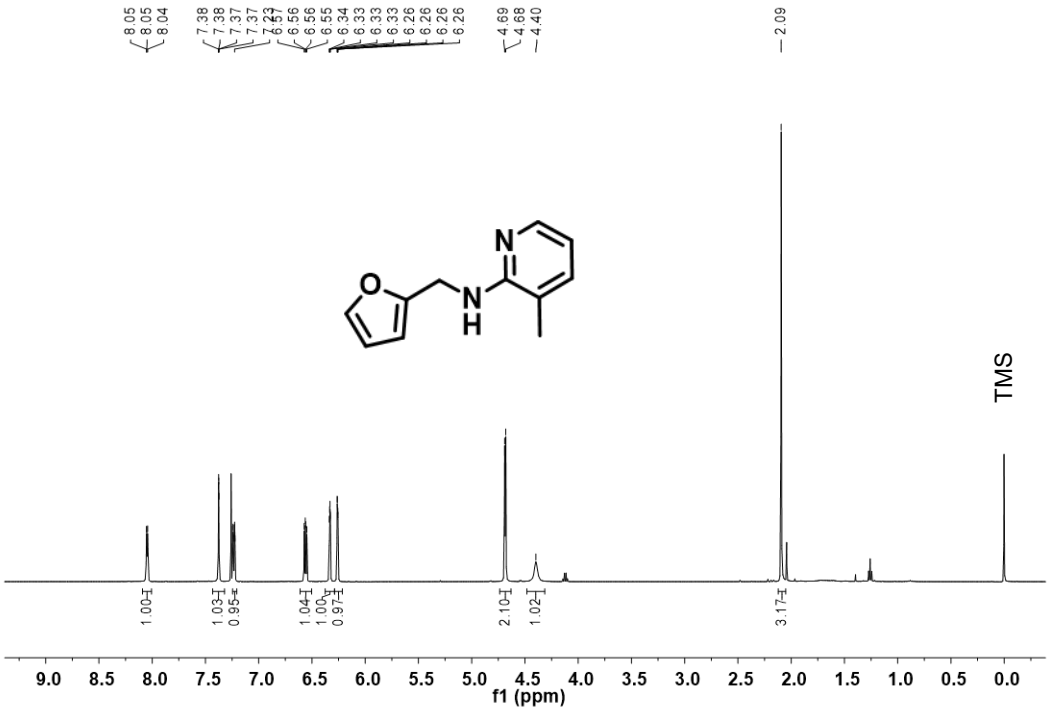

Figure A14. ^{13}C{^{1}H} UDEFT NMR spectrum of *N*-(furan-2-ylmethyl)-3-methylpyridin-2-amine, **3a** (125.8 MHz, $CDCl_3$).

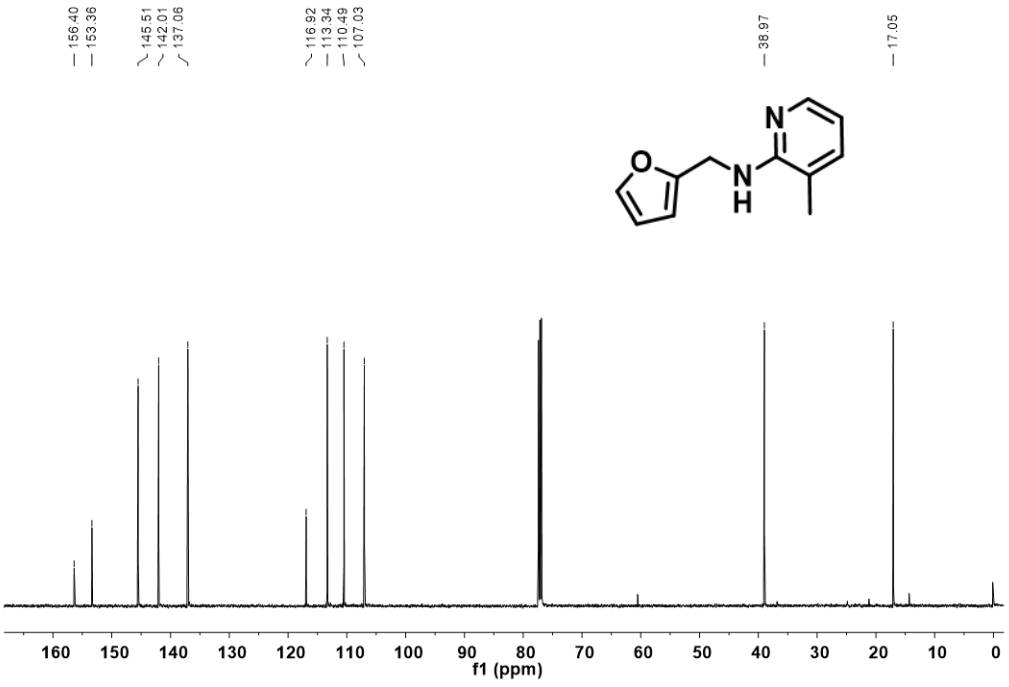

Figure A15. ^{1}H NMR spectrum of 2-(*tert*-butoxy)-3-methylpyridine, **3b'** (500.1 MHz, $CDCl_3$).

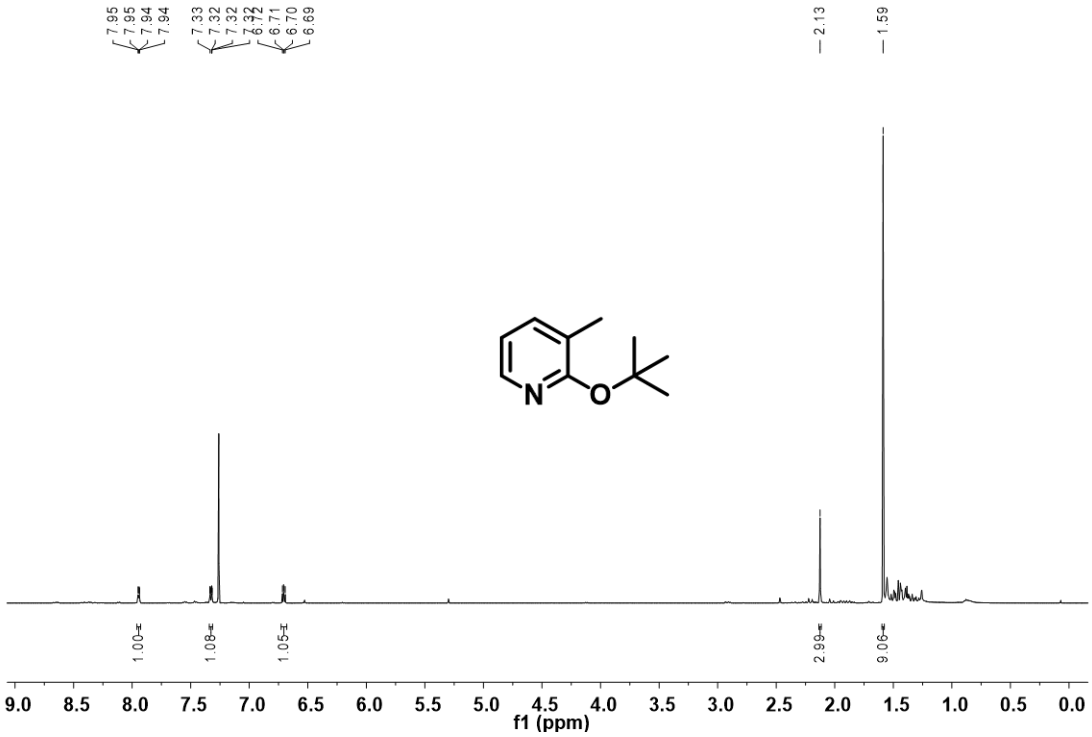

Figure A16. $^{13}C\{^{1}H\}$ UDEFT NMR spectrum of 2-(*tert*-butoxy)-3-methylpyridine, **3b'** (125.8 MHz, $CDCl_3$).

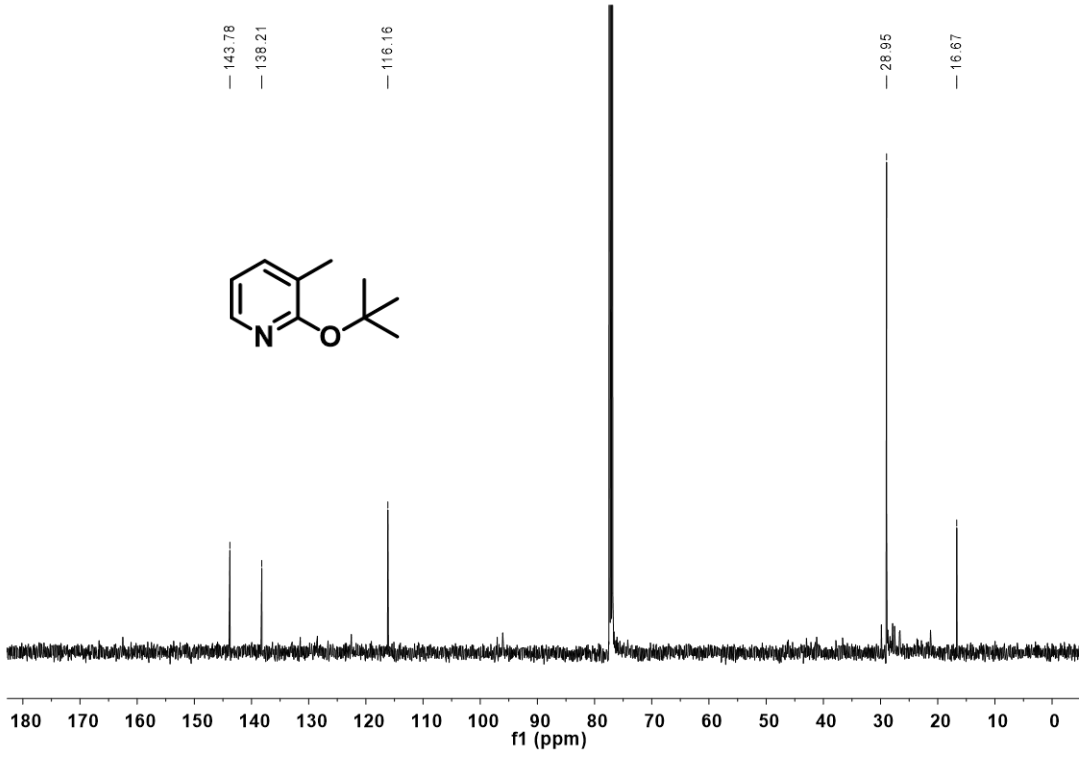

Figure A17. ^{1}H NMR spectrum of 4-(3-methylpyridin-2-yl)morpholine, **3c** (500.1 MHz, $CDCl_3$).

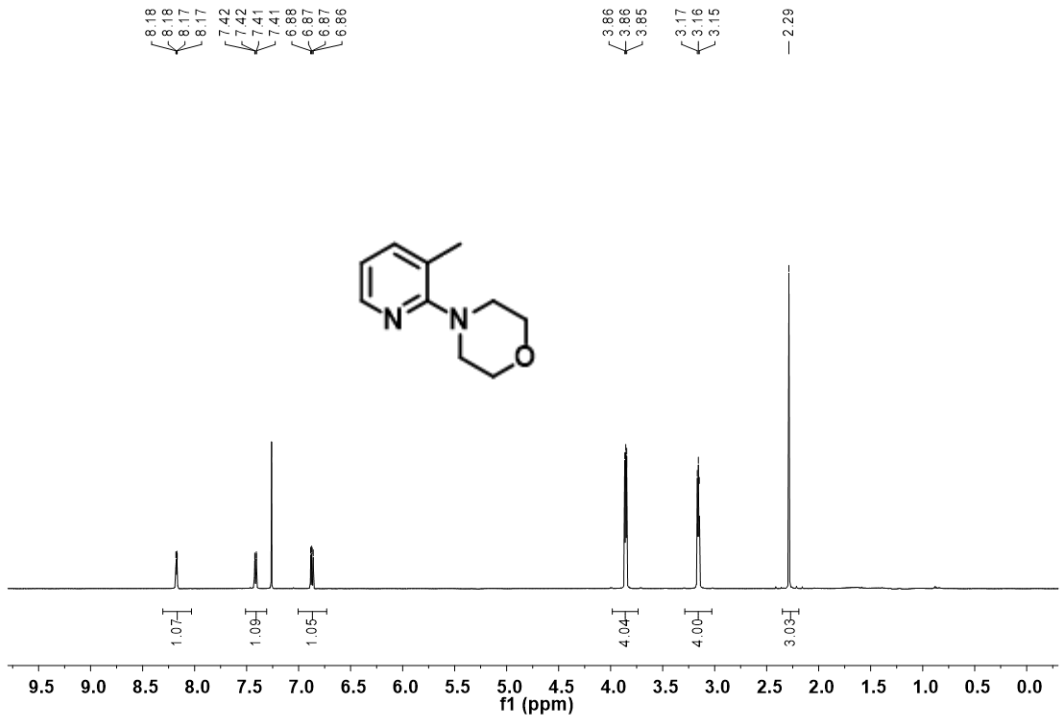

Figure A18. $^{13}C\{^{1}H\}$ UDEFT NMR spectrum of 4-(3-methylpyridin-2-yl)morpholine, **3c** (125.8 MHz, $CDCl_3$).

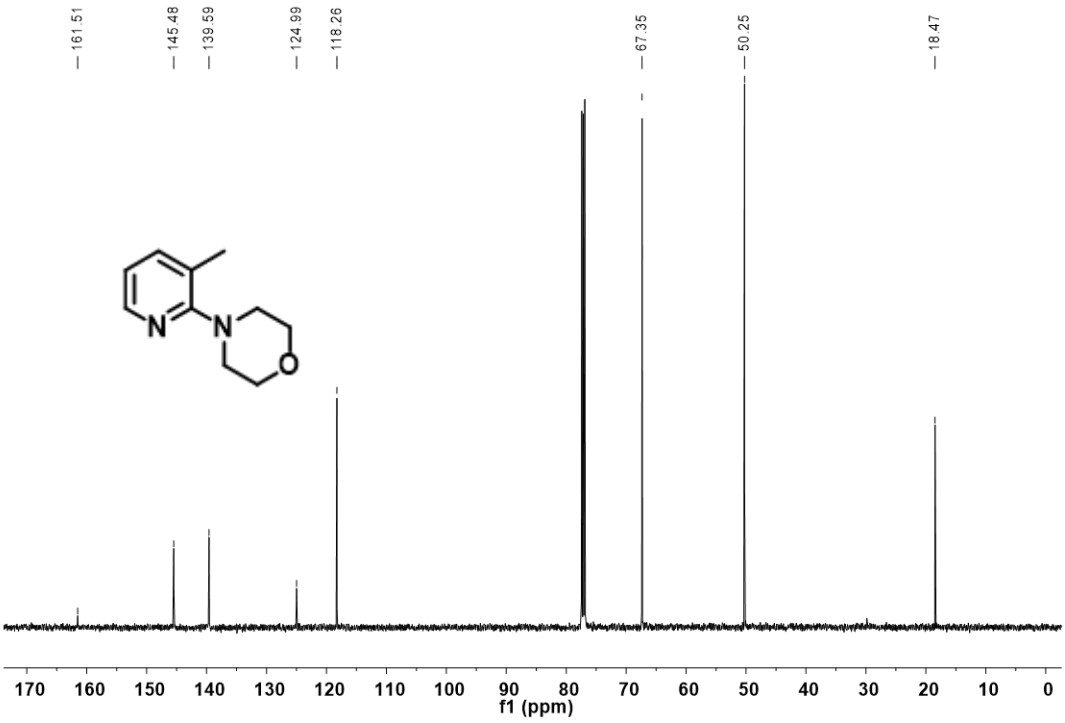

Figure A19. ^{1}H NMR spectrum of 3-methyl-*N*-(3-methyl-1-phenyl-1*H*-pyrazol-5-yl)pyridin-2-amine, **3d** (500.1 MHz, $CDCl_3$).

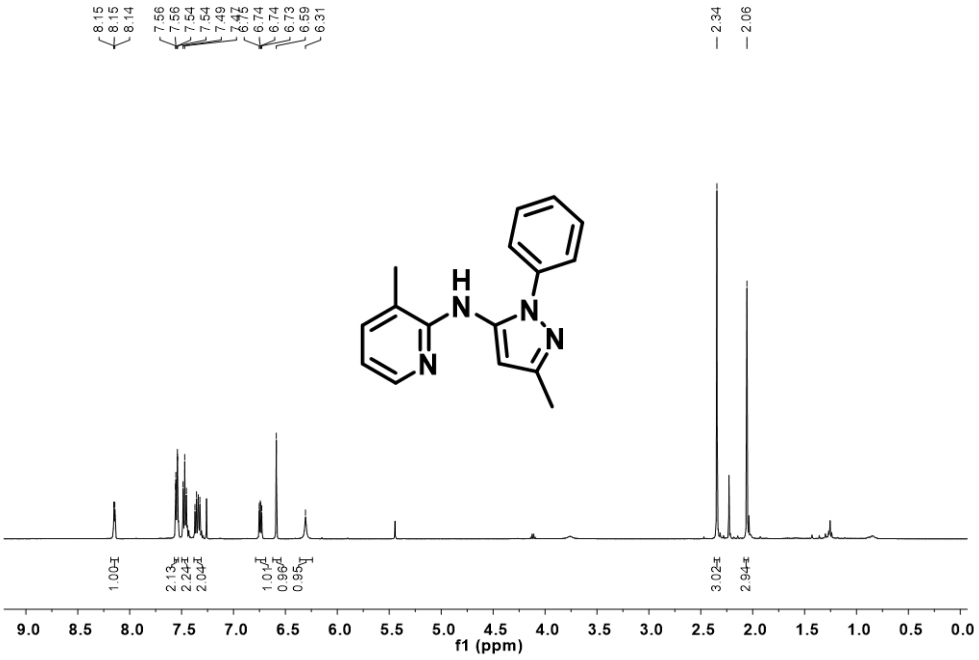

Figure A20. ^{13}C{^{1}H} UDEFT NMR 3-methyl-*N*-(3-methyl-1-phenyl-1*H*-pyrazol-5-yl)pyridin-2-amine, **3d** (125.8 MHz, $CDCl_3$).

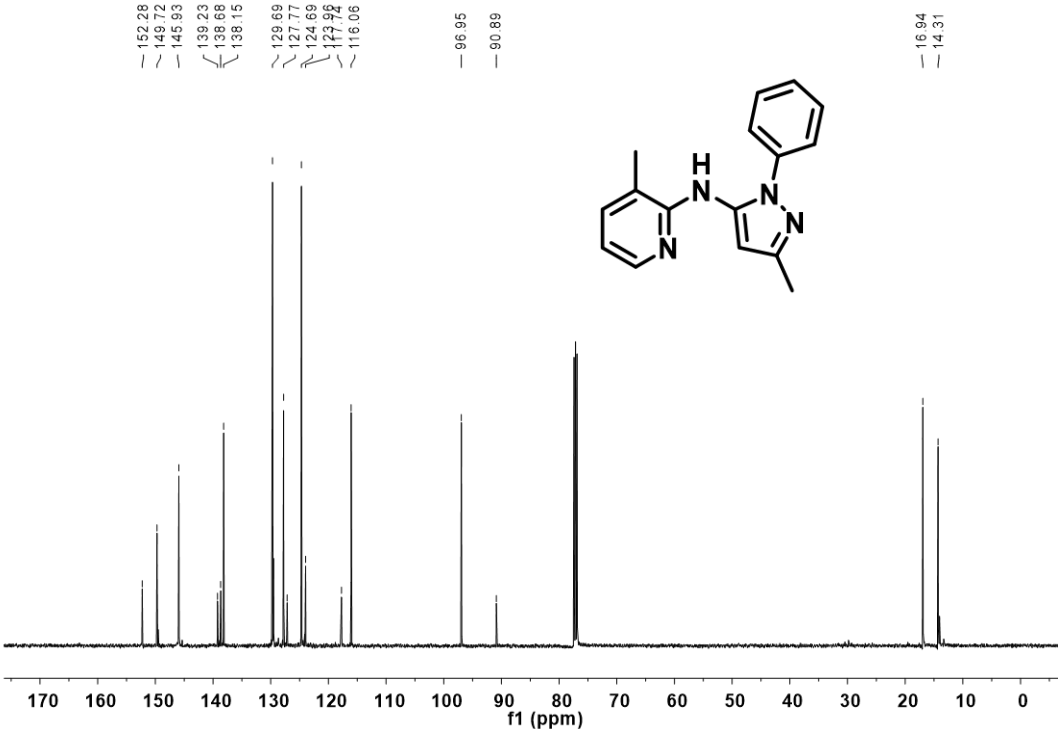

Figure A21. ^{1}H NMR spectrum of *N*-(*tert*-butyl)-2-methylquinolin-4-amine, **4b** (500.1 MHz, $CDCl_3$).

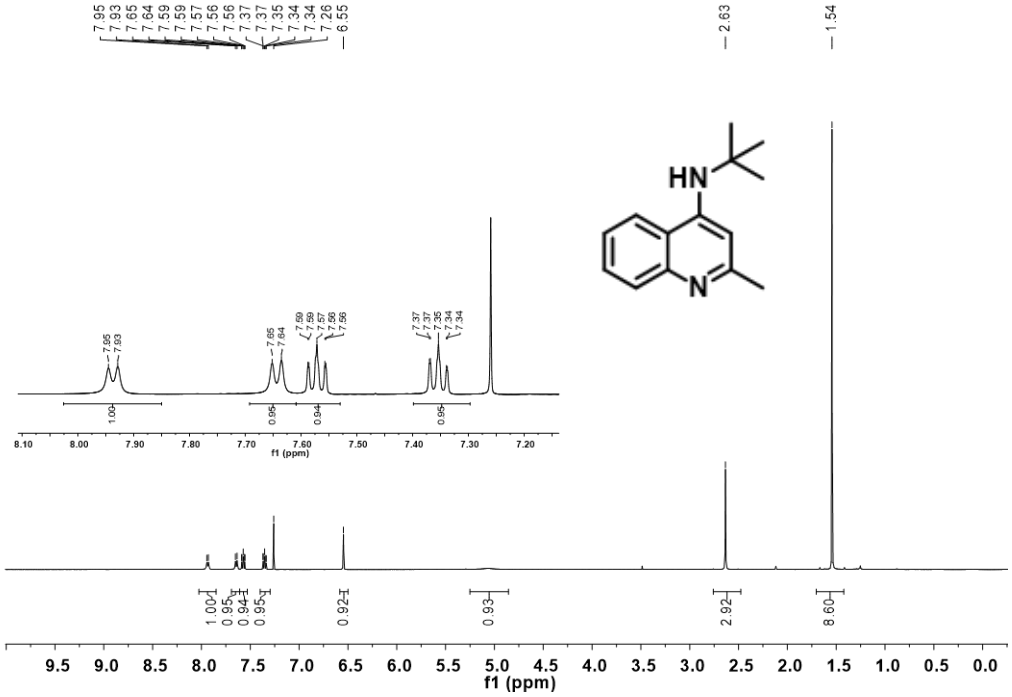

Figure A22. ^{13}C{^{1}H} UDEFT NMR spectrum of *N*-(*tert*-butyl)-2-methylquinolin-4-amine, **4b** (125.8 MHz, $CDCl_3$).

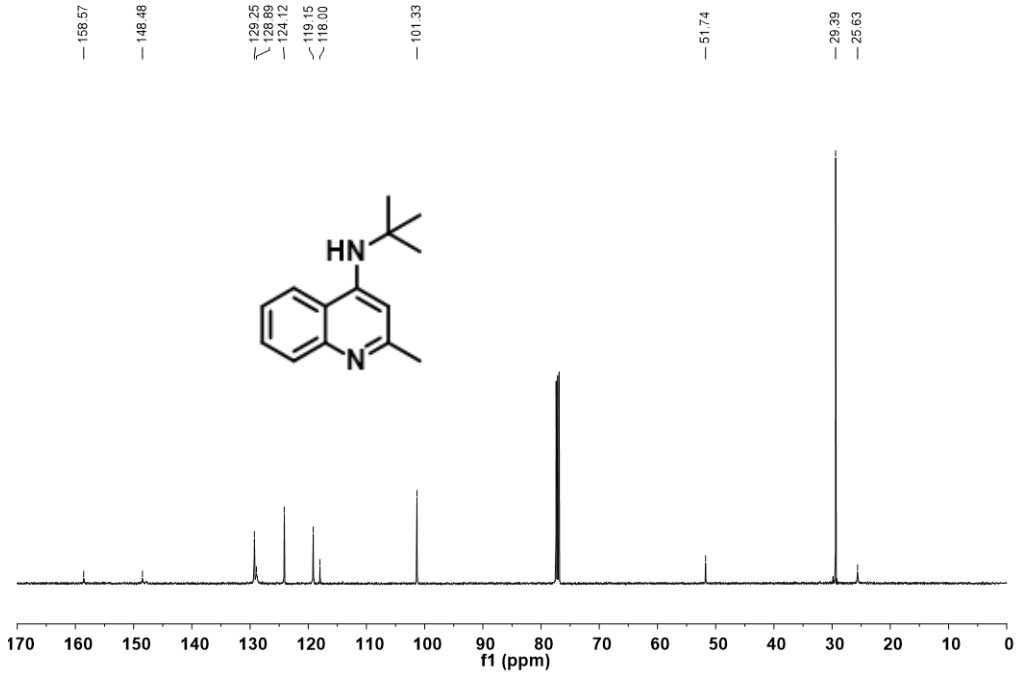

Figure A23. ^{1}H NMR spectrum of 4-(*tert*-butoxy)-2-methylquinoline, **4b'** (500.1 MHz, $CDCl_3$).

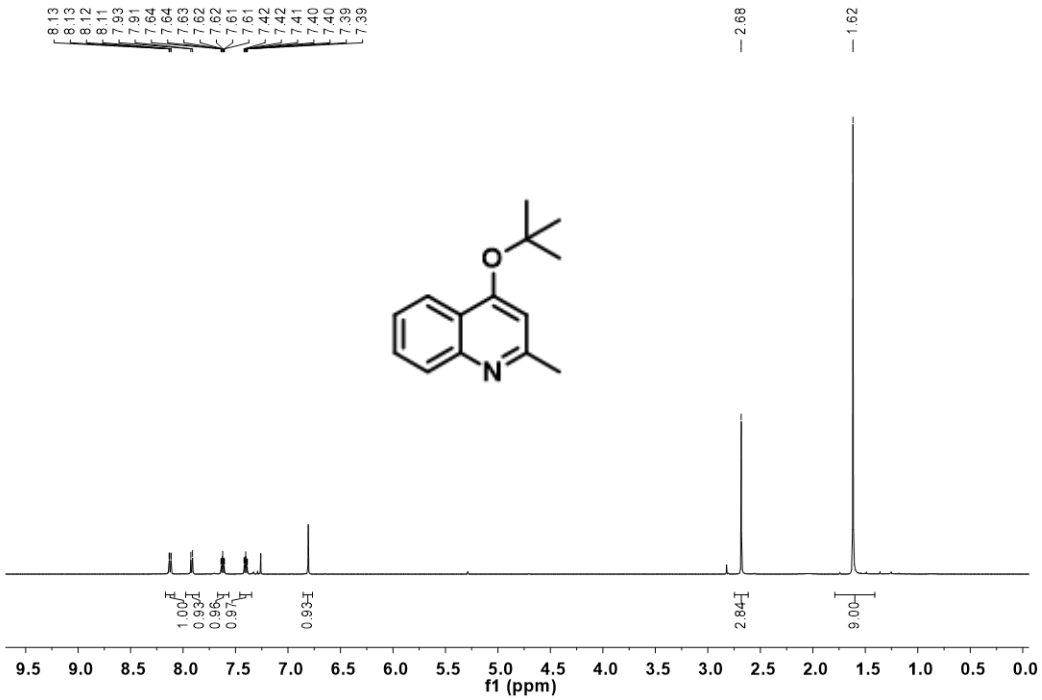

Figure A24. $^{13}C\{^{1}H\}$ UDEFT NMR spectrum of 4-(*tert*-butoxy)-2-methylquinoline, **4b'** (125.8 MHz, $CDCl_3$).

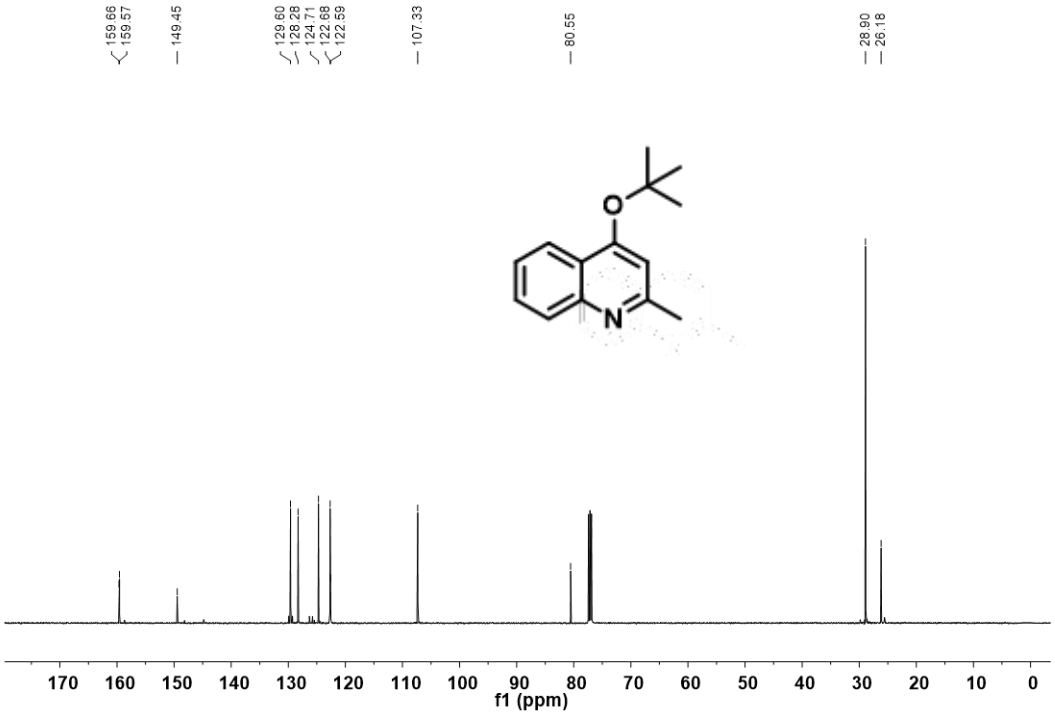

Figure A25. ^{1}H NMR spectrum of 2-methyl-*N*-(3-methyl-1-phenyl-1*H*-pyrazol-5-yl)quinolin-4-amine, **4d** (500.1 MHz, $CDCl_3$).

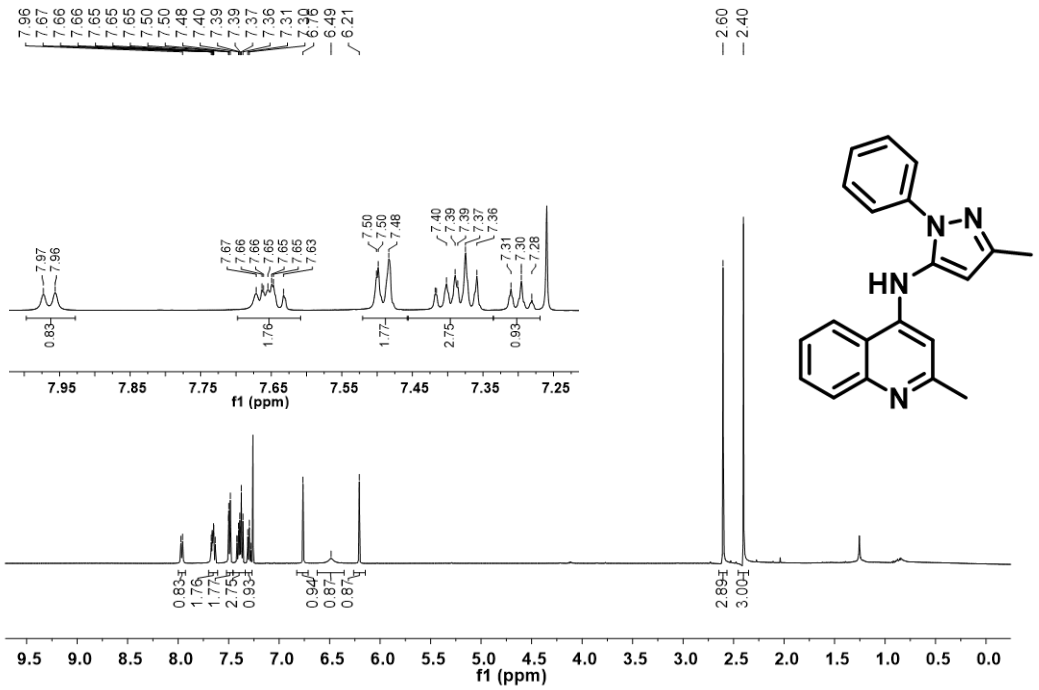

Figure A26. ^{13}C{^{1}H} UDEFT NMR spectrum of 2-methyl-*N*-(3-methyl-1-phenyl-1*H*-pyrazol-5-yl)quinolin-4-amine, **4d** (125.8 MHz, $CDCl_3$).

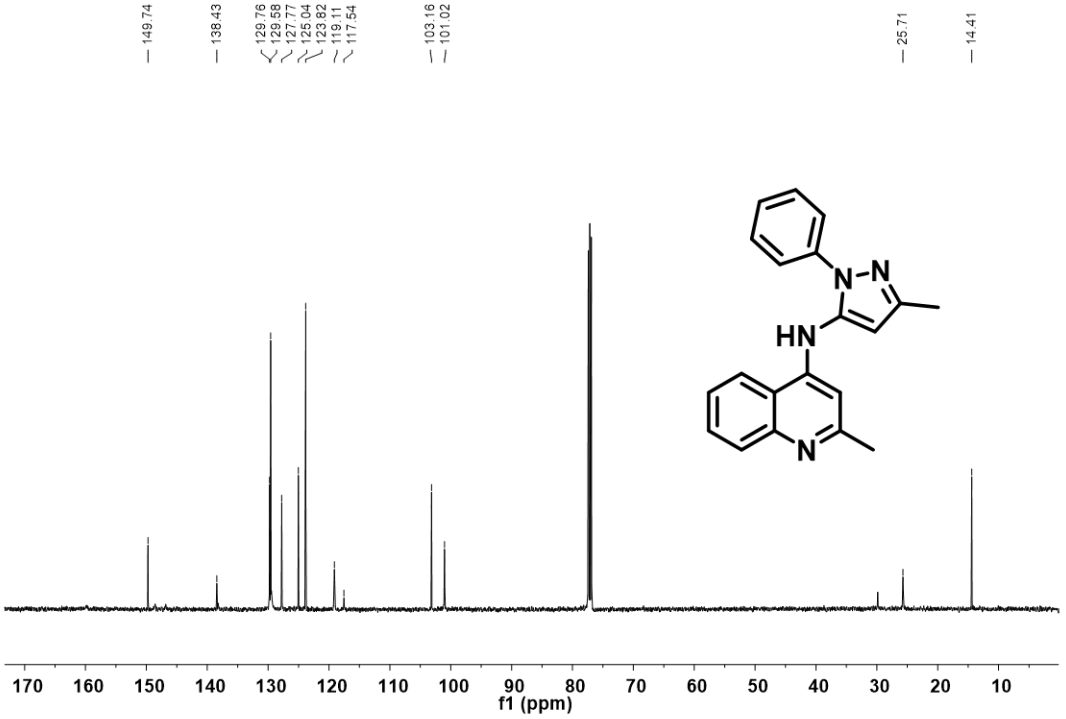

Figure A27. ^{1}H NMR spectrum of 4-((3-methyl-1-phenyl-1*H*-pyrazol-5-yl)amino)benzonitrile, **5a** (500.1 MHz, $CDCl_3$).

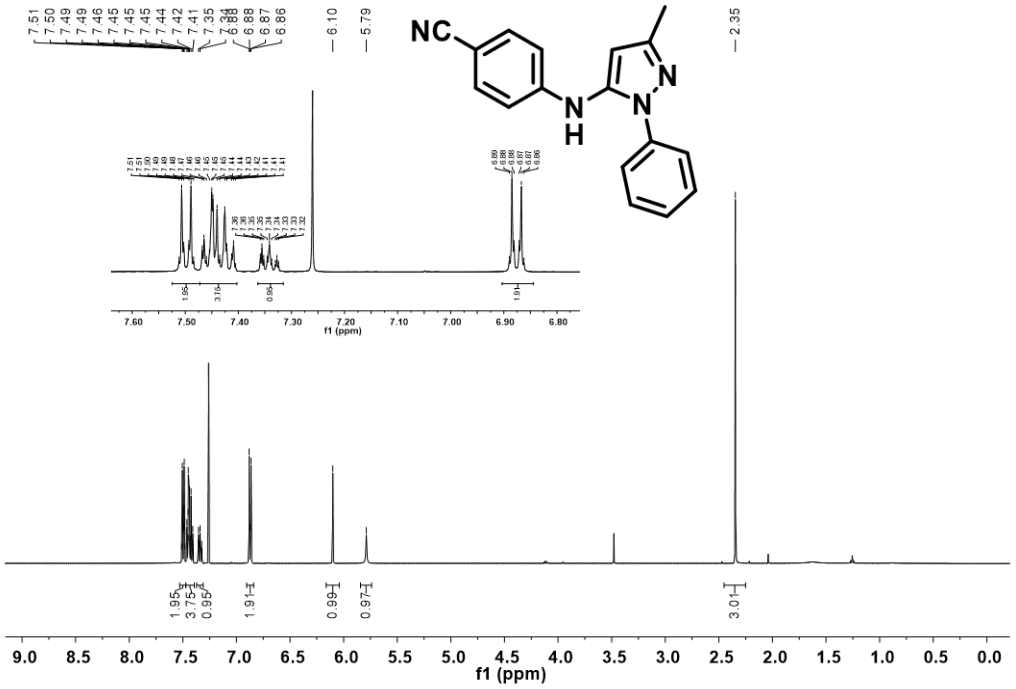

Figure A28. $^{13}C\{^{1}H\}$ UDEFT NMR spectrum of 4-((3-methyl-1-phenyl-1*H*-pyrazol-5-yl)amino)benzonitrile, **5a** (125.8 MHz, $CDCl_3$).

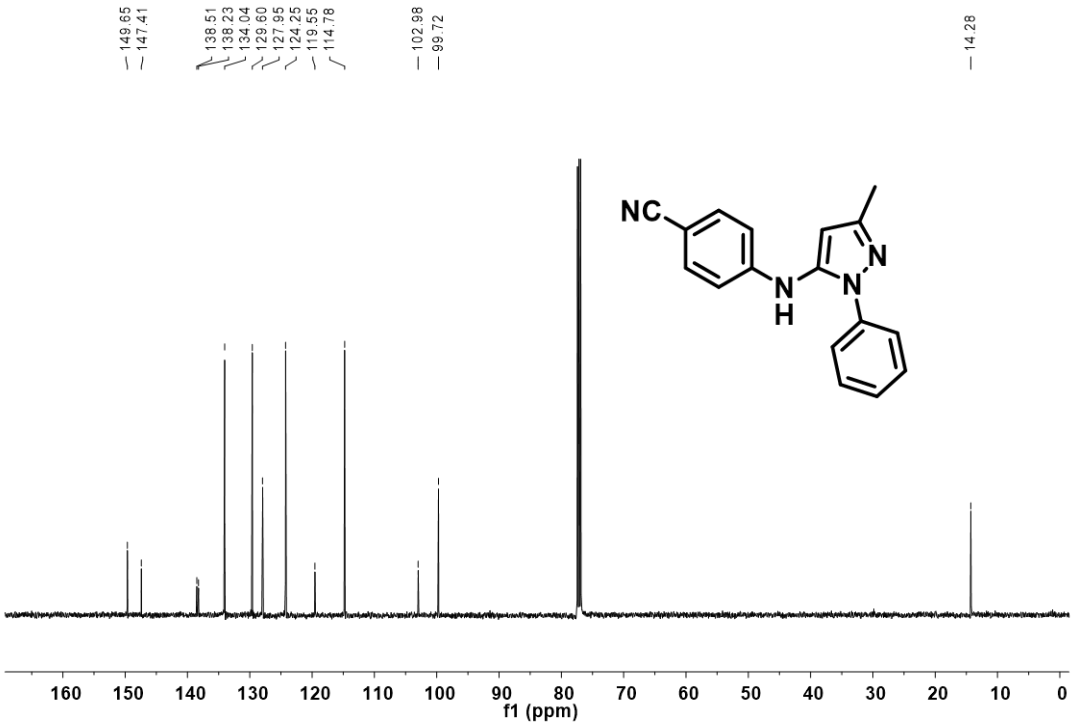

Figure A29. ^{1}H NMR spectrum of *N*-(1,3-dimethyl-4-phenyl-1*H*-pyrazol-5-yl)quinoxalin-6-amine, **5b** (500.1 MHz, $CDCl_3$).

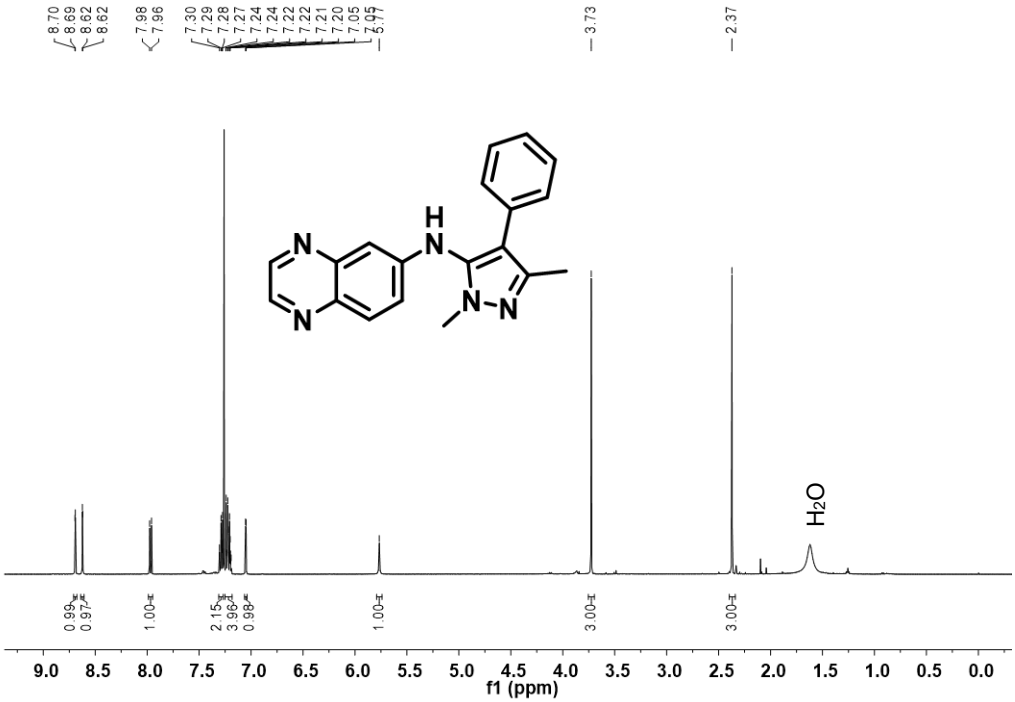

Figure A30. ^{13}C{^{1}H} UDEFT NMR spectrum of *N*-(1,3-dimethyl-4-phenyl-1*H*-pyrazol-5-yl)quinoxalin-6-amine, **5b** (125.8 MHz, $CDCl_3$).

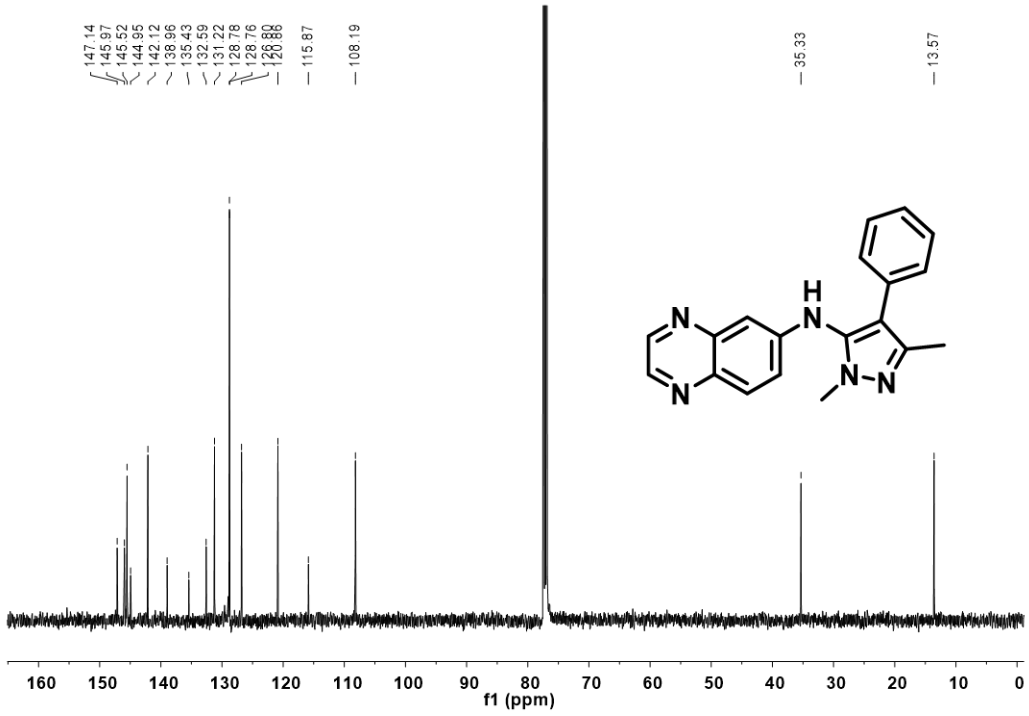

Figure A31. ^{1}H NMR spectrum of 3-methyl-*N*-(1-methyl-3-phenyl-1*H*-pyrazol-5-yl)pyridin-2-amine, **5c** (500.1 MHz, $CDCl_3$).

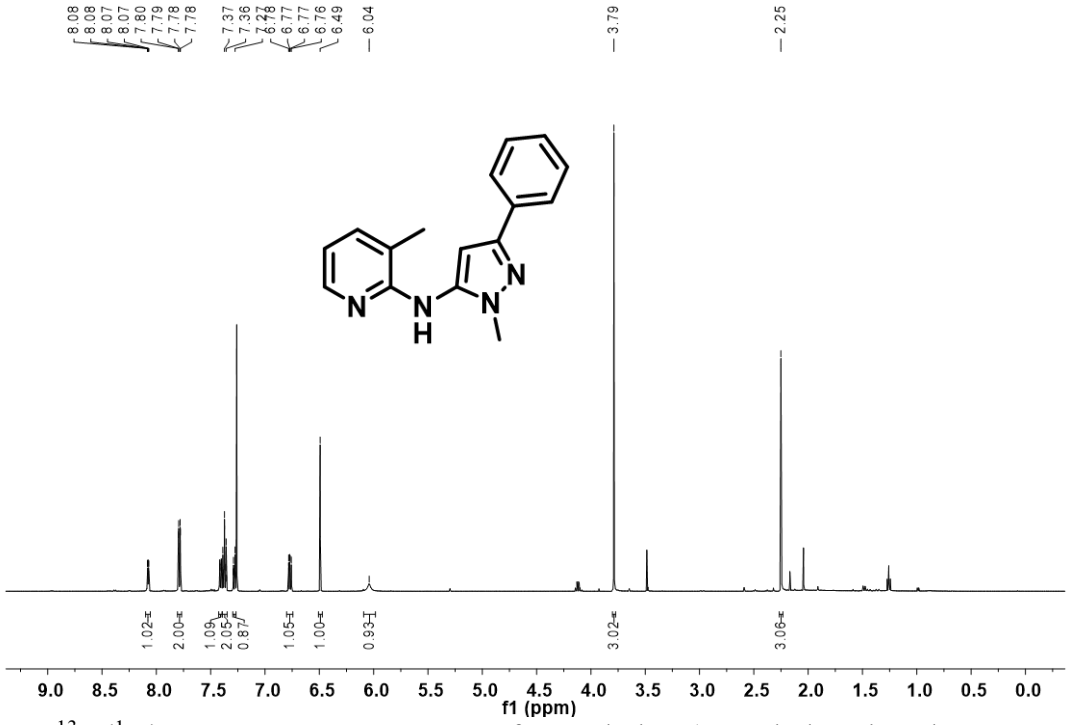

Figure A32. $^{13}C\{^{1}H\}$ UDEFT NMR spectrum of 3-methyl-*N*-(1-methyl-3-phenyl-1*H*-pyrazol-5-yl)pyridin-2-amine, **5c** (125.8 MHz, $CDCl_3$).

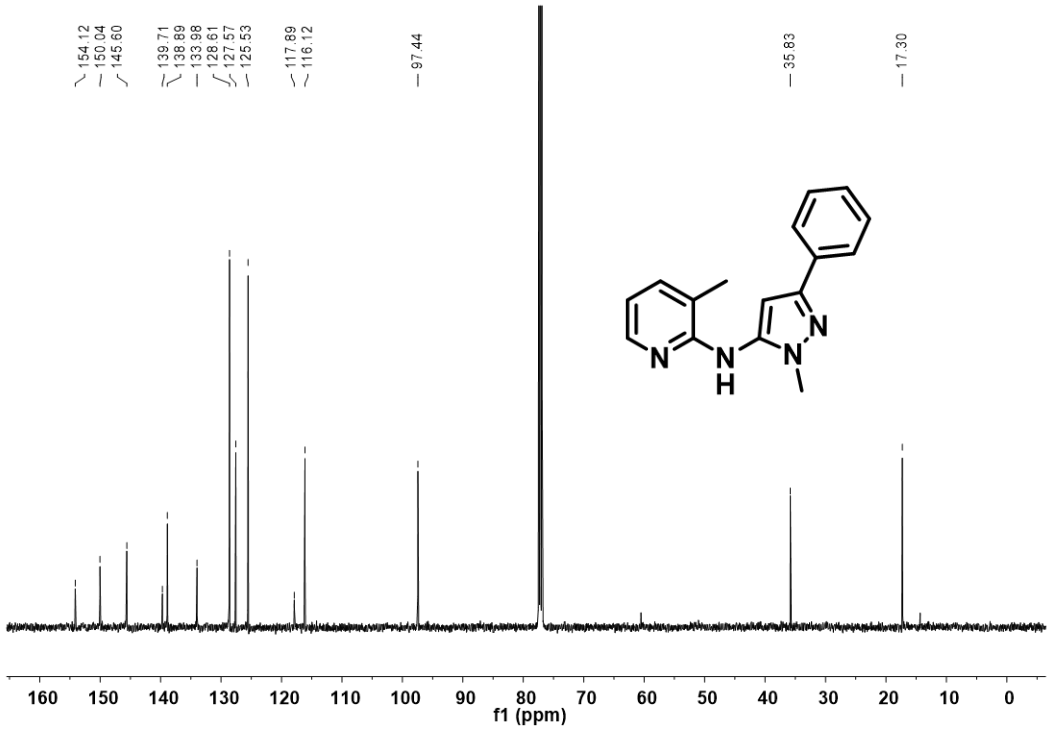

Figure A33. ^{1}H NMR spectrum of *N*-(1,3-diphenyl-1*H*-pyrazol-5-yl)-2-methylquinolin-7-amine, **5d** (500.1 MHz, $CDCl_3$).

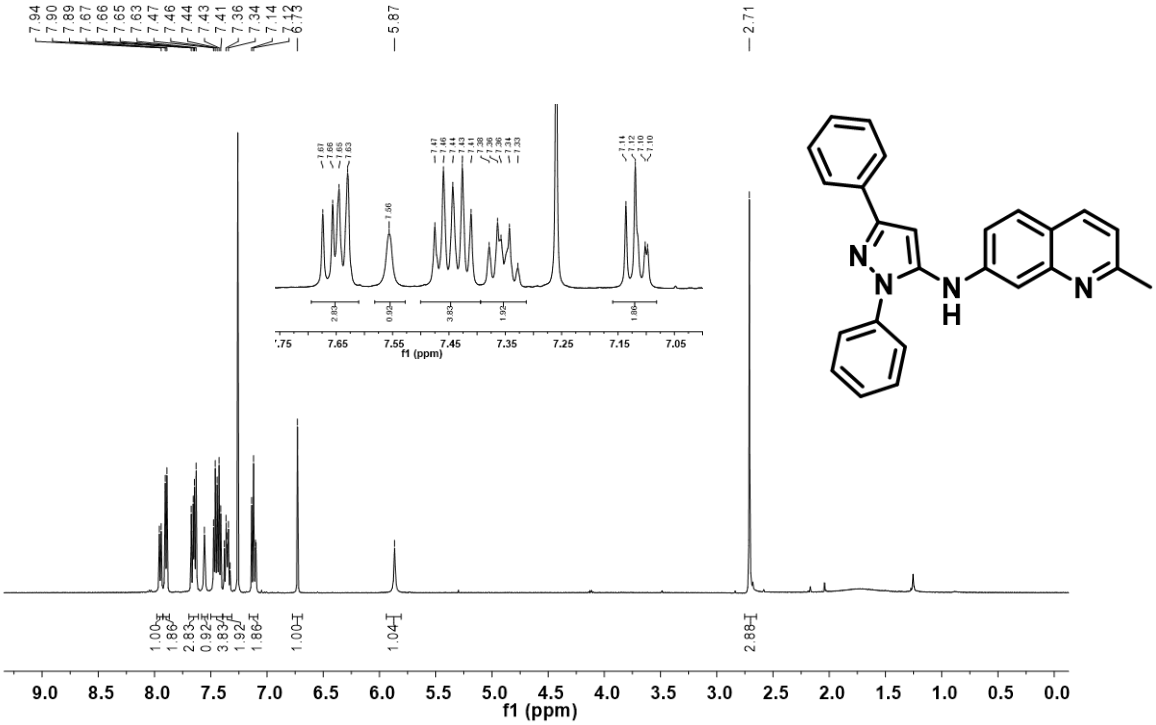

Figure A34. $^{13}C\{^{1}H\}$ UDEFT NMR spectrum of *N*-(1,3-diphenyl-1*H*-pyrazol-5-yl)-2-methylquinolin-7-amine, **5d** (125.8 MHz, $CDCl_3$).

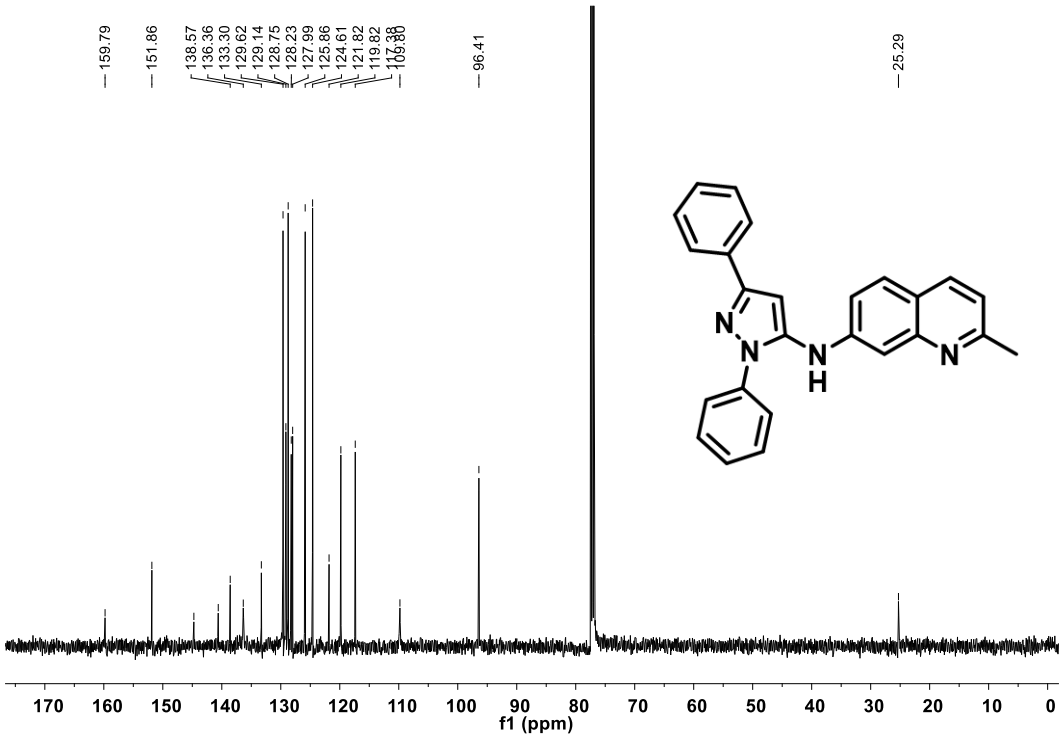

Figure A35. ^{1}H NMR spectrum of *N*-(1-methyl-1*H*-pyrazolo[3,4-*b*]pyridin-3-yl)quinoxalin-2-amine, **5e** (500.1 MHz, $(CD_3)_2SO$).

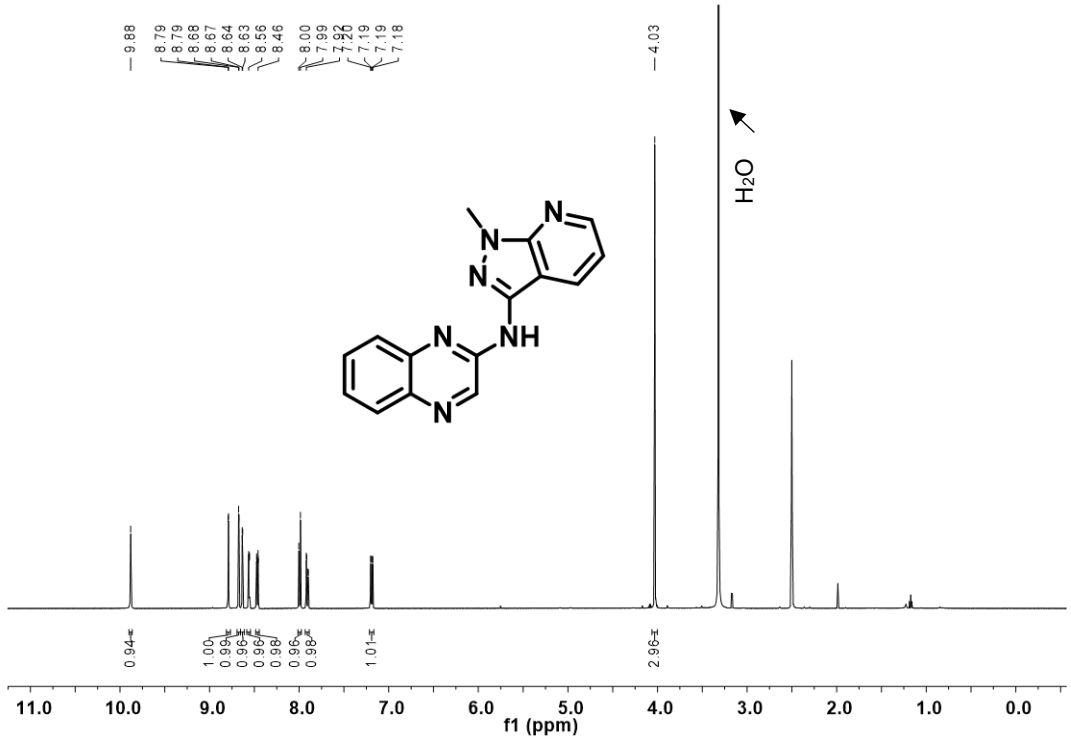

Figure A36. $^{13}C\{^{1}H\}$ UDEFT NMR spectrum of *N*-(1-methyl-1*H*-pyrazolo[3,4-*b*]pyridin-3-yl)quinoxalin-2-amine, **5e** (125.8 MHz, $(CD_3)_2SO$).

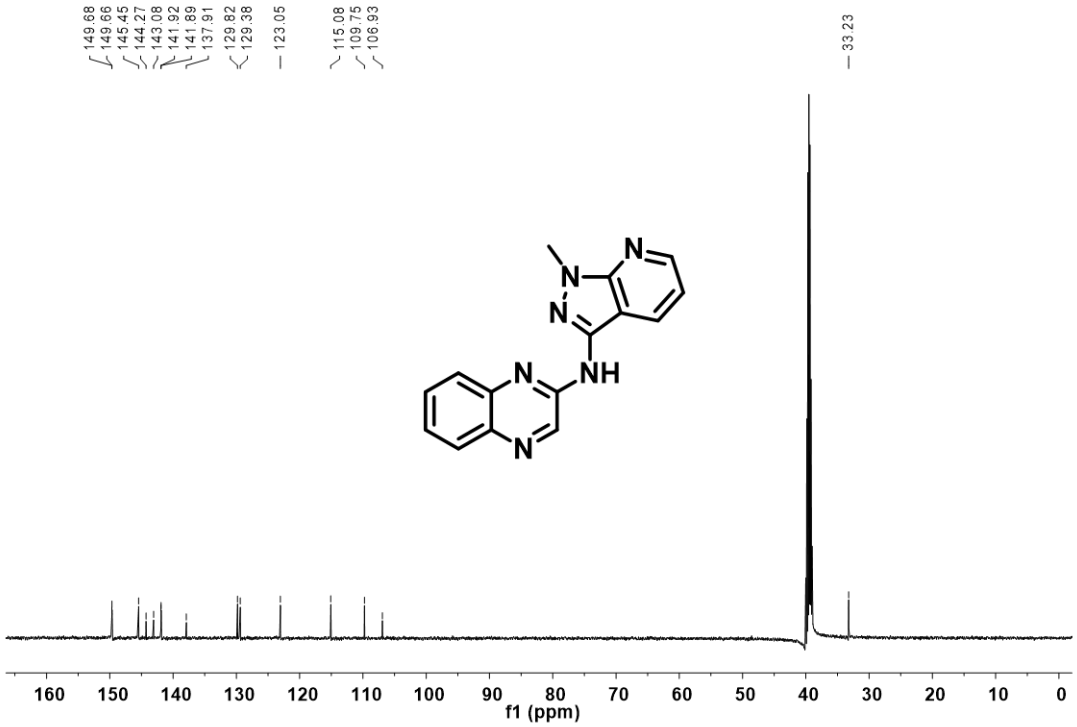

Figure A37. ^{1}H NMR spectrum of *N*-(naphthalen-1-yl)-1*H*-pyrazol-3-amine, **5f** (500.1 MHz, $CDCl_3$).

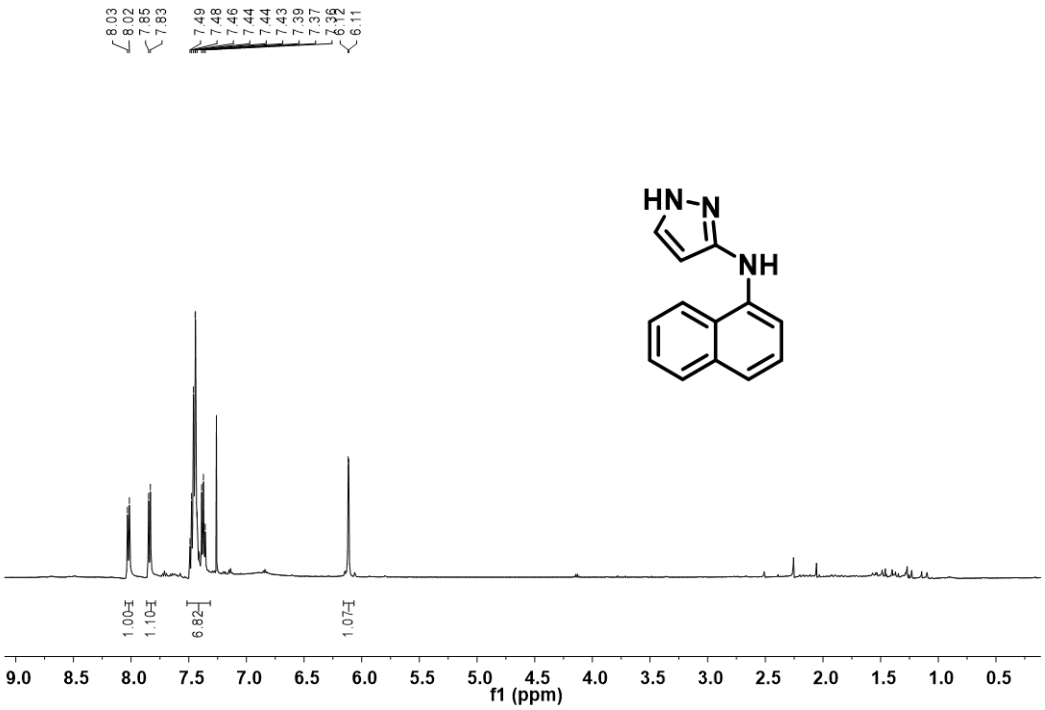

Figure A38. ^{13}C{^{1}H} UDEFT NMR spectrum of *N*-(naphthalen-1-yl)-1*H*-pyrazol-3-amine, **5f** (125.8 MHz, $CDCl_3$).

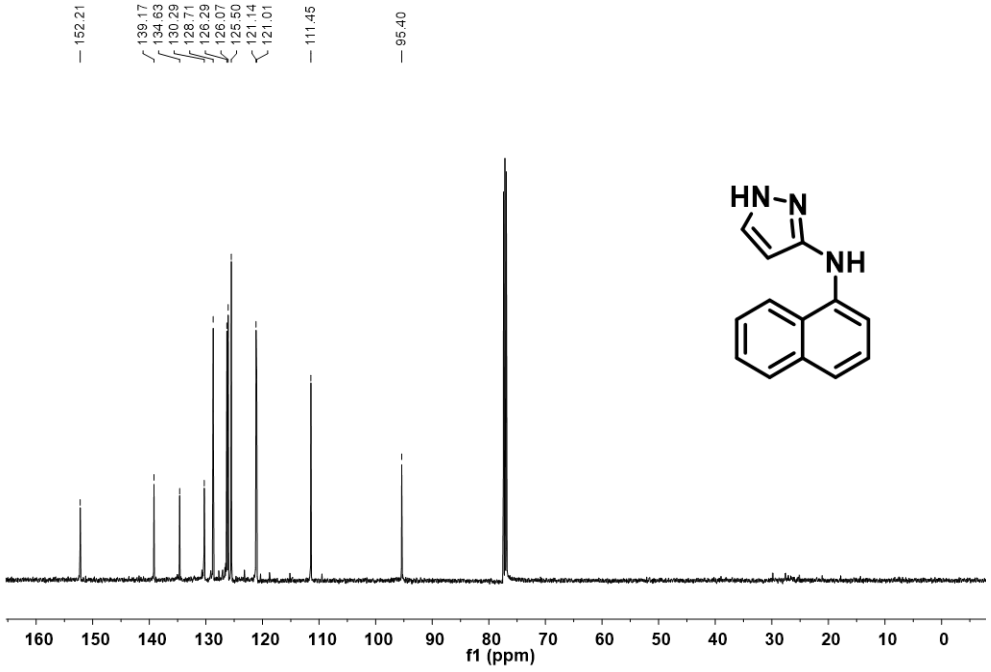

Figure A39. ^{1}H NMR spectrum of 2-methyl-*N*-(1*H*-pyrazol-3-yl)quinolin-4-amine, **5g** (500.1 MHz, $(CD_3)_2SO$).

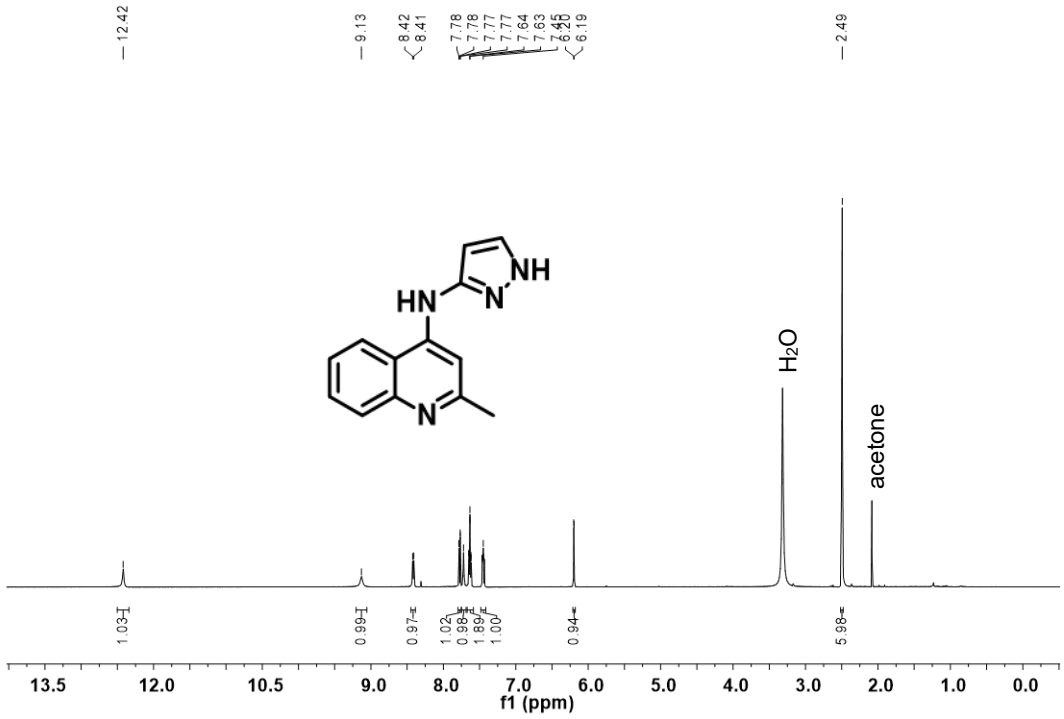

Figure A40. $^{13}C\{^{1}H\}$ UDEFT NMR spectrum of 2-methyl-*N*-(1*H*-pyrazol-3-yl)quinolin-4-amine, **5g** (125.8 MHz, $(CD_3)_2SO$).

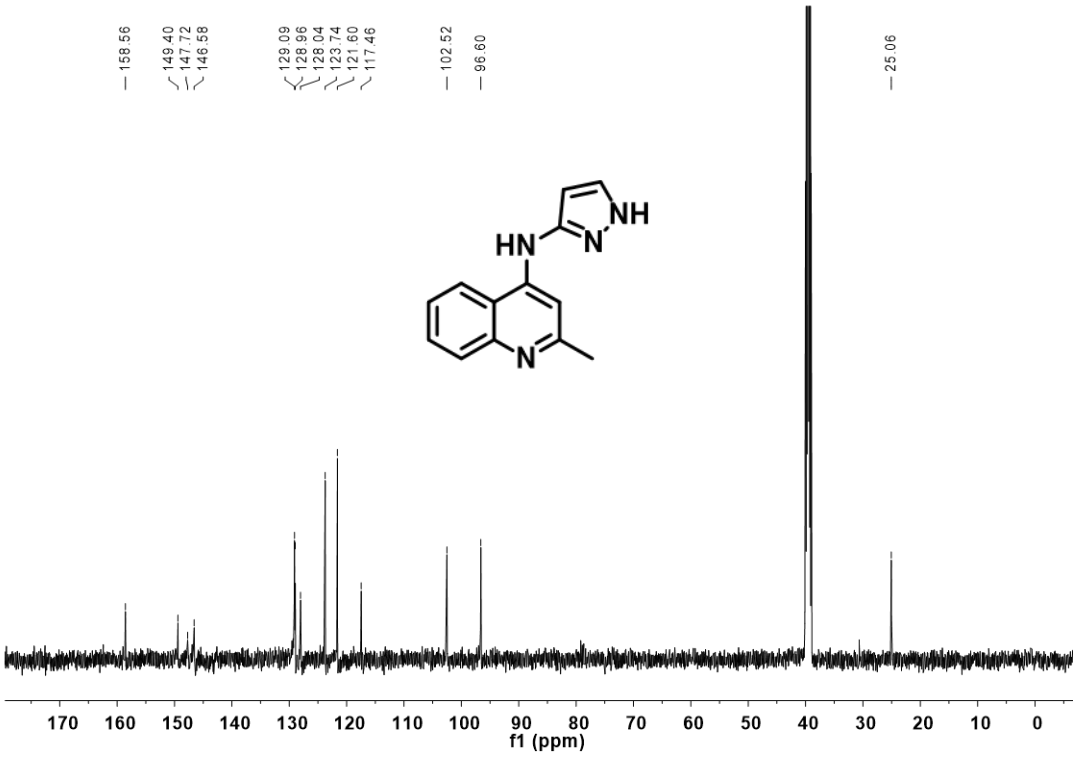

Figure A41. ^{1}H NMR spectrum of 4-((2-(1*H*-pyrazol-1-yl)phenyl)amino)benzonitrile, **5h** (500.1 MHz, $CDCl_3$).

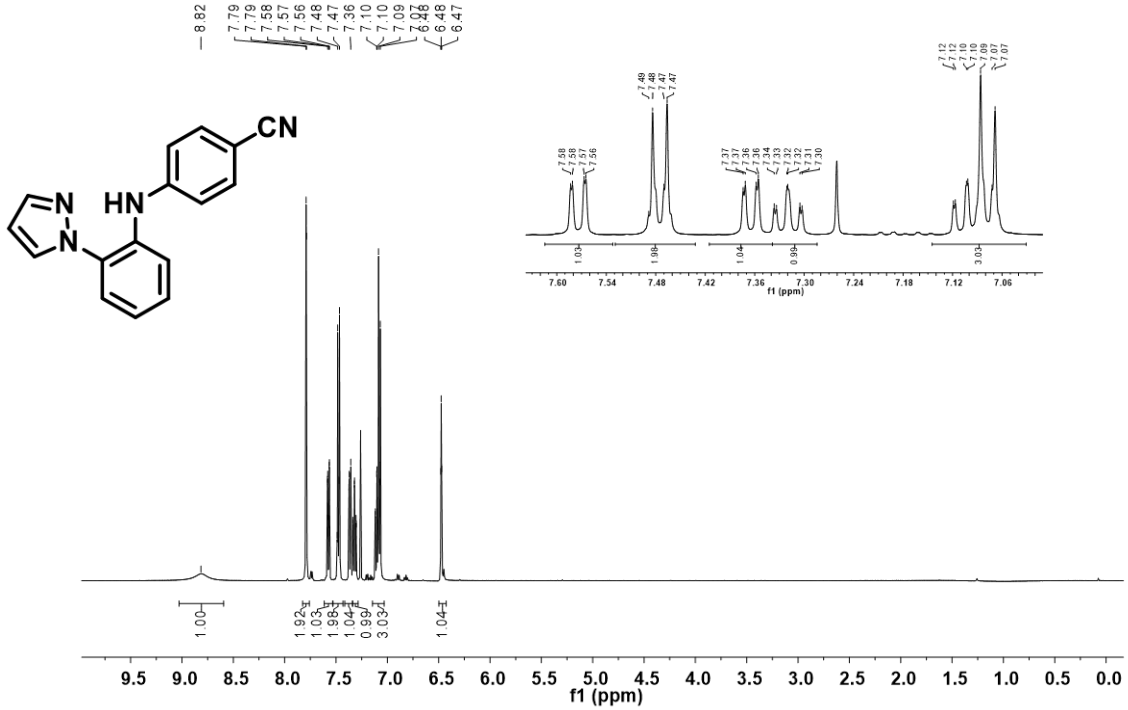

Figure A42. ^{13}C{^{1}H} UDEFT NMR spectrum of 4-((2-(1*H*-pyrazol-1-yl)phenyl)amino)benzonitrile, **5h** (125.8 MHz, $CDCl_3$).

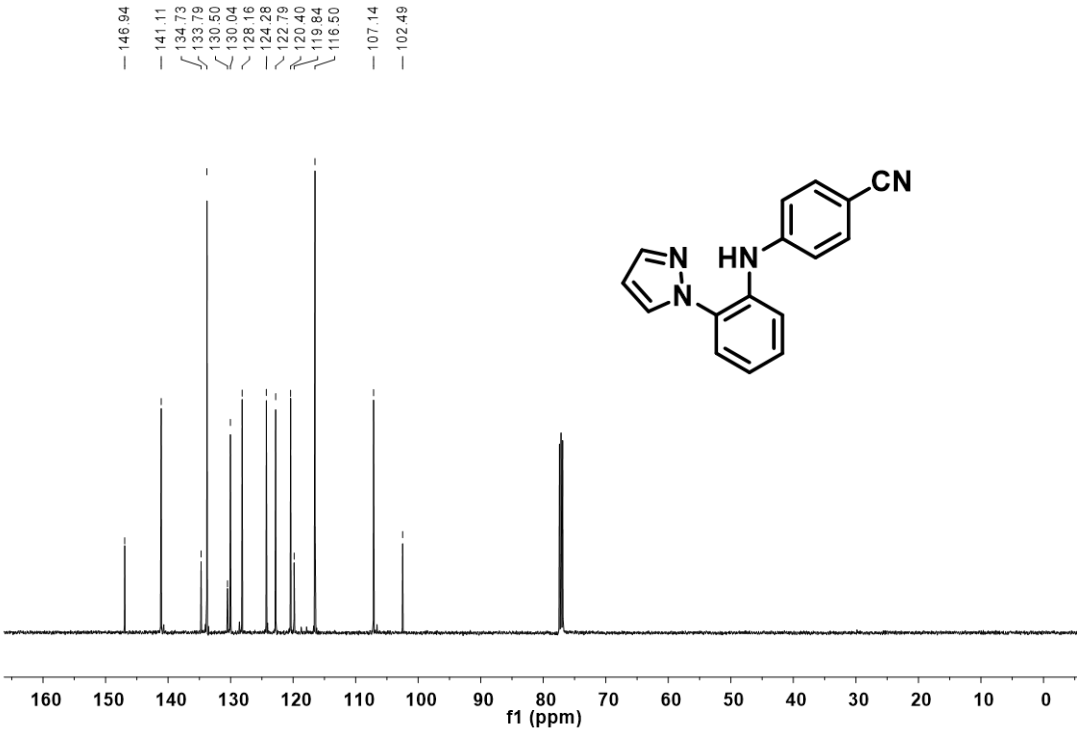

Figure A43. ^{1}H NMR spectrum of *N*-(2-(1*H*-pyrazol-1-yl)phenyl)-3-methylpyridin-2-amine, **5i** (500.1 MHz, $CDCl_3$).

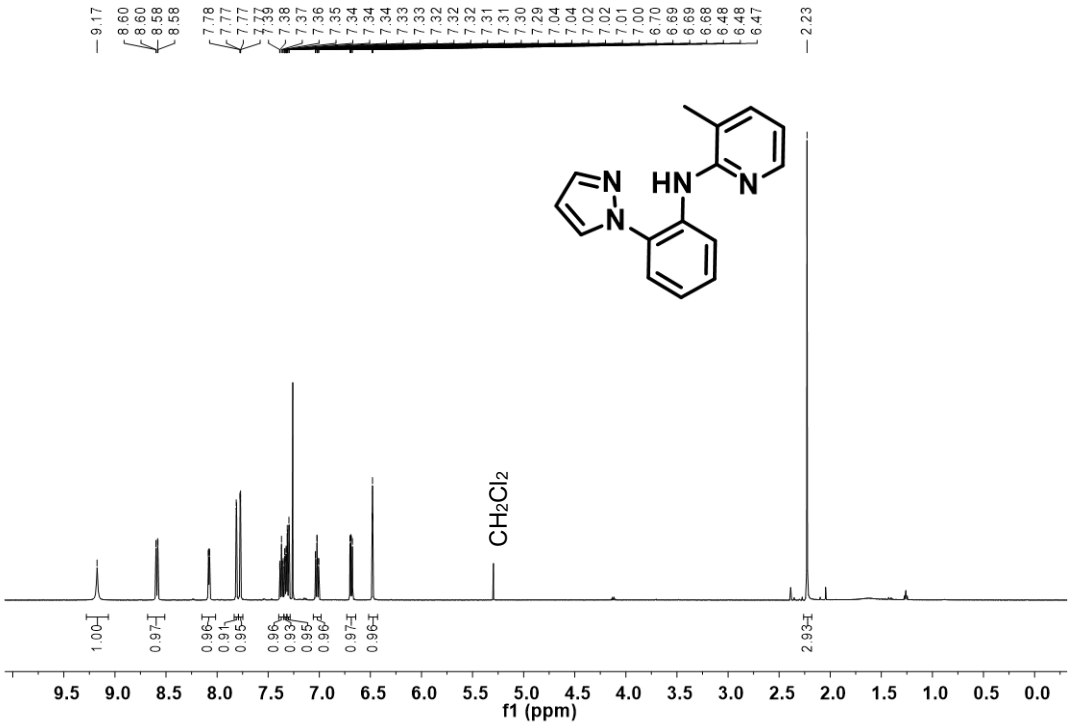

Figure A44. $^{13}C\{^{1}H\}$ UDEFT NMR spectrum of *N*-(2-(1*H*-pyrazol-1-yl)phenyl)-3-methylpyridin-2-amine, **5i** (125.8 MHz, $CDCl_3$).

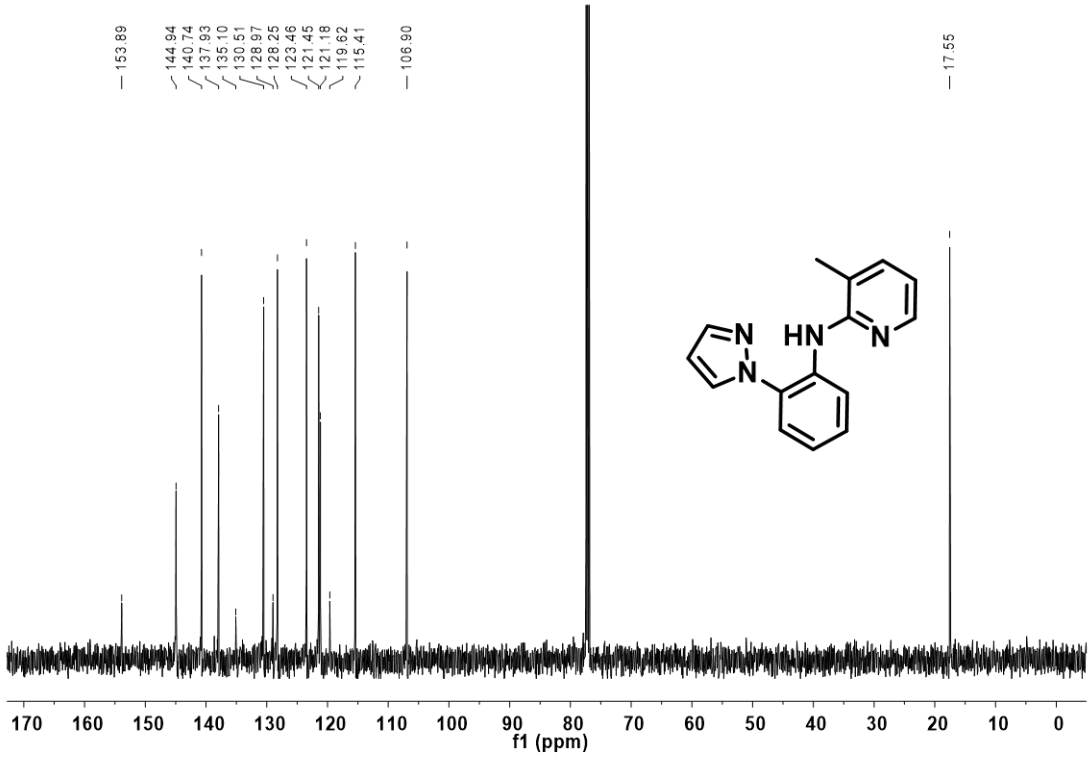

Figure A45. ^{1}H NMR spectrum of *N*-(2-(1*H*-pyrazol-1-yl)phenyl)-2-methylquinolin-4-amine, **5j** (500.1 MHz, $CDCl_3$).

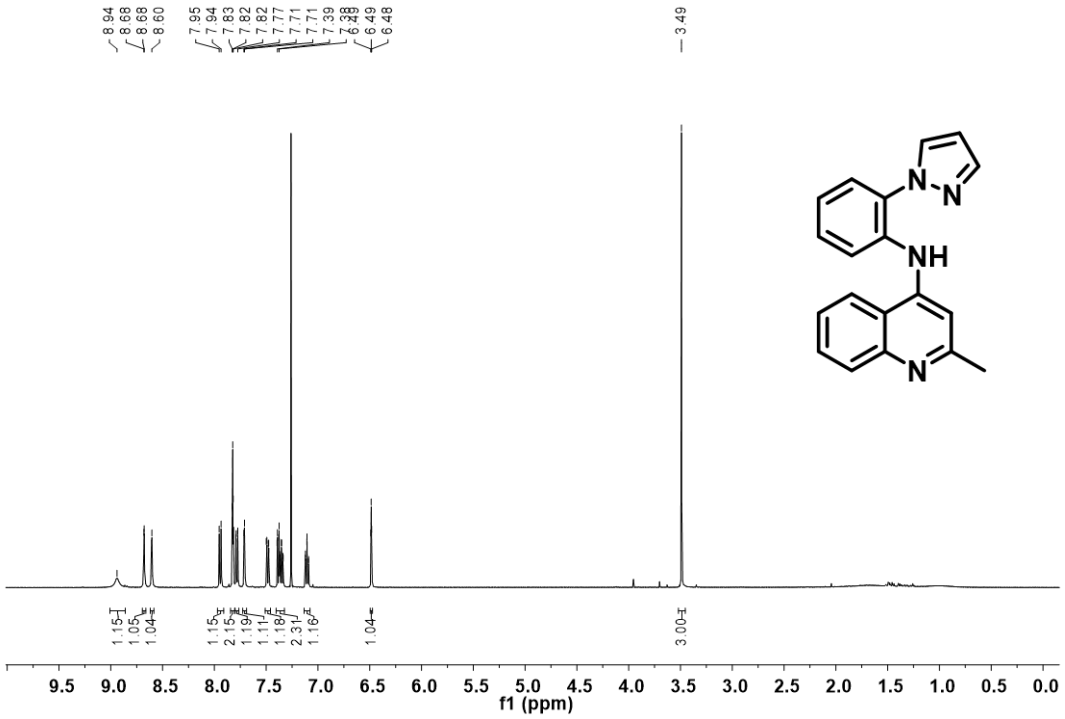

Figure A46. $^{13}C\{^{1}H\}$ UDEFT NMR spectrum of *N*-(2-(1*H*-pyrazol-1-yl)phenyl)-2-methylquinolin-4-amine, **5j** (125.8 MHz, $CDCl_3$).

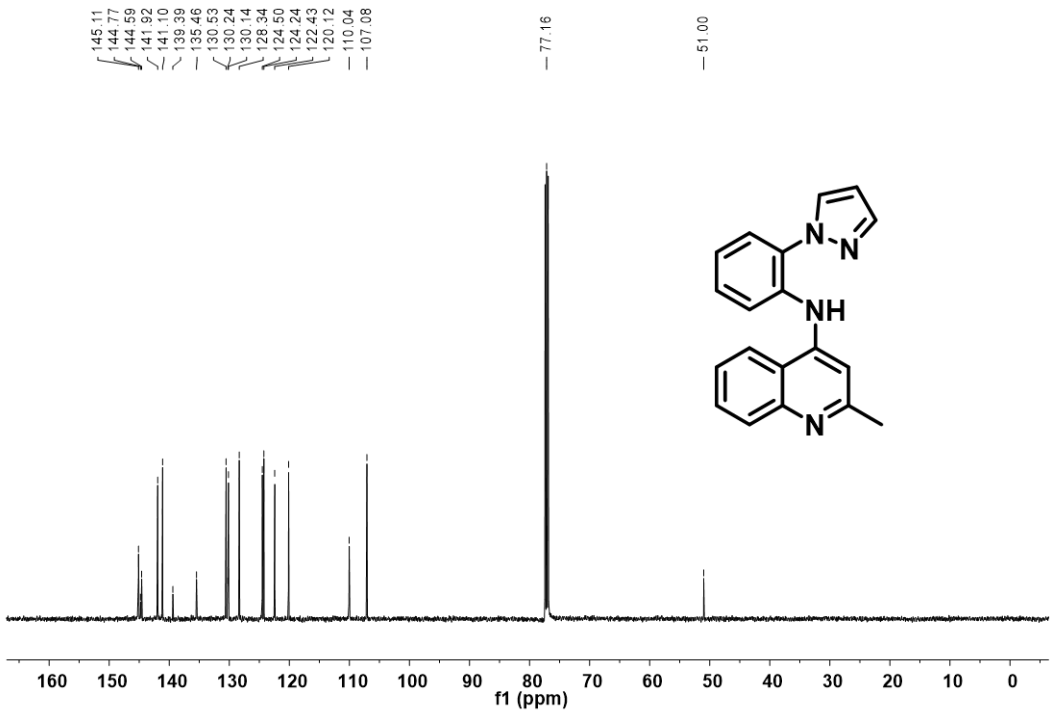

Appendix C. Copyright Permissions

JOHN WILEY AND SONS LICENSE
TERMS AND CONDITIONS

Feb 10, 2023

This Agreement between Dalhousie University -- Nicole Martinek ("You") and John Wiley and Sons ("John Wiley and Sons") consists of your license details and the terms and conditions provided by John Wiley and Sons and Copyright Clearance Center.

License Number	5485500211897
License date	Feb 10, 2023
Licensed Content Publisher	John Wiley and Sons
Licensed Content Publication	Chemistry - A European Journal
Licensed Content Title	Comparative Screening of DalPhos/Ni Catalysts in C-N Cross-couplings of (Hetero)aryl Chlorides Enables Development of Aminopyrazole Cross-couplings with Amine Base
Licensed Content Author	Nicole Martinek, Kathleen M. Morrison, Justin M. Field, et al
Licensed Content Date	Dec 8, 2022
Licensed Content Volume	29
Licensed Content Issue	7
Licensed Content Pages	10

Requestor type	Author of this Wiley article
Format	Electronic
Portion	Full article
Will you be translating?	No
Title	A Comparative Study of Ni Catalysts in C-N Cross-Couplings
Institution name	Dalhousie University
Expected presentation date	Mar 2023
Publisher Tax ID	EU826007151